AEROLEASTIC ANALYSES OF AN UNMANNED HELICOPTER

A THESIS SUBMITTED TO
THE GRADUATE SCHOOL OF NATURAL AND APPLIED SCIENCES
OF
MIDDLE EAST TECHNICAL UNIVERSITY

BY

ALAADDİN FURKAN UZUNKAYA

IN PARTIAL FULFILLMENT OF THE REQUIREMENTS
FOR
THE DEGREE OF MASTER OF SCIENCE
IN
AEROSPACE ENGINEERING

APRIL 2023

Approval of the thesis:

AEROLEASTIC ANALYSES OF AN UNMANNED HELICOPTER

submitted by **ALAADDİN FURKAN UZUNKAYA** in partial fulfillment of the requirements for the degree of **Master of Science** i**n Aerospace Engineering, Middle East Technical University** by,

Prof. Dr. Halil Kalıpçılar
Dean, Graduate School of **Natural and Applied Sciences** _____

Prof. Dr. Serkan Özgen
Head of the Department, **Aerospace Engineering** _____

Prof. Dr. Yavuz Yaman
Supervisor, **Aerospace Engineering, METU** _____

Examining Committee Members:

Prof. Dr. Serkan Özgen
Aerospace Engineering, METU _____

Prof. Dr. Yavuz Yaman
Aerospace Engineering, METU _____

Prof. Dr. Altan Kayran
Aerospace Engineering, METU _____

Assoc. Prof. Dr. Ercan Gürses
Aerospace Engineering, METU _____

Prof. Dr. Erdem Acar
Mechanical Engineering, TOBB ETU _____

Date: 14.04.2023

I hereby declare that all information in this document has been obtained and presented in accordance with academic rules and ethical conduct. I also declare that, as required by these rules and conduct, I have fully cited and referenced all material and results that are not original to this work.

Name, Surname: Alaaddin Furkan Uzunkaya

Signature:

ABSTRACT

AEROLEASTIC ANALYSES OF AN UNMANNED HELICOPTER

Uzunkaya, Alaaddin Furkan
Master of Science, Aerospace Engineering
Supervisor: Prof. Dr. Yavuz Yaman

April 2023, 148 pages

In helicopter comprehensive analysis tools, helicopter blades could be modeled as rigid beams in torsional direction; however, it is well known that helicopter blades are very flexible structures. One of the main purposes of this thesis is to analyze the effects of torsional twist on the helicopter's performance characteristics and to examine validity of rigid blade assumption. To perform the analyses, aerodynamic loads are calculated by using blade element momentum theory. In elastic blade analyses, aerodynamic loads cause a torsional twist which increments aerodynamic load field on the blade. On the other hand, there is no torsional twist and aerodynamic load increment in the rigid blade assumption. A trim code is written to obtain trim points for a level flight at sea level by using rigid and elastic blade in which the only difference is the torsional twist and aerodynamic increments due to the torsional twist.

In the second part of the thesis, flutter analyses are conducted for the reference blade by using steady aerodynamic loads, Theodorsen's, Loewy's and a modified version of Loewy's unsteady aerodynamic theories.

Keywords: Aeroelasticity, Unmanned Helicopter, Flutter, Theodorsen, Loewy.

ÖZ

İNSANSIZ BİR HELİKOPTERİN AEROELASTİK ANALİZLERİ

Uzunkaya, Alaaddin Furkan
Yüksek Lisans, Havacılık ve Uzay Mühendisliği
Tez Yöneticisi: Prof. Dr. Yavuz Yaman

Nisan 2023, 148 sayfa

Kapsamlı helikopter analiz araçlarında helikopter palleri burulma yönünde rijit kirişler olarak modellenebilmektedir ancak bilinmektedir ki helikopter palleri son derece esnek yapılardır. Bu tezin ana amaçlarından birisi de palin esnek yapısından kaynaklanan burulmanın helikopterin performans özelliklerine etkisini araştırmak ve rijit pal varsayımının ne kadar geçerli bir varsayım olduğunu sorgulamaktır. Analizleri gerçekleştirebilmek için aerodinamik yükler Pal Elemanı Momentum Teorisi (*İng. Blade Element Momentum Theory*) kullanılarak hesaplanmıştır. Esnek pal analizleri sırasında aerodinamik yüklerin sebep olduğu burulma aerodinamik yük dağılımını etkilemiştir. Öte yandan, rijit pal varsayımında herhangi bir burulma olmadığı için aerodinamik yük dağılımında bir değişme olmamıştır. Rijit ve esnek pal yapısı için deniz seviyesinde ve yatay düzlemde sabit hızdaki uçuş noktalarını elde eden bir kod yazılmış olup, bu kodun rijit ve esnek pal için tek farkı esnek palin tecrübe ettiği burulmadan dolayı aerodinamik yük dağılımının etkilenmesidir.

Tezin ikinci kısmında ise zamandan bağımsız aerodinamik yükler, Theodorsen'in ve Loewy'nin zamana bağlı aerodinamik teorileri ile Loewy'nin teorisinin değiştirilmiş bir hali referans alınan palin çırpınma analizleri için kullanılmıştır.

Anahtar Kelimeler: Aeroelastisite, İnsansız Helikopter, Çırpınma, Theodorsen, Loewy.

to Him… (ﷺ, p.b.u.h)

ٱقْرَأْ وَرَبُّكَ ٱلْأَكْرَمُ ۝ ٱلَّذِى عَلَّمَ بِٱلْقَلَمِ ۝ عَلَّمَ ٱلْإِنسَـٰنَ مَا لَمْ يَعْلَمْ ۝

Read! And your Lord is the Most Generous, who taught by the pen, taught humanity what they knew not. *(Surah Al-'Alaq)*

ACKNOWLEDGMENTS

Firstly, I would like to thank to my thesis advisor Prof. Dr. Yavuz Yaman for his guidance, support, and endless patience during writing period of this work.

I cannot express how grateful and lucky I am for having such a good family. Without them, nothing would be possible and imaginable. Especially I would like to thank my brother Abdullah Taha for being such a good man, friend, and brother. I miss our childhood days so much.

I also would like to thank my company ASELSAN A.Ş. for providing me such a perfect environment to be a researcher and an engineer.

I feel so much lucky to be an apprentice to Dr. Fahri Ersel Ölçer who is the person who taught me whatever I know about the helicopters. He is always there whenever I needed, he always knows whatever I ask.

I would like to thank to Dr. Aykut Tamer for accepting me his course as a guest and kind responds to my questions about my thesis work.

I would like to mention the people I greatly respect Yusuf Uyar, Abdurrahim Atalay, and Gökhan Karaca for being the light I needed to find the correct path.

I am so grateful to have such a good man like Gökhan Güneruz from the very beginning. If I had the chance, I would have spent a second life by doing the same things with you. Thank you very much man for being from the beginning to the end.

Being a part of our high school group “2010-B-2014 + Furkan Uzgur” is one of the best things happen to me. The days we spent together are the best days of my life.

Lastly, I would like to thank my wife Sümeyye Nur. Without her understanding, patience, love, support and all the things she has done so far, I am not sure whether I could finish my thesis. I don’t know how to thank God for being your husband. You are the sun of my life. I love you.

TABLE OF CONTENTS

LIST OF TABLES

TABLES

LIST OF FIGURES

FIGURES

LIST OF ABBREVIATIONS

ABBREVIATIONS

AoA: Angle of attack.

BEM: Blade Element.

LE: Leading edge.

NFP: No-Feathering Plane.

TE: Trailing edge.

TPP: Tip-Path Plane.

LIST OF SYMBOLS

LATTIN SYMBOLS

A	Main rotor disk area. (πR^2)
B	Tip loss factor.
b	Semi-chord.
$C_{D,F}$	Non-dimensional fuselage aerodynamic drag coefficient.
$C_{M,F}$	Non-dimensional fuselage aerodynamic pitching moment coefficient.
$C(k)$	Theodorsen's lift deficiency function.
$C'(k)$	Loewy's lift deficiency function.
$C'_N(k)$	Finite wake lift deficiency function.
C_P	Non-dimensional main rotor power coefficient. ($P/\rho A(\Omega R)^3$)
C_T	Non-dimensional main rotor thrust coefficient. ($T/\rho A(\Omega R)^2$)
c	Chord of the main rotor blade.
c_d	Non-dimensional drag coefficient. ($c_{d_0} + c_{d_{\alpha^2}}\alpha^2$)
c_{d_0}	Zero-lift drag coefficient.
$c_{d_{\alpha^2}}$	Second order drag coefficient.
c_l	Non-dimensional lift coefficient. ($c_{l_\alpha}\alpha$)
c_{l_α}	Lift curve slope of the airfoil.
c_m	Non-dimensional aerodynamic pitching moment coefficient.
D	Fuselage aerodynamic drag force.

D'	Drag force per unit span.
E	Young's modulus.
e	Non-dimensional flap hinge offset.
F_A	Fuselage effective aerodynamic area.
F_f	Ratio of the lift-curve slope of the airfoil to the lift-curve slope of thin-airfoil theory. $(c_{l_\alpha}/2\pi)$
F_L	Fuselage effective aerodynamic length.
F_x	Parallel force to the disk plane of the airfoil.
F_z	Normal force to the disk plane of the airfoil.
G	Shear modulus.
g	Damping coefficient.
H	Main rotor longitudinal force.
$H^{a,b}$	Harmonic solution parameter. $\left(\frac{1}{N_{az}}\sum_{n=1}^{n=N_{az}}\frac{sin^a\psi_n\, cos^b\psi_n}{\sqrt{1-M_n^2}}\right)$
h	Plunging displacement.
$\hat{h}$	Non-dimensional wake spacing.
I_b	Moment of inertia of the blade about the rotor center.
$\widehat{I_a}$	Main rotor blade second-order inertia.
$\widehat{I_b}$	Main rotor blade hinged second-order inertia w.r.t flap-hinge.
i	Incidence angle or pitch angle of the aircraft.
i_s	Longitudinal tilt of the rotor shaft.
J	Torsional constant.

K	Kinetic energy of the system.
k	Non-dimensional reduced frequency. $(\omega b/U)$
L'	Lift per unit span.
M	Mach number.
M'	Sectional aerodynamic torque.
M_H	Main rotor hub moment.
M_X	Rotor hub rolling moment.
M_{XF}	Fuselage aerodynamic rolling moment.
M_{XX}	Lateral component of the rotor hub rolling moment.
M_Y	Rotor hub pitching moment
M_{YF}	Fuselage aerodynamic pitching moment.
M_{YY}	Longitudinal component of the rotor hub pitch moment.
m	Blade mass per unit length.
m	Non-dimensional frequency ratio. (ω/Ω)
N_{az}	Number of azimuth step.
N_b	Number of blades of the main rotor.
N_{bem}	Number of blade elements of the main rotor.
Q	Main rotor torque.
Q_i	Generalized forces of the system.
q	Dynamic pressure. $\left(\frac{1}{2}\rho U^2\right)$
q_i	Generalized coordinates of the system.

P	Potential energy of the system.
P_c	Climb power.
P_i	Induced power.
P_o	Profile power.
P_p	Parasite power.
P_{req}	Required power.
R	Main rotor radius.
Δr	Length of the blade elements in the radial direction. $(\Delta r = R/N_{bem})$
r	Radial location on the blade from center of the rotor.
r_a	Non-dimensional radius of gyration.
r_R	Aerodynamic root cutout.
T	Main rotor total thrust.
U	Resultant air speed.
U_D	Divergence speed of the blade.
u_P	Experienced axial speed by the airfoil.
u_r	Experienced radial speed by the airfoil.
u_T	Experienced tangential speed by the airfoil.
V	Forward flight velocity of the helicopter.
V_c	Climb velocity of the helicopter.
V_F	Flutter speed of the blade.
V_w	Non-dimensional speed of the air, reduced velocity.

W'	Loewy's returning wake effect.
W'_N	Returning finite wake effect.
X_{CG}	Distance between c.g. of the aircraft and rotor hub in x-axis of body-fixed frame.
x_o	Position of the elastic axis (shear center) from the leading edge.
x_{ac}	Position of the aerodynamic center from the leading edge.
x_{cg}	Position of the c.g. of the airfoil.
x_θ	Non-dimensional distance between shear center and c.g. of the airfoil.
Y	Main rotor lateral force.
Y_{CG}	Distance between c.g. of the aircraft and rotor hub in y-axis of body-fixed frame.
Y_F	Fuselage aerodynamic side force.

GREEK SYMBOLS

α	Angle of attack.
α_r	Rigid angle of attack.
β_0	Main rotor coning angle.
β_{1s}	Main rotor 1st harmonic lateral tip-path plane-tilt.
β_{1c}	Main rotor 1st harmonic longitudinal tip-path plane-tilt.
δ	Elastic increment of the angle of attack.
ζ_0	Main rotor mean lag angle.
ζ_{1c}	Main rotor 1st harmonic lateral shift.
ζ_{1s}	Main rotor 1st harmonic longitudinal shift.

η	Non-dimensional vertical displacement of the blade section.
θ	Blade pitch angle. ($\theta_{con} + \theta_{tw}$)
θ_0	Main rotor collective input.
θ_{1c}	Main rotor 1st harmonic lateral cyclic input.
θ_{1s}	Main rotor 1st harmonic longitudinal cyclic input.
θ_{con}	Main rotor control input. ($\theta_0 + \theta_{1c} \cos\psi + \theta_{1s} \sin\psi$)
θ_{FP}	Flight path angle.
θ_{tw}	Elastic twist of the blade.
λ	Nondimensional rotor inflow ratio. ($v/\Omega R$)
λ_i	Nondimensional rotor induced inflow ratio. ($v_i/\Omega R$)
μ	Advance ratio. ($Vcos\ i/\Omega R$)
μ_z	Climb velocity advance ratio. ($Vsin\ i/\Omega R$)
μ_m	Non-dimensional mass ratio.
ν	Induced inflow.
ν_i	Induced inflow in hover.
ξ	Ratio of the first bending natural frequency of the blade to the main rotor nominal rotational speed. (ω_h/Ω)
ρ	Air density.
σ	Solidity of the main rotor. ($N_b c/\pi R$)
Φ	Lateral tilt or roll angle of the aircraft.
φ	Ratio of the plunging natural frequency to the pitching natural frequency. (ω_h/ω_θ)

ϕ	Inflow angle.
ψ	Blade azimuth angle. (Ωt)
Ω	Main rotor nominal RPM.
ω	Oscillation frequency of a state.
ω_h	First bending natural frequency.
ω_θ	First torsional natural frequency.

CHAPTER 1

INTRODUCTION

Helicopter is a type of aircraft which rotates its blades in order to produce the lift necessary to take-off. Since these rotating blades could produce lift even when the aircraft is stationary, helicopters have the ability of vertical take-off and landing. Thanks to the vertical take-off and landing capability, helicopters are one of the most important and precious vehicles for different civilian and military objectives such as transporting, rescuing, and exploring.

Since objectives of a helicopter vary, there are different helicopter designs to accomplish these different objectives successfully. These designs are usually named according to the main rotor configurations and orientations. The first and most common helicopter design is the **conventional helicopters** which has one main rotor and one tail rotor. Purpose of the main rotor is to produce the necessary thrust, whereas the tail rotor is used to balance the main rotor torque and provide yaw motion.

Figure 1.1. Turkish Aerospace T129 Atak Helicopter. [22]

Advantages of the conventional helicopters could be listed as:

- Their design is simple and generally lighter than other design types.
- Tail rotor could provide a significant control power in yaw direction.

Whereas disadvantages are:

- Tail rotor requires power which increases total power needed to fly the helicopter.
- The tail rotor operates in an aerodynamic environment where the wakes coming from the main rotor and the fuselage is highly effective. Therefore, the tail rotor operates in an aerodynamically inefficient environment.
- Due to the wakes coming from the fuselage and the main rotor, tail rotor may produce excessive vibrations.

Co-axial helicopters could be given as second helicopter design. In the co-axial design, there are two counter rotating rotors sharing same shaft with some vertical separation. Since the main rotors rotates in different directions, no tail rotor is needed. Yaw control is obtained by the differential torque. Advantages of the co-axial design are:

- Necessary rotor diameter to produce same thrust could be lower compared to conventional helicopters since there are two main rotors.
- More thrust could be obtained compared to a conventional helicopter having same radius.

Disadvantages of the co-axial design could be listed as:

- Yaw control is generally weak since the yaw is achieved by the torque difference.
- Co-axial design of the rotor is complicated in terms of transmission and rotor control.

Figure 1.2. Kamov KA-32 co-axial helicopter. [13]

The third helicopter design is **tandem rotor helicopters** which has two main rotors as co-axial helicopters; however, these rotors are separated in longitudinal direction. Since the rotor rotates in opposite directions, tail rotor is not necessary.

Figure 1.3. Boeing CH-47 Chinook tandem helicopter. [5]

Tandem helicopters main advantages are:

- Thanks to the two main rotors they are capable of lifting heavy weights.
- Yaw control is achieved by differential lateral cyclic which provides significant control power in yaw direction.

Disadvantages of the tandem helicopters could be given as:

- Since the fuselage of the aircraft is large which returns with high gross-weight, two main rotors are needed.
- Two engines are necessary to operate the main rotors.

As it is stated before, helicopters could produce lift without having a relative speed w.r.t the air. This lift is produced by rotating the blade which are connected to the **rotor hub**. Rotor hub is a helicopter component where not only the connection between the blades and the main shaft is obtained but also blades are controlled. There are different types of rotor hub design to control the blades. **Articulated rotor**, **teetering rotor**, **hingeless rotor** and **bearingless rotor** designs could be given as examples for different rotor hub designs.

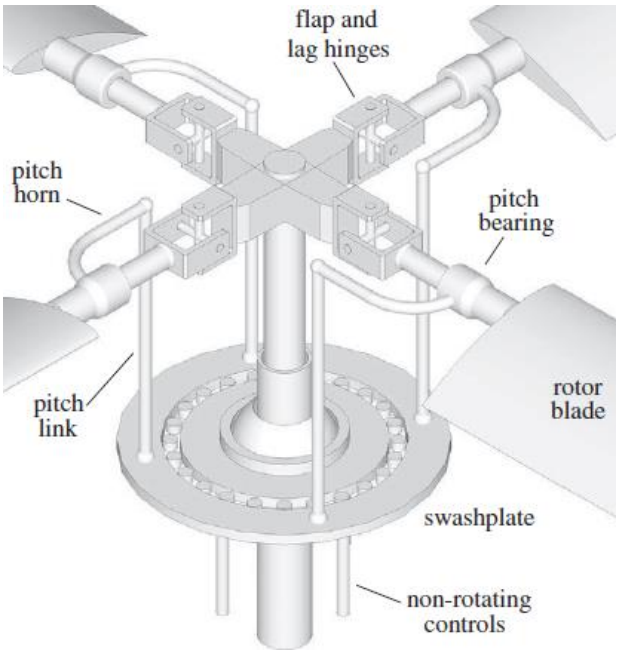

Figure 1.4. Articulated rotor schematic. [12]

In articulated design, blades are connected to the rotor hub with hinges which frees the blades motion in out-of-plane motion (flapping) and in-plane motion (lead-lag). These hinges are called as **flap-hinge** and **lead-lag-hinge** respectively. Main purpose of flap-hinges and lag-hinges is reducing the stress coming from the blades at the connection points between the blades and the rotor hub by freeing flap and lead-lag motion.

In teetering rotor design, there are two blades, and these blades are connected to the rotor shaft with a hinge similar to a flapping-hinge. Since the blades are connected to each other, flapping motion occurs as a whole.

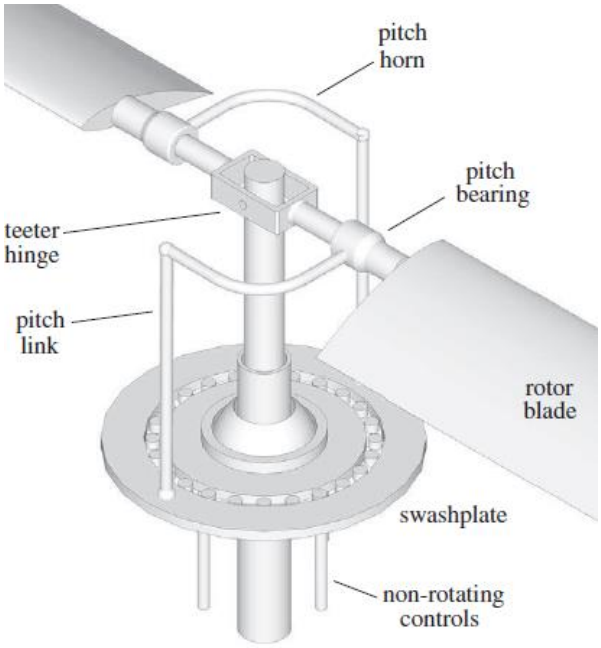

Figure 1.5. Teetering rotor schematic. [12]

Hingeless rotor design could be given as the third rotor hub configuration. As its name suggests, no flap-hinge or lead-lag-hinge is implemented between the rotor shaft and the blades; however, there exists a pitching bearing to control the blades. Blades are connected to the main rotor hub with a flexible medium. Material and design of this medium depends on the rotor design. Main advantages of the hingeless rotor design are mechanical simplicity, low maintenance costs and low aerodynamic drag. However, since the blades are connected to the rotor hub with an elastic medium, a strong connection must be implemented which generally returns with a heavier rotor hub [12]. Another critical issue regarding the hingeless rotors is connecting the blades to the rotor hub with a flexible medium creates a coupling between the flapping, lead-lag and pitching motions. Therefore, aeroelastic and aeromechanic analyses should be carefully conducted for hingeless rotors.

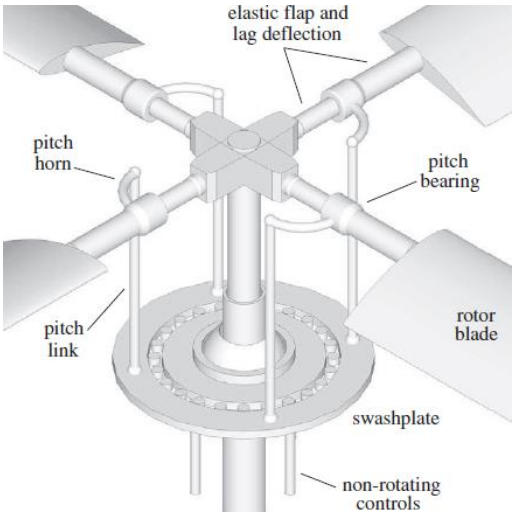

Figure 1.6. Hingeless rotor schematic. [12]

Bearingless rotors are the fourth rotor design. They are like hingeless rotors in terms of not having flap and lead-lag hinges. On the other hand, bearingless rotors do not have any pitch bearing or hinge. Instead, the control of the blades is obtained by twisting a relatively soft beam which connects the blade to the rotor hub. Bearingless rotors has an advantage over hingeless rotors in terms of maintenance cost. However, design and analysis stage of the bearingless rotors are more complicated than the hingeless rotors since designing the beam through which control and connection are obtained might be a challenging task.

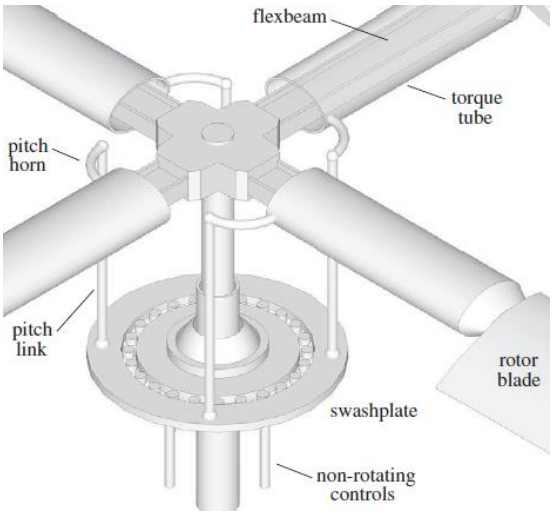

Figure 1.7. Bearingless rotor schematic. [12]

CHAPTER 2

LITERATURE REVIEW

As it is discussed in the previous section, helicopter blades are flexible structures and the loads are harmonic; therefore, the blades are subjected to high vibratory loads with structural deformations. If the structural deformations are excessive, control of the helicopter could be very hard. On the other hand, if the vibratory loads exceed the structural limits, the structure could fail. Moreover, as the airspeed increases flutter phenomenon could occur which may result in a fatal failure. Due to these problems, there are lots of studies conducted in terms of aeroelastic analyses helicopter blades. In this section, some of the previous works are discussed.

In comprehensive helicopter analysis tools, the rotor hub, the blades, and the connection between the hub and blades could be modeled as rigid by neglecting their structural flexibilities [12]. In his work, Özturan [17] modeled the main rotor hub, the blades, and the connection of the blades to the rotor hub as flexible structures of an articulated rotor configuration with root spring-damper system by using a finite element analysis tool and a multibody dynamic analysis tool. In addition, centrifugal stiffening and large deformations blades experiencing are included as nonlinearities to the analyses he conducted. Therefore, he was able to find stress concentrated points and actual deformations of the blades in hover and forward flight conditions.

In Akel's [2] study, torsional deformations experienced by the blades and their effects to the trim points are examined for a full-scale helicopter having an articulated rotor design. Aerodynamic loads are calculated using an in-house helicopter comprehensive analysis tool by implementing blade element method. Then these aerodynamic loads are transferred to a finite element analysis in which structural deformations are calculated. After finding the structural deformations from the finite element analyses, these deformations are transferred to the blade element

method as an angle of attack input. Akel found that torsional deformation of the blade could reach up to 1.5 degrees in hover and 2 degrees in forward flight which could be considered as a relatively high deformation. Therefore, to increase the fidelity of the analysis tool, effect of the torsional deformations should be considered in the analysis tool to obtain the necessary control inputs.

In the study which is done by the Siearadzki [20], UH-60A blades are modeled according to the Euler-Bernoulli Beam Theory and the main purpose of the study is to determine the deformation of the blades and influence of the deformations on the blade loads and general performance characteristics in hover condition. In the study, results obtained from the rigid blade assumption and results obtained elastic blade model are compared as well. In Sieradzki work, tip deflection of the blade in vertical direction is found as about 0.65 m, whereas the tip deflection of the elastic blade is found as about 0.40 m if the collective input is given as 10 degrees. The main reason elastic blade deforms less than the rigid blade is that torsional deformation of the blade is experienced as negative in the elastic blade which decreases the lift produced by the blade. Therefore, to be able to produce same thrust of the rigid blade, collective input for an elastic blade must be higher than the rigid blade collective input. The situation is also showed in Sieradzki's study. To obtain similar load distribution on the blade for the rigid blade where the collective input is 10 degrees, 16 degrees collective input is needed for the elastic blade. The difference is considerably high; therefore, to increase the fidelity of the performance calculations, flexibility of the blades should be included in the analyses.

Farsadi and Kayran [9] examined the aeroelastic stability of a composite wind turbine blade for different rotational speed. In the study, blades of the wind turbine are modeled as thin-walled composite box beams. For the unsteady aerodynamic loads, Theodorsen's and Loewy's unsteady aerodynamic theories and lift deficiency functions are used. In their work, it is found that for a relatively lower rotational speed, the difference between the flutter speed prediction by Theodorsen's and Loewy's unsteady aerodynamics are very close to each other. However, as rotational speed of the wind turbine blades increases, difference between the flutter speed

predictions widens as well since the returning wake effect is corelated with the rotational speed in Loewy's unsteady aerodynamic theory. The study also examined the effects of the number of blades on the flutter speed. It is found that, as the number of blades of the wind turbine increases, the flutter speed prediction coming from the Loewy's unsteady aerodynamics increases as well, whereas there is no change for the Theodorsen's unsteady theory. The reason behind this fact is that in Loewy's theory, wake returning from the blades are considered as well. In other words, number of blades is an argument for the Loewy's lift deficiency function. Therefore, as the number of blades changes flutter speed prediction changes as well in Loewy's theory.

In Çiçek's [7] study, different flutter speed prediction methodologies are investigated for fixed-wing and rotary-wing aircrafts. In his study, Theodorsen's, Loewy's, Wagner's unsteady aerodynamic theories and Pitt-Peters, Peters-He inflow theories are used to calculate the aerodynamic loads, whereas a simple beam theory expanded by Rayleigh-Ritz and Galerkin methods is used in the structural equations. To expand the scope of the work, Çiçek also examined the effects of the locations of the shear center and the mass center of the blade to the flutter speed for a helicopter in forward flight. In the study, it is shown that flutter speed predictions of the inflow theories are more conservative than the flutter speed predictions of the unsteady aerodynamic theories for a rotary-wing aircraft. Therefore, to be on the safe side flutter analyses could be conducted by implementing inflow theories as well. Another important outcome of the study is that if the center of mass is coincident with the shear center, no flutter instability is experienced.

CHAPTER 3

REFERENCE HELICOPTER

In this chapter, details of the structure of the unmanned helicopter's will be given.

Reference helicopter is an unmanned helicopter with a 160 kg maximum take-off weight. The helicopter could carry 40 kg payload. 10 kg of the payload is the optical systems. 30 kg of the payload is the cargo which could be dropped during the flight. Maximum forward flight speed of the helicopter is approximately 125 km/h.

Platform's length is 2.07 m, width is 0.78 m and height is 1.22 m. Platform's mass center is intersecting with the rotor hub in x-y plane in body-fixed frame, whereas platform center of gravity is 40 cm below the rotor hub.

Table 3.1 Reference helicopter's specifications.

MTOW	160 kg
Payload	40 kg
Length	2.07 m
Width	0.78 m
Height	1.22 m
CG Position w.r.t Rotor Hub in x-Body Axis	~0 m
CG Position w.r.t Rotor Hub in y-Body Axis	~0 m
CG Position w.r.t Rotor Hub in z-Body Axis	0.4 m
Max Speed	125 km/h

3.1 Reference Helicopter's Fuselage Aerodynamic Properties

In this work, fuselage of the helicopter is considered as a blunt body. Therefore, the fuselage will create some aerodynamic loads during forward flight. These aerodynamic loads are assumed to be as:

$$D = \frac{1}{2}\rho V^2 F_A C_{D,F}\alpha \tag{3.1}$$

$$M_{YF} = \frac{1}{2}\rho V^2 F_A F_L C_{M,F}\alpha \tag{3.2}$$

where ρ is the air density, V is the helicopter's forward flight speed, F_A and F_L are the aerodynamic effective area and aerodynamic effective length respectively, α is the angle of attack of the fuselage, $C_{D,F}$ and $C_{M,F}$ are non-dimensional aerodynamic drag and pitching moment coefficients respectively which are given w.r.t the angle of attack in Figure 3.1.

In this work, it is assumed that platform does not experience any side-slip angle and aerodynamic lateral force and rolling moment of the fuselage are assumed to be zero at zero side-slip angle. Another important assumption made in this work is that fuselage creates neither aerodynamic force nor aerodynamic yawing moment in z-axis in body-fixed frame.

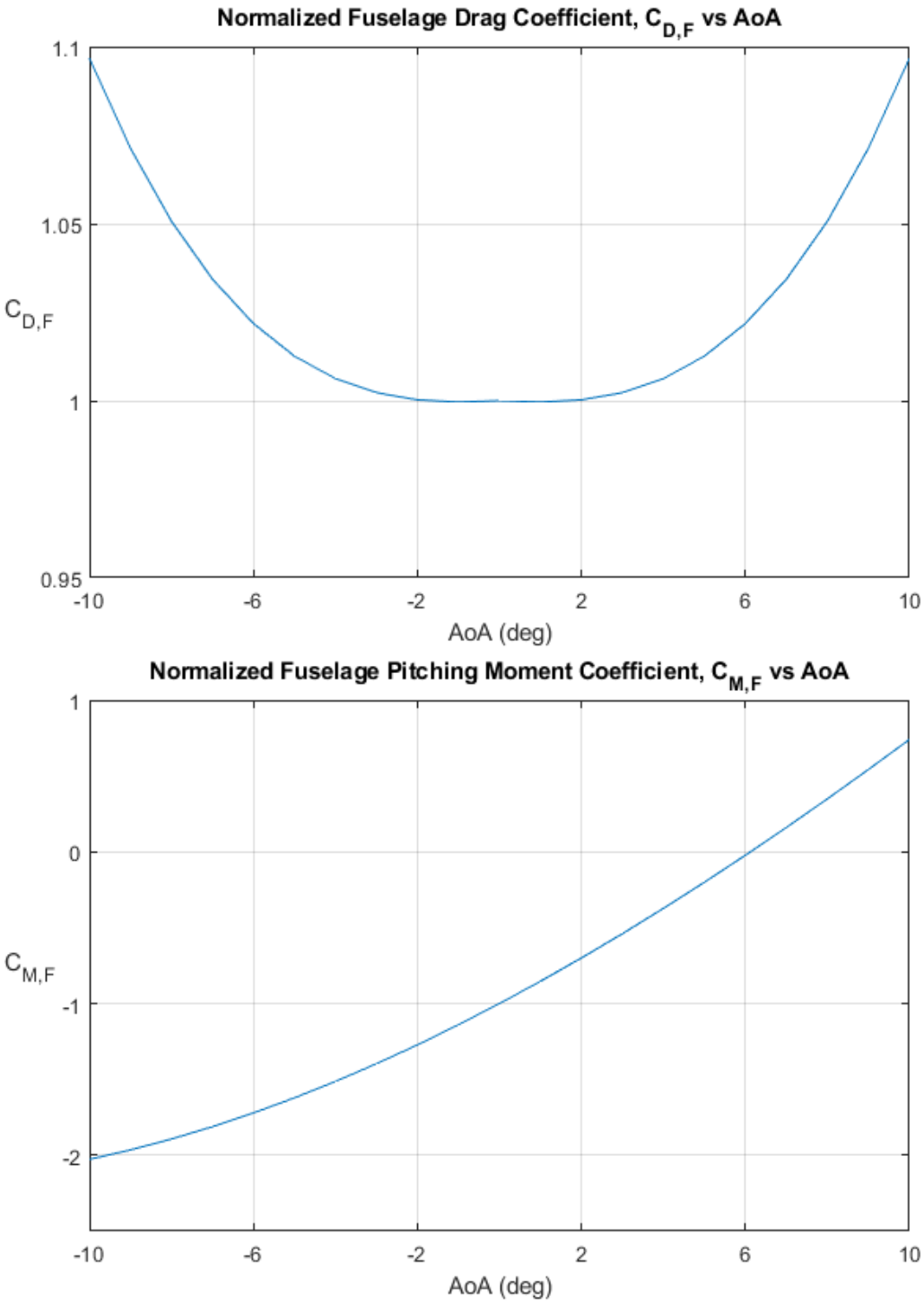

Figure 3.1. Normalized fuselage drag and pitching moment coefficients versus angle of attack of the fuselage.

3.2 Rotor and Blade Properties

Rotor configuration of the reference helicopter is chosen as hingeless. As it is discussed in Section 1, hingeless rotor configurations are mechanically simple. Therefore, hingeless rotors are preferred in most unmanned helicopters such as ASELSAN ARI-1T, Schiebel CAMCOMPTER® S-100, Skeldar V-200 and Anduril Ghost.

The rotor has two blades. Blades have a span of 2 m from the rotor hub. No taper or design twist exists in the blades. First 20 cm of the blade is used for the connection to the hub and pitch links. It is assumed that the connection between rotor hub and the blade is passing through the shear center of the blade.

Airfoil of the blades are chosen as NACA 0012 having a 9 cm chord. Blades are made of aluminum and the structure of the blades are designed as **D-section type**. In D-section structures, the spar and the leading edge is thicker than the trailing edge part since most of the loads are going to be carried by the D-shaped structure. Leading edge's thickness could be as low as one tenth of the thickness of the D-shape.

There is a non-structural mass in the blades installed at about 5 mm behind of the leading edge. There are two main purposes of this non-structural mass. First one is to make the center of gravity of the blades closer to the shear center so that flutter speed is increased. Second one is to increase the out-of-plane bending stiffness of the blades. In helicopter blades, out-of-plane bending stiffness mainly comes from the centrifugal forces due to the rotation of the rotor; therefore, as the mass per unit length increases, blades will be stiffer in out-of-plane bending direction. However, as the centrifugal force increases axial loading at the root will increase as well. Therefore, an optimum mass should be chosen to increase the out-of-plane bending stiffness, whereas staying in the axial load safety limit. Another crucial point regarding the non-structural mass is that since this mass cannot carry any load, it is a deadload. Therefore, not to increase the weight of the blade unnecessarily, mass

of the non-structural should be chosen carefully. A blade design without any additional non-structural mass is more favorable if it could be achieved in the structural design stage.

Table 3.2 Rotor and blade properties.

Number of Blades	2
Rotor Radius, R	2 m
Rotor Speed, Ω	1100 RPM
Rotor Design	Hingeless
Airfoil	NACA 0012
Blade Chord, c	9 cm
CG from the LE	2.46 cm
Shear Center from the LE	2.22 cm
Young's Modulus, E	69 GPa
Shear Modulus, G	26.5 GPa
Torsional Constant, J	1.54×10^{-8} m^4
Density, ρ_{AL}	2700 kg/m^3
Blade Mass, m	~1 kg
Material	Aluminum
Skin thickness,	1 mm to 1.5 mm in D section ~0.1 mm in TE section.
Blade-Hub Connection Length	20 cm
Blade-Hub Connection Material	Stainless Steel

3.2.1 Fan Plot (Campbell Diagram) of the Reference Blade

Due to the centrifugal forces acting on the helicopter blade, stiffness of the blade becomes a function of the rotor speed. Since stiffness changes with the rotor speed, natural frequencies of the blade changes with the rotor speed as well. Fan plot or Campbell Diagram shows how natural frequencies of the blade change with the rotor speed. In Figure 3.2, natural frequencies of the reference blade w.r.t rotational speed are given. These natural frequencies are obtained by using MSC Nastran structural analysis tool.

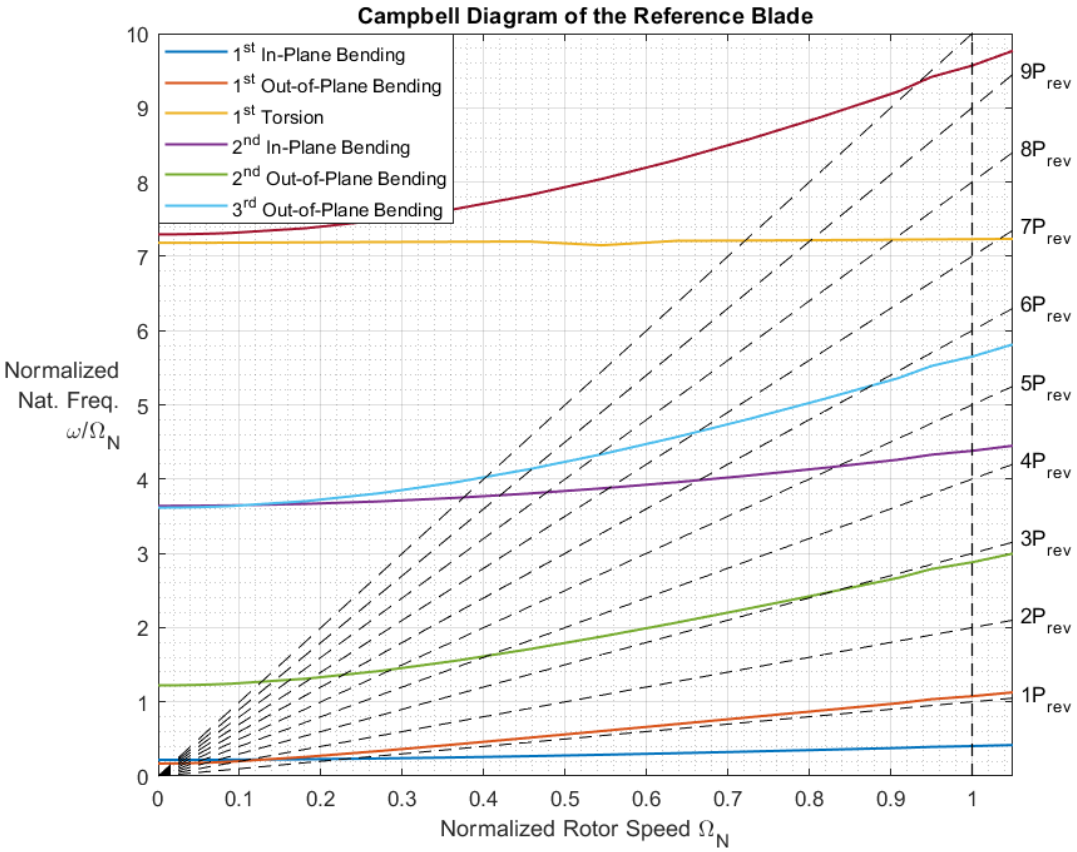

Figure 3.2. Fan plot (Campbell Diagram) of the reference blade.

Dashed lines in Figure 3.2 are called as **N per revolution** lines. "N" is the integer multiply of the nominal rotor speed. For example, $2P_{rev}$ means that the frequency of a state or a loading is 2Ω.

Table 3.3 Reference blade's natural frequencies with rotor speed.

Mode / **RPM**	**1st In-Plane Bending** *(rad/s)*	**1st Out-of-Plane Bending** *(rad/s)*	**2nd Out-of-Plane Bending** *(rad/s)*	**2nd In-Plane Bending** *(rad/s)*	**3rd Out-of-Plane Bending** *(rad/s)*	**1st Torsion** *(rad/s)*	**4th Out-of-Plane Bending** *(rad/s)*
0	25.2	19.5	140.7	419.2	416.5	827.2	840.4
25	25.2	19.7	140.9	419.2	416.6	827.2	840.5
50	25.2	20.3	141.4	419.4	417.1	827.2	840.9
75	25.3	21.2	142.3	419.6	417.9	827.4	841.6
100	25.4	22.5	143.4	420.0	419.0	827.5	842.7
200	26.2	29.8	151.1	422.3	426.6	828.0	849.9
300	27.4	39.0	163.1	426.2	438.9	828.5	862.2
400	29.0	49.0	178.6	431.5	455.4	828.9	879.3
500	30.9	59.4	196.6	438.3	475.8	829.3	900.9
600	33.1	69.9	216.6	446.4	499.4	823.5	926.5
700	35.5	80.6	238.0	455.8	525.8	830.3	955.8
800	38.1	91.4	260.4	466.4	554.5	830.8	988.4
900	40.8	102.2	283.7	478.2	585.1	831.5	1023.8
1000	43.7	113.1	307.5	490.9	617.3	832.1	1061.9
1045	45.3	119.2	321.3	498.6	636.2	832.6	1084.6
1100	**46.6**	**123.9**	**331.7**	**504.6**	**650.8**	**833.0**	**1102.1**
1155	48.2	129.9	345.3	512.5	669.7	833.4	1125.1

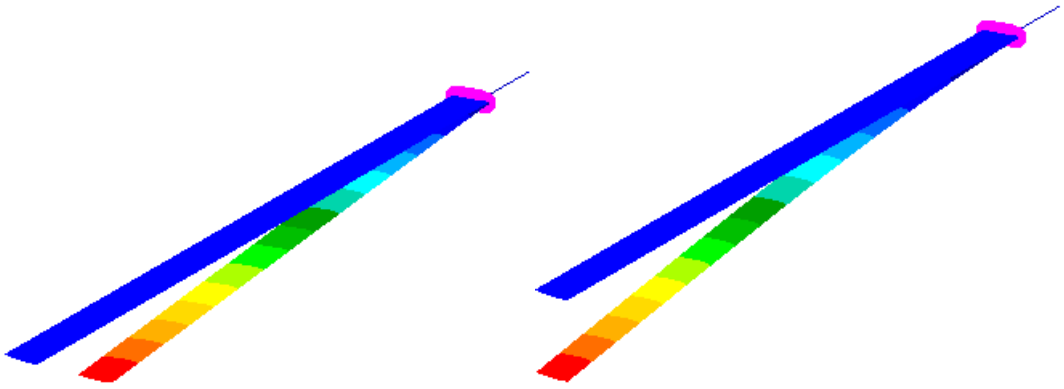

a) First in-plane bending mode, b) First out-of-plane bending mode,

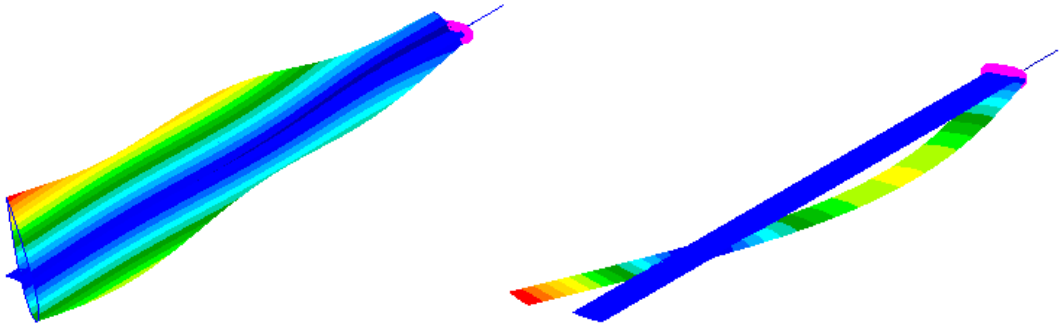

c) First torsion mode, d) Second in-plane bending mode,

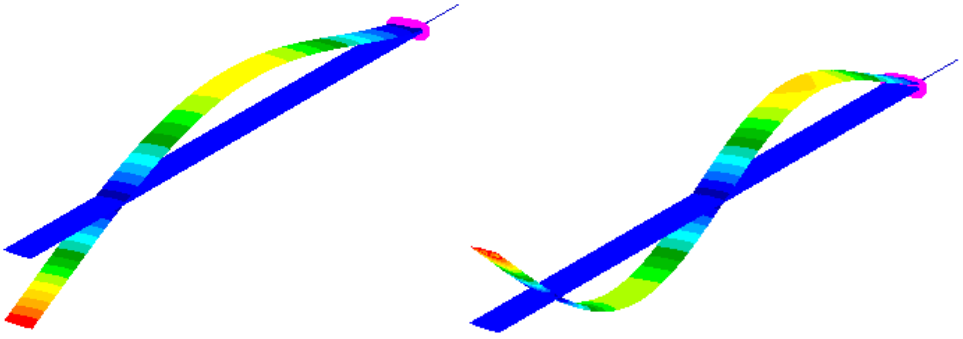

e) Second out-of-plane bending mode, f) Third out-of-plane bending mode,

Figure 3.3. Mode shapes of the reference blade.

For the helicopter blades, frequencies of the blade pitch control are integer multiply of the rotor rotational speed which will be discussed in detail in Section 4.9. Since the loads of the blades are controlled by the cyclic controls, blades are excited at the frequency of rotor rotational speed or its integer multiply. Therefore, any N per revolution lines should not intersect any natural frequency of the blade at the rotor's operational speed to prevent any structural fail. Therefore, fan plot is a useful graph to observe whether any period of the loads acting on the blade will intersect with any natural frequency of the blade. When Figure 3.2 is inspected, it is seen that none of the natural frequencies intersect with any integer multiply of the rotor speed.

Another point which should be emphasized regarding Figure 3.2 is that first out-of-plane bending natural frequency is mostly dominated by the rotor speed due to the centrifugal stiffening effect. Hence, rotor rotational speed could be used to express the structural stiffness of the blade in the out-of-plane bending direction during the rotation.

3.2.2 Reference Blade's Aerodynamic Coefficients

Reference blade's airfoil is chosen as NACA0012 airfoil. Non-dimensional lift and drag coefficients c_l and c_d are given in [16] as:

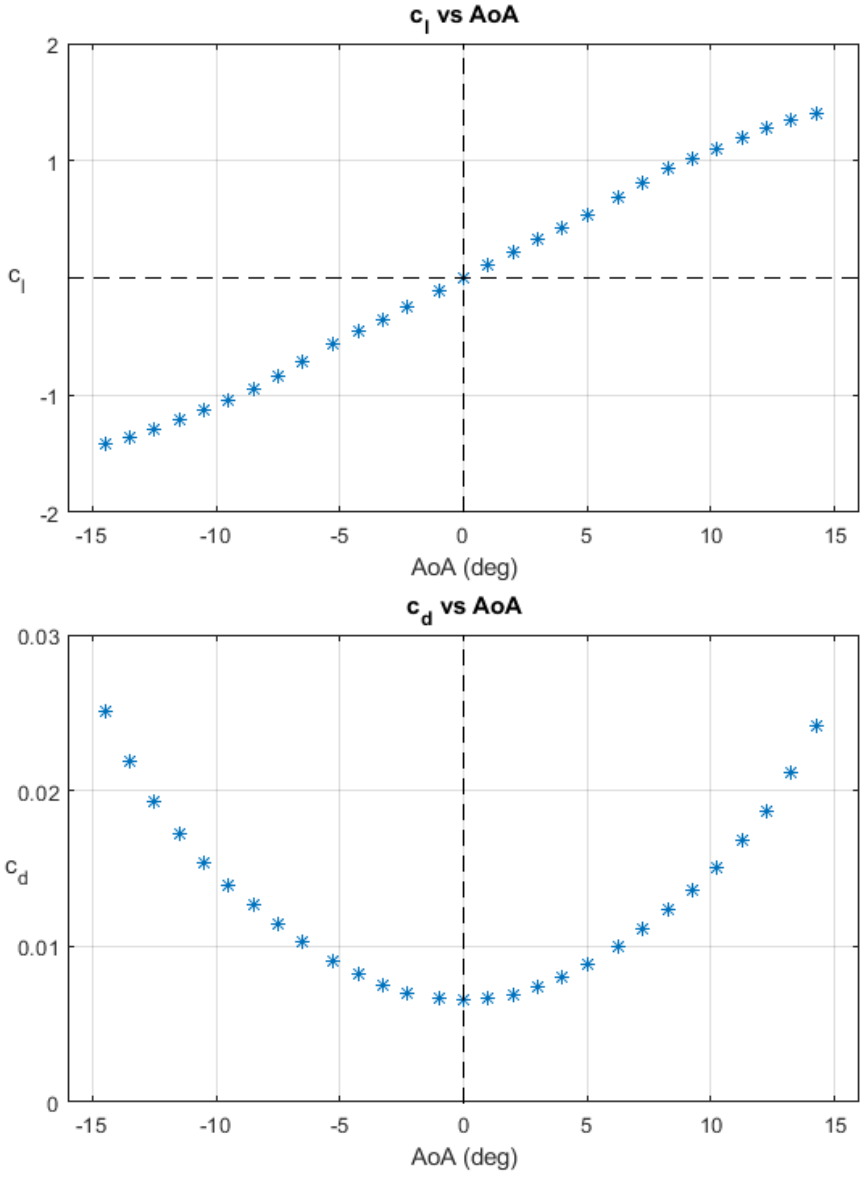

Figure 3.4. Non-dimensional lift and drag coefficient.

As it could be observed from Figure 3.4, c_l has a linear behavior, c_d has a second order polynomial behavior. Therefore, as [19] suggests c_l and c_d could be approximated as:

$$c_l = c_{l_\alpha}\alpha \tag{3.3}$$

$$c_d = c_{d_0} + c_{d_{\alpha^2}}\alpha^2 \tag{3.4}$$

where $c_{l_\alpha} = 5.98$, $c_{d_0} = 0.006533$, $c_{d_{\alpha^2}} = 0.2783$ for the NACA0012 airfoil.

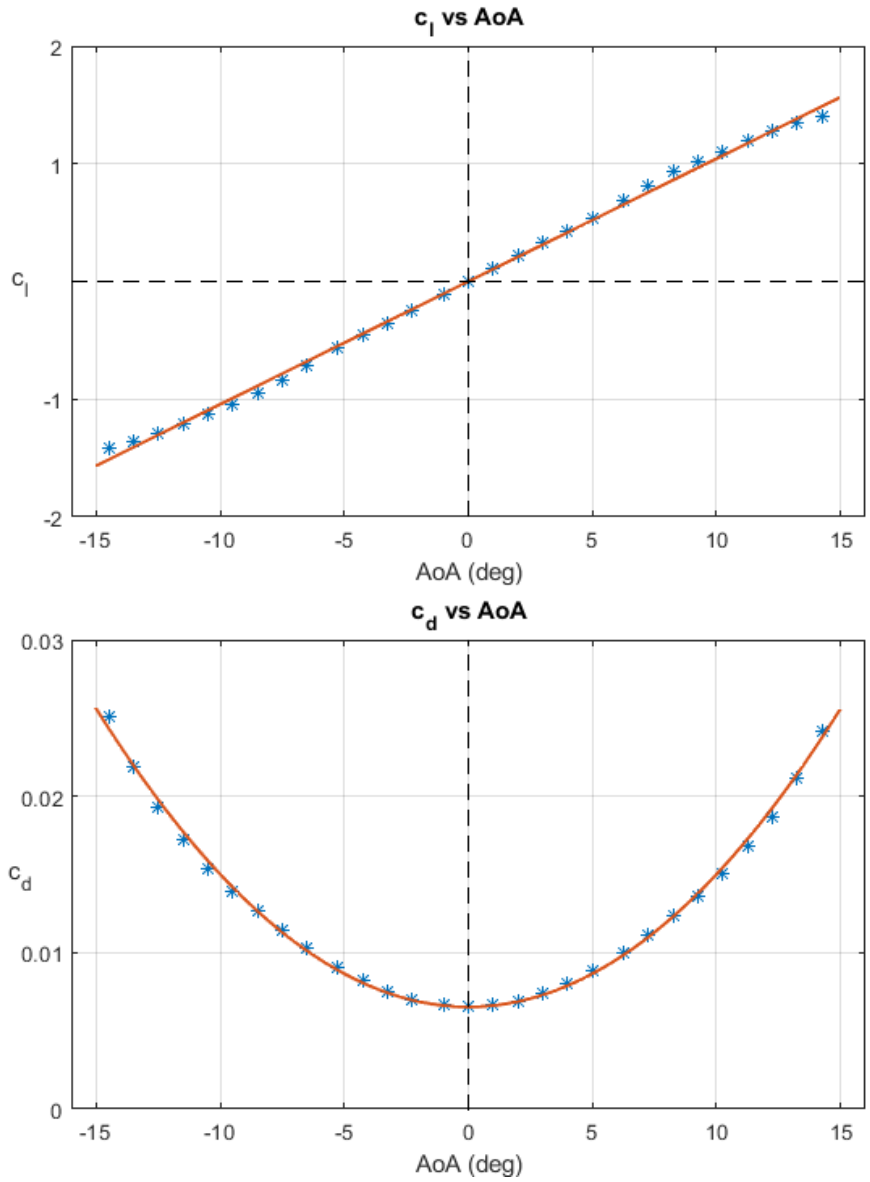

Figure 3.5. Comparison of approximated c_l and c_d values to Ref. [16].

Let us look at the ratio of the c_l to c_d.

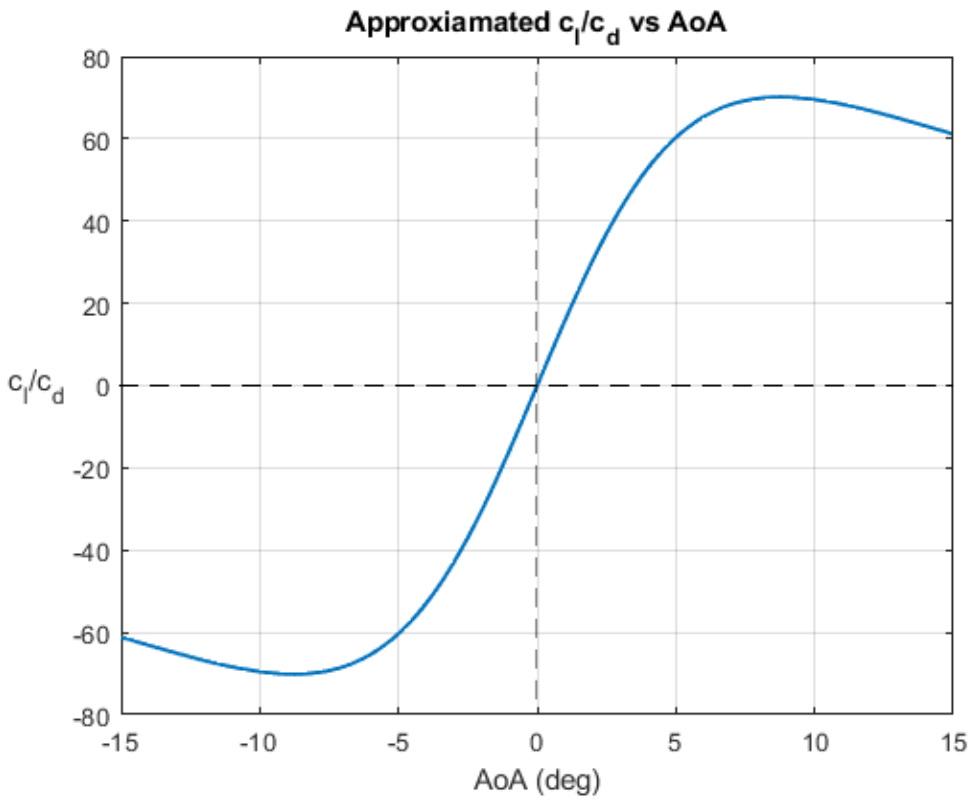

Figure 3.6. Ratio of the approximated c_l to c_d.

From Figure 3.6, it is seen that c_l to c_d ratio reaches about 70 in the operating range of the reference helicopter. Therefore, drag effects in the thrust calculation could be neglected since the drag effect in the thrust would be negligible.

Note that NACA 0012 airfoil is a symmetric airfoil; thus, it is assumed that its non-dimensional aerodynamic pitching moment coefficient c_m is zero.

CHAPTER 4

STATIC AEROELASTICITY

Static aeroelasticity is a brand of the aeroelasticity in which main concern is the interaction between the structure and the aerodynamic loads. In this section, aerodynamic forces, and their relations with the blade in terms of static aeroelasticity will be discussed.

4.1 Momentum Theory

Helicopter rotor produces a thrust by the air's interaction with the blades. According to the Newton's Law there must be an equal reaction of the rotor. Consequently, velocity of the air in the rotor wake increases in the opposite direction of the rotor thrust. Momentum theory studies the relation between the rotor thrust and the air velocity in the wake.

Momentum theory was firstly studied by W.J.M Rankine 1865 and R.E Froude in 1885 to examine marine propellers [12]. Momentum theory estimates the rotor performance by applying basic laws (mass, momentum, and energy conservation laws) of fluid motion to the rotor and the flow. The theory is an overall approach which directly connects the rotor thrust and power to the inflow velocity.

In momentum theory, helicopter rotor is assumed as a circular disk whose thickness is zero and the rotor can support the pressure difference between upper and lower surface. Let us assume a rotor disk whose area is A produces a uniformly distributed thrust T in an incompressible and inviscid air environment.

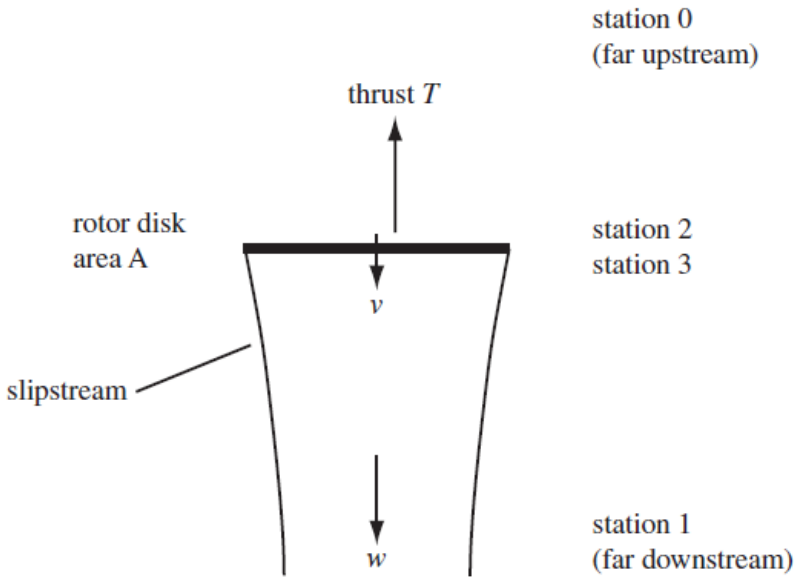

Figure 4.1. Flow of the rotor according to momentum theory in hover. [12]

The mass flux passing through the rotor is $\dot{m} = \rho A v$. According to the momentum conservation law, the rotor thrust must be equal to the rate of change of linear momentum of the air between station 0 (far upstream) and station 1 (far downstream). Since swirl in the wake is neglected, air velocity is zero at station 0 for a hovering rotor which results $T = \dot{m} w$. By using energy conservation law, rate of change of energy of the air must be equal to the work done by the rotor. Rate of change of energy of the air is the difference between station 0 where the air is at rest and station 1 in which the air has a velocity w. Therefore, work done by the rotor could be expressed as $Tv = \frac{1}{2}\dot{m} w^2$. It could be easily showed that $w = 2v$ by combining energy conservation law and momentum conservation law. Since the mass flux and the density assumed to be constant, the area of the slipstream at station 1 is found as $\frac{1}{2}A$.

To find the thrust, Bernoulli's equation could be used between the stations 0 and 2 (just above of the rotor disk), 1 and 3 (just below of the rotor disk). From the station 0 and station 2, Bernoulli's relation states that $p_0 = p_2 + \frac{1}{2}\rho v^2$. From the station 1 to the station 3 Bernoulli's principle gives $p_3 + \frac{1}{2}\rho v^2 = p_0 + \frac{1}{2}\rho w^2$.

When these two equations are combined, it is found that $T/A = p_3 - p_2 = \frac{1}{2}\rho w^2$ from which inflow could be written as:

$$v_i = \sqrt{T/2\rho A} \tag{4.1}$$

After founding induced velocity in Eq. (4.1), total power could be found from the relation:

$$P = Tv = T\sqrt{T/2\rho A} \tag{4.2}$$

Let us define some non-dimensional parameters in terms of induced velocity, thrust and induced power by using blade tip speed ΩR.

$$C_T = T/\rho A(\Omega R)^2 \tag{4.3}$$

$$\lambda_i = \frac{v_i}{\Omega R} = \sqrt{C_T/2} \tag{4.4}$$

$$C_P = C_T^{3/2}/\sqrt{2} \tag{4.5}$$

These equations are valid for the condition where the rotor is hovering in the air. Now let us examine the case where the rotor is climbing in the air by making same assumptions as made in hovering case: rotor is modeled as disk, thrust is uniformly distributed over the rotor, induced velocity is uniform, slipstream is smooth, fluid is ideal and swirl in the wake is neglected.

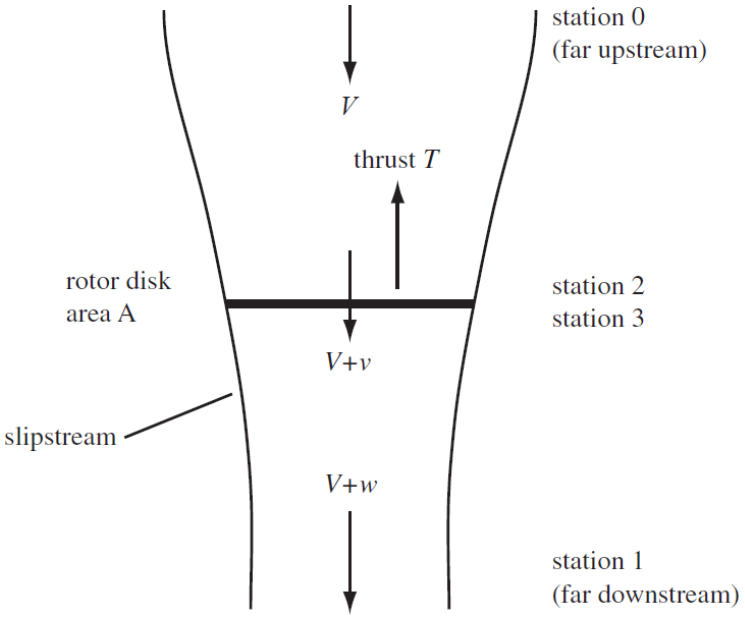

Figure 4.2. Flow of the rotor according to momentum theory in climbing. [12]

Mass flux passing through the rotor is now $\dot{m} = \rho A(V + v)$. Where V is the climb velocity. By applying energy and momentum conservation laws between the stations 0 and 1, $T(V + v) = \frac{1}{2}\dot{m}(V + w)^2 - \frac{1}{2}\dot{m}V^2$ and thrust is found as $T = \dot{m}(V + w) - \dot{m}V$. When these two equations are combined, it is found that $w = 2v$ as in the hover case. However, if the Bernoulli's principle is applied between the stations 0 and 1, $p_0 + \frac{1}{2}\rho(V + w)^2 = p_0 + \frac{1}{2}\rho V^2 + T/A$. When the equation is simplified, it is found that $T/A = \frac{1}{2}\rho(2Vw + w^2)$. Since it is showed that $w = 2v$, thrust could be expressed as $T = 2\rho A(V + v)v$. If Eq. (4.1) is used, the relation between induced inflow and the climb velocity could be shown as:

$$v(V + v) = v_i^2 \tag{4.6}$$

The solution of Eq. (4.6) w.r.t the total inflow v is:

$$v = -\frac{V}{2} + \sqrt{\left(\frac{V}{2}\right)^2 + v_i^2} \tag{4.7}$$

Total power relation in the climb condition could be found as:

$$P = T(V + v) = T\left(\frac{V}{2} + \sqrt{\left(\frac{V}{2}\right)^2 + v_i^2}\right) \tag{4.8}$$

Note that induced inflow is assumed to be uniform on the rotor and swirl effects in the air flow are neglected.

4.2 Momentum Theory in Forward Flight

Glauert introduced a momentum theory analysis for rotors in forward flight by combining inflow and forward flight speed. [11]

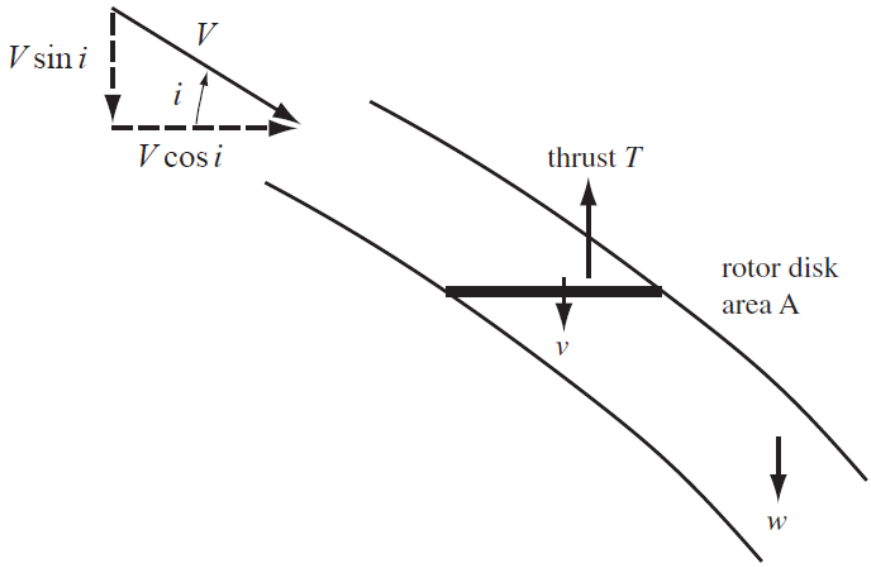

Figure 4.3. Glauert inflow model for forward flight. [12]

According to momentum conservation law, rotor thrust is expressed as $T = \dot{m}2v$ where the mass flux $\dot{m} = \rho AU$. U is the resultant velocity of air passing the rotor disk and U is given as:

$$U^2 = (V\,cos\,i)^2 + (V\,sin\,i + v)^2 = V^2 + 2Vv\,sin\,i + v^2 \tag{4.9}$$

By combining Eq. (4.9) with thrust and mass flux equalities, rotor thrust is obtained as:

$$T = 2\rho A v U = 2\rho A v\sqrt{V^2 + 2Vv\,sin\,i + v^2} \tag{4.10}$$

From the relation given in Eq. (4.8), rotor power for forward flight is found as:

$$P = T(V\,sin\,i + v) \tag{4.11}$$

To express velocity components which are parallel and normal to the rotor disk, let us define two non-dimensional parameters: advance ratio μ and inflow ratio λ which are expressed as:

$$\mu = \frac{V\,cos\,i}{\Omega R} \tag{4.12}$$

$$\lambda = \frac{V\,sin\,i + v_i}{\Omega R} = \mu\,sin\,i + \lambda_i = \mu_z + \lambda_i \tag{4.13}$$

By using Eq's. (4.3) and (4.10), non-dimensional induced inflow ratio could be found as:

$$\lambda_i = \frac{C_T}{2\sqrt{\mu^2 + \lambda^2}} \tag{4.14}$$

Eq. (4.14) is called as **Glauert Inflow Formula**. Although the equation is a fourth order polynomial equation, a Newton-Raphson solution could be implemented for inflow ratio λ [11]:

$$(\lambda_i)_n = \frac{C_T}{2\sqrt{\mu^2 + (\lambda^2)_n}} \tag{4.15}$$

$$(\lambda)_{n+1} = (\lambda)_n - \frac{(\lambda)_n - \mu_z - (\lambda_i)_n}{1 + (\lambda_i)_n(\lambda)_n/((\lambda^2)_n + \mu^2)}f \tag{4.16}$$

f is the relaxation factor, and it could be taken as 0.5. Less than five iterations are usually enough to converge from the starting point:

$$(\lambda)_1 = \frac{\lambda_h^2}{\sqrt{\mu^2 + (\lambda_h + \mu_z)^2}} + \mu_z \tag{4.17}$$

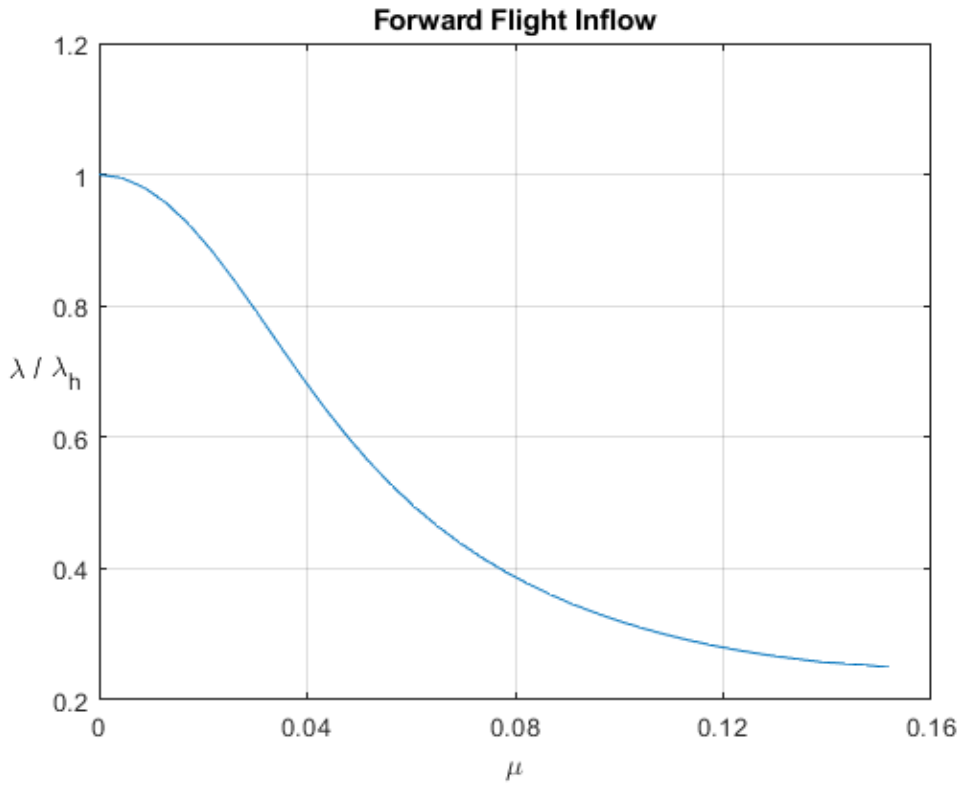

Figure 4.4. Non-dimensional induced inflow ratio in trimmed forward flight.

As it could be observed from Figure 4.4, total inflow could decrease up to ~%80 w.r.t hover as the forward flight speed increases in a trimmed flight. From Eq. (4.11), it could be stated that if the thrust is constant, a decrease in induced inflow would decrease the induced power since induced power is related to the thrust and magnitude of the inflow.

4.3 Blade Element Theory

Blade Element Theory is a lifting-line-based theory. To apply blade element theory on a wing, wing's aspect ratio should be high. [11] Since most of the helicopter blades have high aspect ratio, blade element theory could be thought as the foundation of most of helicopter aerodynamic analyses.

In blade element theory, each finite length section of the blade is considered as an individual two-dimensional airfoil. Therefore, most of the design parameters of the

blade such as span or radius, chord, airfoil shape etc. are dealt with in detail in the blade element theory. Whereas momentum theory is stated to be an overall system analysis which could give useful information; however, a more detailed analysis is essential to design and analyze a rotor.

According to [12], there were two main lines in the early development stages of the rotary-wing theories. First one was the momentum theory, second one was the blade element theory. In the 1920s, these two theories were combined.

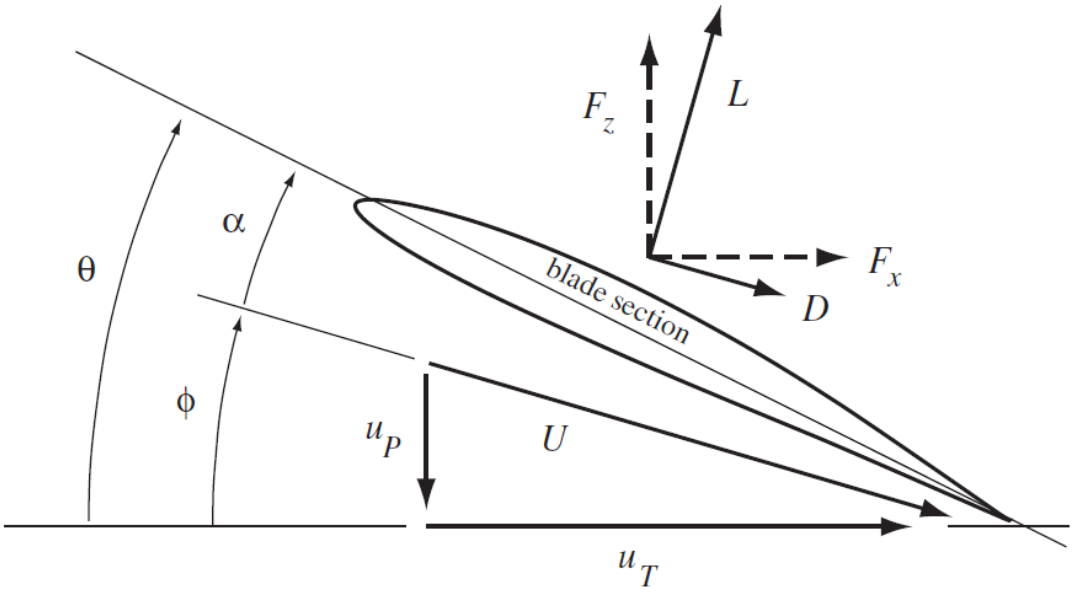

Figure 4.5. Blade section aerodynamics in hover. [12]

In Figure 4.5, air velocities, aerodynamic forces and incidences are shown for a blade section. θ is the pitch angle of the section. Total air velocity experienced by the section is denoted as U which has two components u_T and u_P. u_T is the tangential velocity component in the parallel direction to the disk plane. Whereas u_P is the axial velocity which is in the normal direction to the disk plane.

$$u_T = \Omega r \tag{4.18}$$

$$u_P = v \tag{4.19}$$

$$U = \sqrt{u_T^2 + u_p^2} \cong u_T \tag{4.20}$$

Since $u_T \gg u_P$, resultant velocity U could be approximated as u_T. Let us define the inflow angle:

$$\phi = tan^{-1}\left(\frac{u_P}{u_T}\right) \cong \frac{u_P}{u_T} \tag{4.21}$$

α is the angle of attack of the blade section and it is defined as the difference between pitch angle of the blade θ and inflow angle ϕ.

$$\alpha = \theta - \phi \tag{4.22}$$

Blade section produces aerodynamic lift and drag which are in the direction to the normal and parallel to the resultant airflow velocity, respectively. Sectional lift and drag force for a thin airfoil are given as:

$$L' = \frac{1}{2}\rho U^2 c c_l = \frac{1}{2}\rho U^2 c c_{l_\alpha}(\theta - \phi) \tag{4.23}$$

$$D' = \frac{1}{2}\rho U^2 c c_d = \frac{1}{2}\rho U^2 c\left(c_{d_0} + c_{d_{\alpha^2}}(\theta - \phi)^2\right) \tag{4.24}$$

ρ is the air density, c is the chord of the blade. c_{l_α}, c_{d_0} and $c_{d_{\alpha^2}}$ are non-dimensional lift curve slope, zero-lift and second order drag coefficients, respectively. If the aerodynamic forces in Figure 4.5 are resolved in the directions normal and parallel to the disk plane, resolved forces will be:

$$F_z = L' cos\,\phi - D' sin\,\phi \cong L' \tag{4.25}$$

$$F_x = L' sin\,\phi + D' cos\,\phi \cong L'\phi + D' \tag{4.26}$$

Hence, total thrust, torque and profile power of the rotor could be found as:

$$T = N_b \int F_z dr \tag{4.27}$$

$$Q = N_b \int F_x r dr \tag{4.28}$$

$$P_o = \Omega Q = \Omega N_b \int F_x r dr \tag{4.29}$$

where N_b is the number of blades of the rotor.

In Blade Element Theory, every blade element has a finite length. Therefore, integrals, infinitesimal lengths and radial locations in Eq's. (4.27), (4.28) and (4.29) could be replaced with summation symbol, length of the blade elements and radial location of the blade elements respectively:

$$T = N_b \sum_{n=1}^{n=N_{bem}} (F_z)_n \, \Delta r \tag{4.30}$$

$$Q = N_b \sum_{n=1}^{n=N_{bem}} (F_x)_n r_n \, \Delta r \tag{4.31}$$

$$P_o = \Omega Q = \Omega N_b \sum_{n=1}^{n=N_{bem}} (F_x)_n r_n \Delta r \tag{4.32}$$

where Δr is the blade element length and it is given as R/N_{bem}.

4.3.1 Blade Element Number

To be able to calculate rotor thrust, torque and required power adequately, sufficient number of blade element must be chosen. To observe how blade element number affects the calculated thrust for the reference blade, Figure 4.6 is drawn.

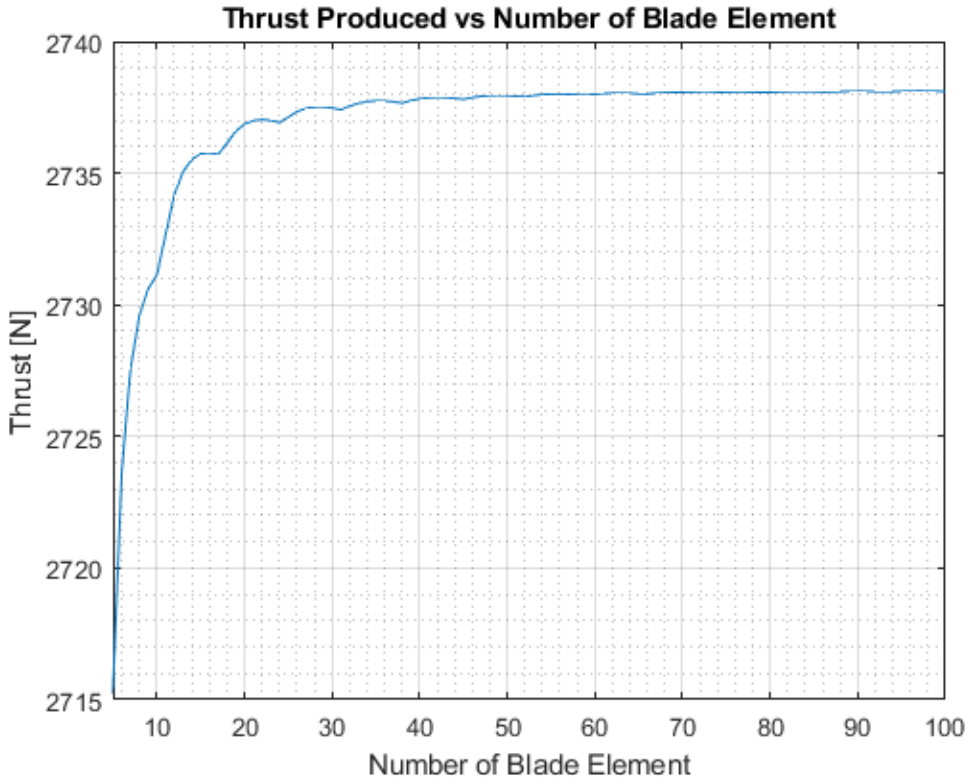

Figure 4.6. Calculated thrust versus the number of blade element.

From Figure 4.6, it could be observed that even 5 elements could represent the thrust sufficiently since the thrust calculated between 5 number of blade elements and 100 number of blade element deviates only about %0.84. However, to not lose any information and according to the suggestion of [14], 40 blade elements are chosen.

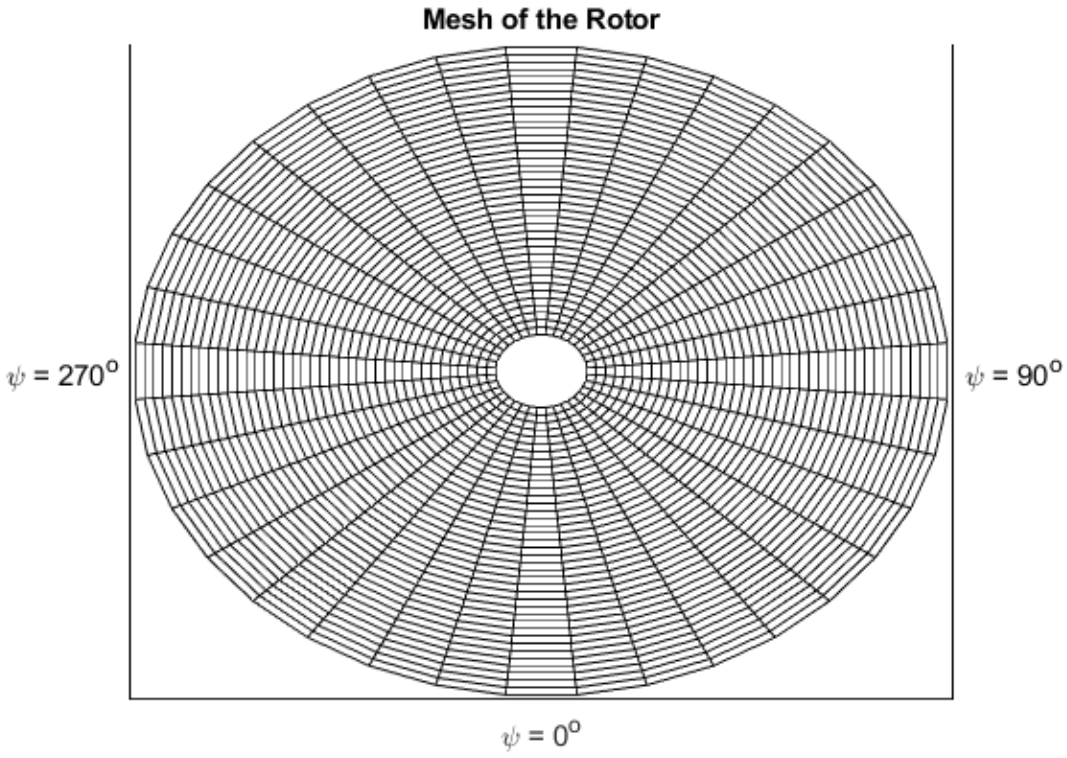

Figure 4.7. Blade elements and azimuth steps of the rotor (40 elements, 10° azimuth steps).

4.4 Aerodynamic Root Cutout

Due to the low tangential velocity, inner section of the blade experiences a low dynamic pressure resulting low aerodynamic forces. Therefore, this portion of the blade is neglected in terms of aerodynamic effects. Neglected portion of the blade is called as **aerodynamic root cutout** or **root cutout**. Root cutout is shown as r_R and generally taken as between 10% to 30% of the blade span [11]. Performance integrals such as Eq's. (4.27), (4.28) and (4.29) should be taken from r_R to R rather than 0 to R.

$$T = N_b \int_{r_R}^{R} F_z dr \tag{4.33}$$

$$Q = N_b \int_{r_R}^{R} F_x r dr \tag{4.34}$$

$$P = \Omega Q = N_b \Omega \int_{r_R}^{R} F_x r dr \tag{4.35}$$

Since the dynamic pressure is lower in the aerodynamic root cutout region compared to the radially outer sections of the blade, neglecting this portion of the blade has minor effect on performance calculations. Therefore, in Blade Element analysis, Eq.'s (4.30), (4.31) and (4.32) become respectively:

$$T = N_b \sum_{n=1}^{n=N_{bem}} (F_z)_n \tag{4.36}$$

$$Q = N_b \sum_{n=1}^{n=N_{bem}} (F_x)_n r_n \Delta r \tag{4.37}$$

$$P = \Omega Q = \Omega N_b \sum_{n=1}^{n=N_{bem}} (F_x)_n r_n \Delta r \tag{4.38}$$

4.5 Tip Losses

As discussed in Section 4.3, Blade Element Theory is a lifting-line theory. However, blade element theory fails near the blade tip since blade element theory calculates a lift profile through the blade span, whereas actual lift profile drops sharply to the zero near blade tip due to three-dimensional aerodynamic effects. To add tip loss effect in to the thrust, it is assumed that the blade produces no lift but continues having profile drag after radial station BR, where B is called as tip loss factor. If the tip loss effect is not implemented to the calculations, the thrust and

power calculations will be overestimated since dynamic pressure over the blade is proportional to r^2.

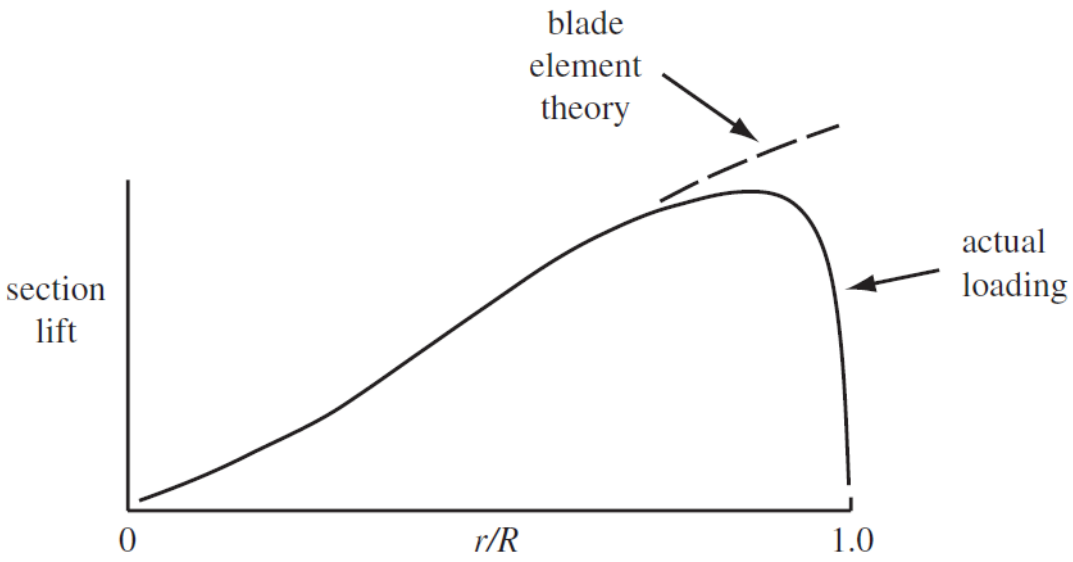

Figure 4.8 Sectional lift profile over the blade span. [12]

If the tip loss factor is included to the thrust integral with aerodynamic root cutout, thrust equation will be:

$$T = N_b \int_{r_R}^{BR} F_z dr \tag{4.39}$$

If Eq. (4.38) is re-written by using blade element analysis:

$$T = N_b \sum_{n=1}^{n=N_{bem}} (F_z)_n \tag{4.40}$$

In this work, root cutout is taken as %20. In blade element analysis, first 5 blade elements of the rotor mesh in Figure 4.7 do not create any aerodynamic force. Therefore, in Eq's. (4.37), (4.38) and (4.40) the summation should start from 6th element for the reference blade. Whereas tip loss effect B could be taken as between 0.95 and 0.98 according to Leishman [14]. In this work, B is taken as 0.97 which corresponds the last element of the rotor mesh. Hence, in Eq. (4.40) the summation should end at 39th element for the reference blade.

4.6 Blade Element Momentum Theory

To calculate thrust and power of the rotor, Momentum Theory and Blade Element Theory could be combined, and it is called as **Blade Element Momentum Theory.**

According to Blade Element Momentum Theory, lift and drag forces of the airfoil are obtained by using Blade Element Theory, whereas Momentum Theory is used to find inflow which directly effects lift and drag forces since inflow decreases the angle of attack experienced by the airfoil section as showed in Eq's. (4.21) and (4.22).

Since the thrust is affected by the inflow and inflow is related with the thrust, to be able to solve the thrust and the inflow, an iterative solution procedure could be implemented such that:

1. Assume a starting thrust value. Usually, it is wise to start from thrust is equal to total weight of the aircraft.
2. Find the uniform induced inflow according to the thrust value by using Eq. (4.14). (If the forward speed of the helicopter is zero, $\mu = 0$ and $\lambda = \lambda_i$)
3. Insert the inflow found in step-2 in to Eq. (4.40) and calculate new thrust.
4. Return to step-2 until a defined convergence criterion is satisfied such as $\lambda_{err} \geq |\lambda_n - \lambda_{n-1}|$ or $T_{err} \geq |T_n - T_{n-1}|$ where λ_{err} and T_{err} are the error tolerances, n is the iteration step number.

4.7 Helicopter Rotor in Forward Flight

Forward flight analysis needs more concern than hover analysis since helicopter rotor experiences not only rotational speed but also forward velocity in forward flight which creates an unsymmetrical airspeed profile on the rotor.

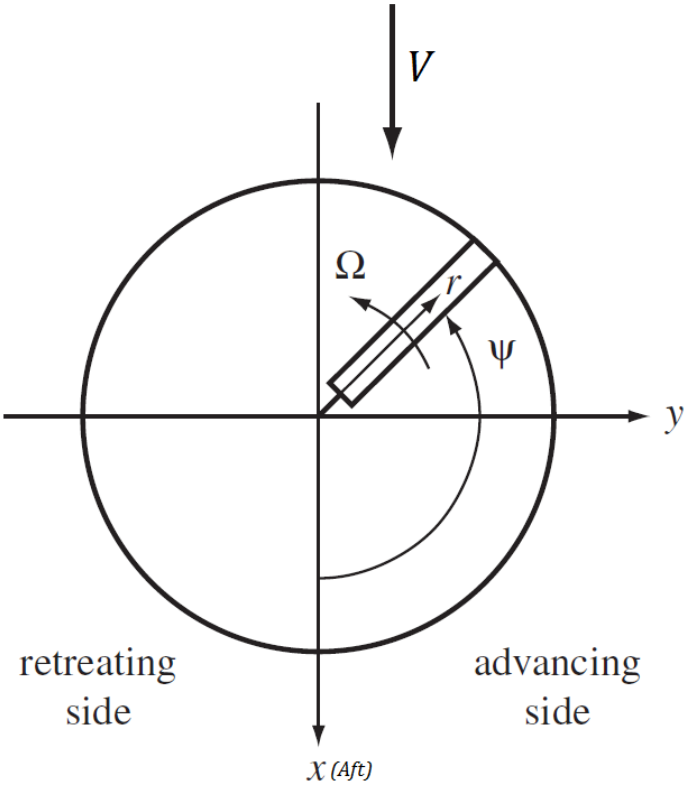

Figure 4.9. Helicopter rotor in forward flight. [12]

In Figure 4.9, it is seen that one side of the rotor is called as **advancing side** since airspeed experienced by the rotor is the summation of the rotational speed and forward speed, whereas the other side is called as **retreating side**. This portion of the rotor is called as retreating since airspeed of this side is the difference of the rotational speed and forward speed. If this difference is negative, there occurs a special region which is called as **reverse flow region**. In reverse flow region, airflow is passing the airfoil not from leading edge to trailing edge but from trailing edge to leading edge. Therefore, special considerations are necessary to obtain aerodynamic loads in this region.

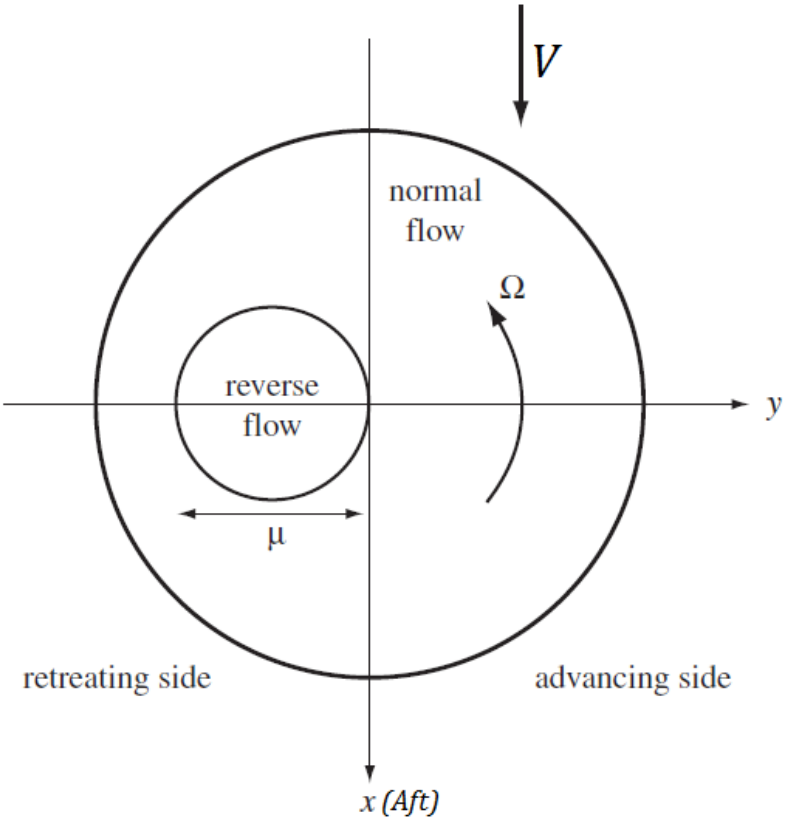

Figure 4.10. Reverse flow region in forward flight. [12]

In Figure 4.10, reverse flow region is illustrated exaggeratedly. The ratio of rotor radius to reverse flow region's diameter is equal to the advance ratio μ. Although reverse flow illustration covers about %70 radius of the rotor in Figure 4.10, its maximum is usually about %40 of the rotor radius since conventional helicopter's maximum advance ratio is about 0.4.

As stated above, serious aerodynamic analyses are needed since the flow characteristics are different from the rest of the rotor in reverse flow region. However, in this work, reference helicopter reaches advance ratio up to 0.15. In the first %10 of the rotor, there is no airfoil. The region between %10 and %20 of the blade lies on the aerodynamic root cutout region in which all aerodynamic forces are neglected. Hence, the reverse flow region is not a concern for this work under the given assumptions.

4.7.1 Experienced Tangential Velocity by the Blade

As discussed in the very beginning of Section 4.7, experienced airspeed by the blade changes with both radial location and azimuth angle ψ. Let us define tangential and radial velocity component for the blade in a rotating frame with the blade:

$$u_T = \Omega r + V \sin\psi \tag{4.41}$$

$$u_R = V \cos\psi \tag{4.42}$$

Tangential velocity distribution over the rotor in forward flight is illustrated in Figure 4.11. Maximum tip speeds of the blade are $\Omega R + V$ and $\Omega R - V$ in the advancing side and in the retreating side respectively.

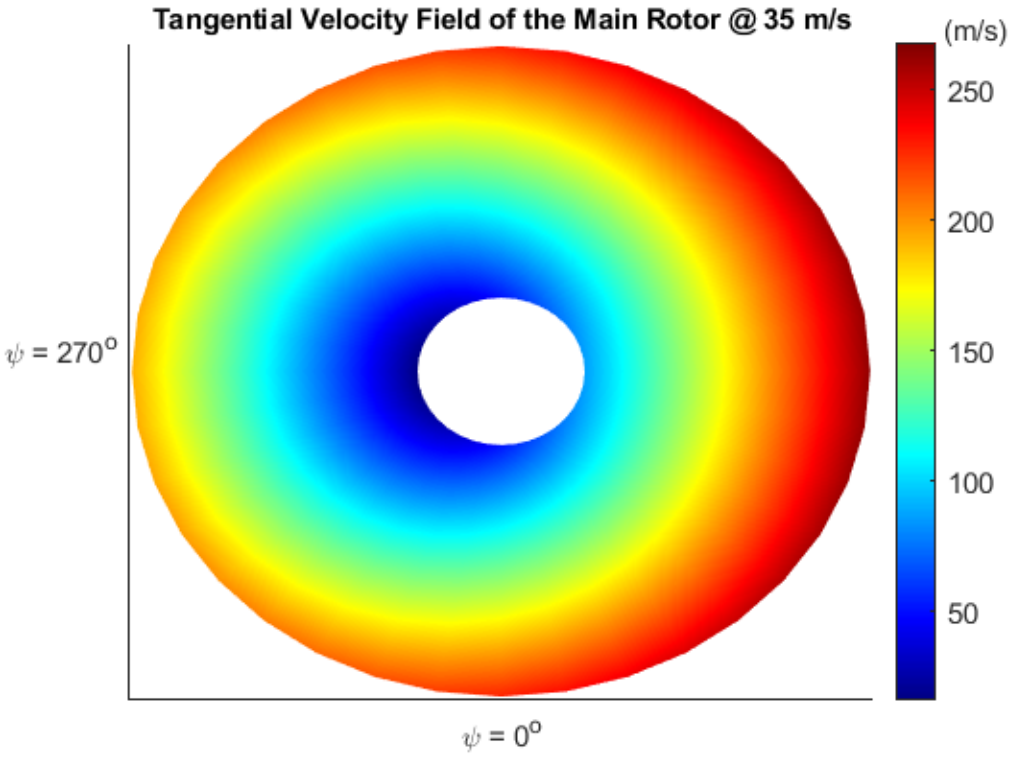

Figure 4.11. Tangential velocity field of the main rotor at 35 m/s.

4.8 Compressibility Corrections

Compressibility effects become more important as Mach Number increases and as it could be seen in Figure 4.12, reference blade's Mach Number reaches almost 0.7 Mach in hover and exceeds 0.75 in maximum forward flight speed; therefore, compressibility effects should be included in the analyses.

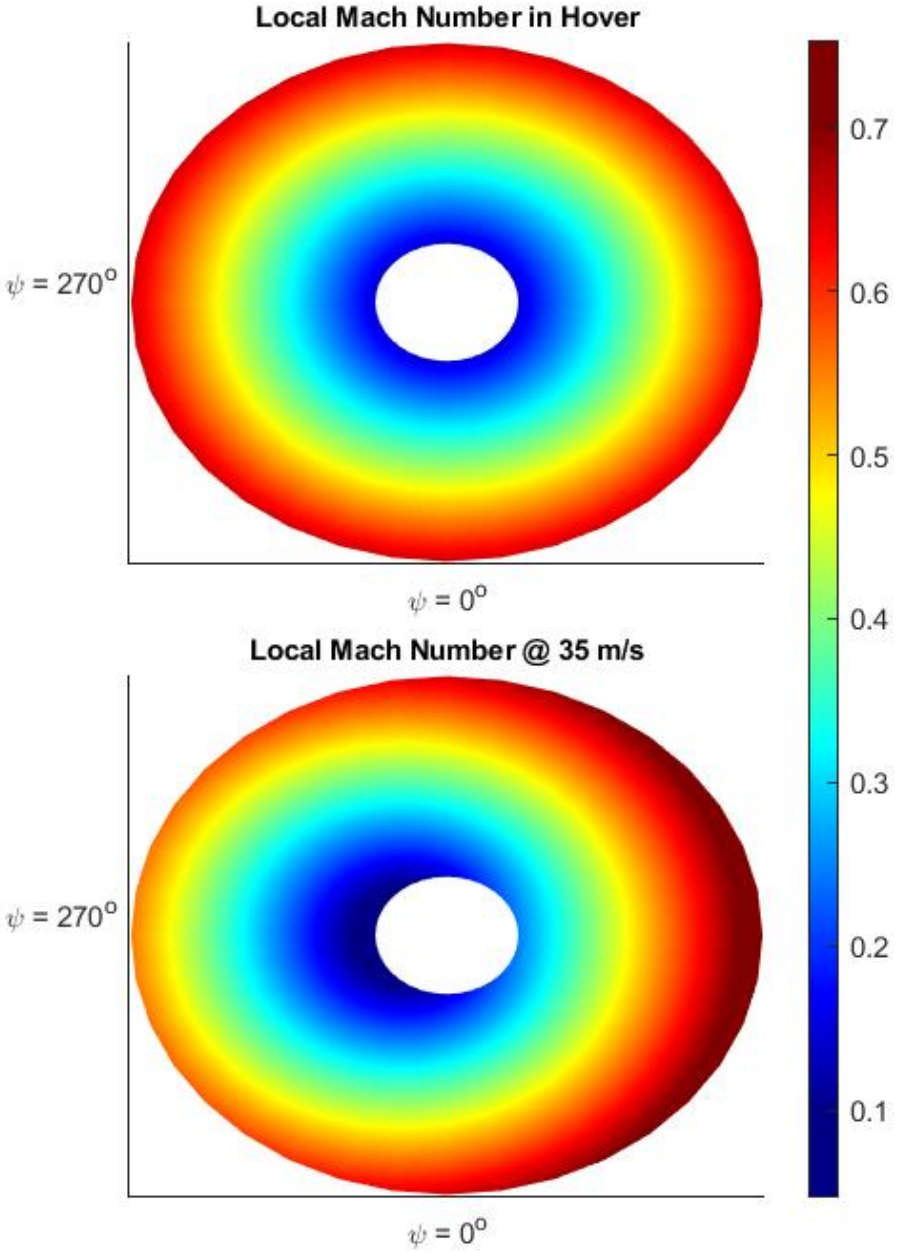

Figure 4.12. Reference blade's local Mach Number in hover and at 35 m/s.

By referring Ref. [1], non-dimensional lift and drag coefficients c_l and c_d could be written in a compressible regime as:

$$c_d = \frac{c_{l_{incomp}}}{\sqrt{1-M^2}} \tag{4.43}$$

$$c_d = \frac{c_{d_{incomp}}}{\sqrt{1-M^2}} \tag{4.44}$$

where $c_{l_{incomp}}$ and $c_{d_{incomp}}$ are the c_l and c_d expressed in Section 3.2.2 and $\frac{1}{\sqrt{1-M^2}}$ is called as compressibility correction factor.

Figure 4.13 shows that the compressibility correction factor could increase up to %30 in hover and %50 in forward flight. In other words, local lift coefficient c_l and local drag coefficient c_d could increase up to %30 in hover and %50 in forward flight. Therefore, compressibility effect must be considered to increase the fidelity of the performance calculations.

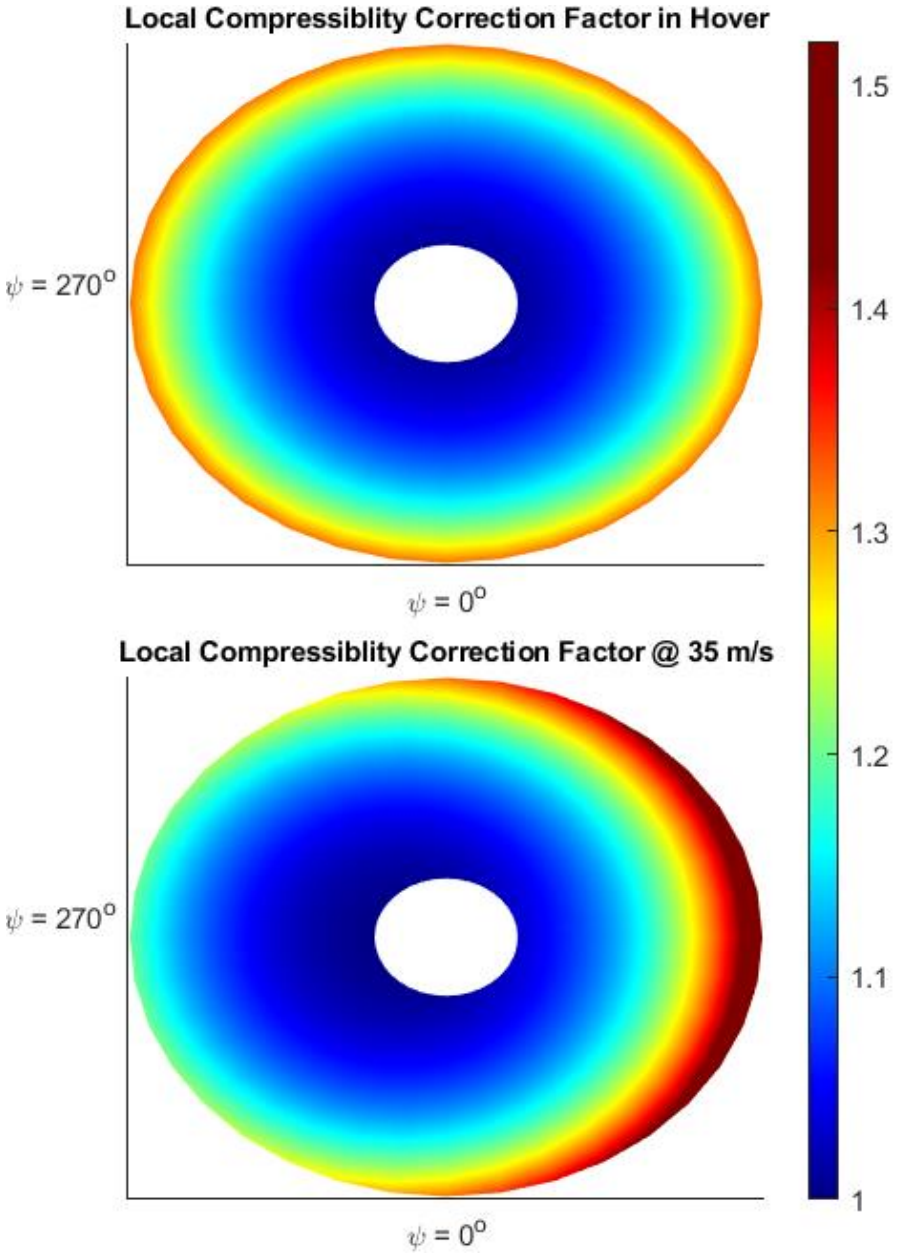

Figure 4.13. Local compressibility correction factor in hover and at 35 m/s.

4.9 Rotor Blade Control

Control of the blades are done by the swashplate. Moving up and down the swashplate controls the collective pitch input, whereas tilting the swashplate creates the cyclic pitch input.

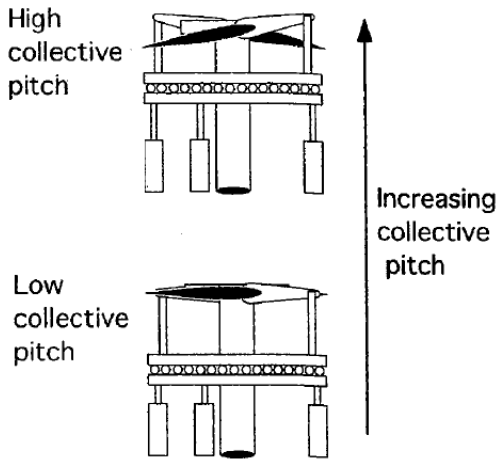

Figure 4.14. Collective pitch control. [14]

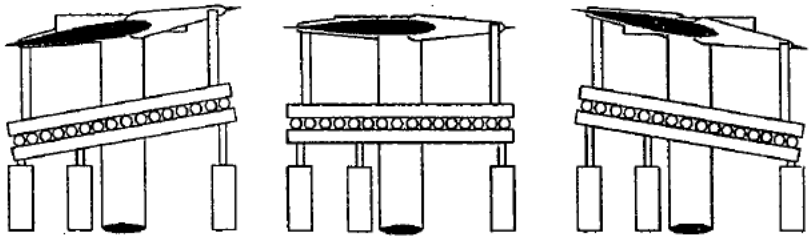

Figure 4.15. Cyclic pitch control. [14]

Swashplate rotates with the main rotor shaft; therefore, cyclic control is a periodic function having period of blade azimuth angle ψ. Periodic functions could be represented by a Fourier Series [11]; therefore, cyclic input could be defined as:

$$\theta(r,\psi) = \theta_0 + \theta_{tw}(r,\psi) + \theta_{1c}\cos\psi + \theta_{1s}\sin\psi + \theta_{2c}\cos 2\psi + \theta_{2s}\sin 2\psi + \cdots + \theta_{Nc}\cos N\psi + \theta_{Ns}\sin N\psi \quad (4.45)$$

θ_{tw} is the twist of the blade which contains both torsional deformation and blade design twist. Since the reference blade does not have a twist in design, θ_{tw} is

considered as elastic twist only. Although θ_{tw} is not a control input, it has an effect over the blade loads and performance of the aircraft. Note that since all the loads acting on the blade are harmonic, θ_{tw} is a function of azimuth angle ψ as well.

4.9.1 Rotor Planes

There could be relative motions between the rotor and the main frame of the helicopter. To describe these relative motions and make the calculations, some reference planes are defined.

4.9.1.1 Reference Plane (Horizontal Plane)

As the name of the plane suggests, this plane lies on the horizontal axis and global motion of the airframe is defined w.r.t this plane.

4.9.1.2 Disk Plane (Hub Plane)

Disk plane is the plane whose normal is in the direction of the rotor shaft. In other words, disk plane is perpendicular to the rotor shaft. Rotor's relative motions w.r.t the fuselage are defined in this plane.

4.9.1.3 Tip-Path Plane

Tip-path plane is defined by connecting the tip positions of the blades during one complete revolution of the rotor. Orientation of the tip-path plane defines the flapping angles; therefore, the thrust is perpendicular to the TPP.

4.9.1.4 No-Feathering Plane

This plane is defined firstly by Gessow & Myers in 1952 [14]. This plane is defined by cyclic pitch. Cyclic controls θ_{1c} and θ_{1s} are observed as zero w.r.t the no-feathering plane.

4.9.2 Blade Motion

Due to the asymmetrical velocity over the blade, aerodynamic loads on the blade would have an asymmetrical distribution as well. Since the velocity field and aerodynamic loads are periodic with azimuth angle ψ, blade motion is also periodic with azimuth angle ψ.

Let us define flap angle β and lag angle ζ. β is the out-of-plane bending angle between the blade and the disk plane and β is called as **flap angle**. β is defined as positive when the blade bends upward direction. ζ is the in-plane bending angle of the blade w.r.t to the hub. ζ is called as **lag angle** and defined as positive when the blade bends in the direction of opposite direction of the rotation.

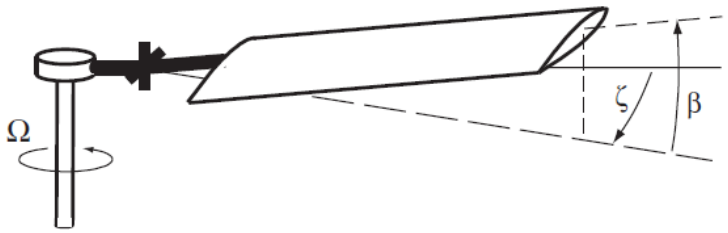

Figure 4.16. Flap and lag angle. [12]

Flap angle β and lag angle ζ are periodic with azimuth angle ψ as well. Therefore, they could be expressed as Fourier Series as well:

$$\begin{aligned}\beta(\psi) &= \beta_0 + \beta_{1c}\cos\psi + \beta_{1s}\sin\psi + \beta_{2c}\cos 2\psi + \beta_{2s}\sin 2\psi + \cdots \\ &= \beta_0 + \sum_{n=1}^{\infty}(\beta_{nc}\cos(n\psi) + \beta_{ns}\sin(n\psi))\end{aligned} \tag{4.46}$$

$$\begin{aligned}\zeta(\psi) &= \zeta_0 + \zeta_{1c}\cos\psi + \zeta_{1s}\sin\psi + \zeta_{2c}\cos 2\psi + \zeta_{2s}\sin 2\psi + \cdots \\ &= \zeta_0 + \sum_{n=1}^{\infty}(\zeta_{nc}\cos(n\psi) + \zeta_{ns}\sin(n\psi))\end{aligned} \tag{4.47}$$

In general, lowest harmonics are enough to describe the blade motion in forward flight accurately [11]. Therefore, mean value and first harmonics are used in this work:

$$\theta(\psi, r) = \theta_0 + \theta_{tw}(\psi, r) + \theta_{1c}\, cos\, \psi + \theta_{1s}\, sin\, \psi \tag{4.48}$$

$$\beta(\psi) = \beta_0 + \beta_{1c}\, cos\, \psi + \beta_{1s}\, sin\, \psi \tag{4.49}$$

$$\zeta(\psi) = \zeta_0 + \zeta_{1c}\, cos\, \psi + \zeta_{1s}\, sin\, \psi \tag{4.50}$$

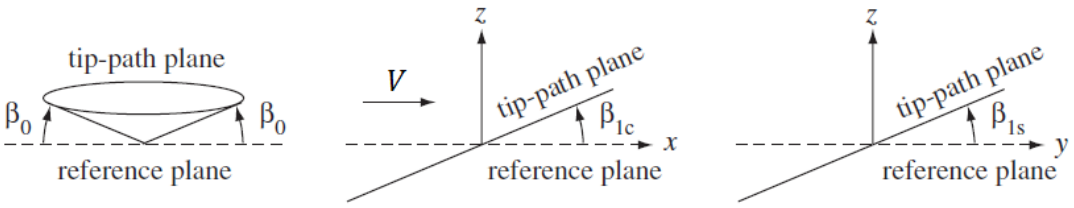

Figure 4.17. Rotor flap angle harmonics. β_0 coning angle, β_{1c} longitudinal tip-path-plane tilt (left view), β_{1s} lateral tip-path-plane tilt (aft view). [12]

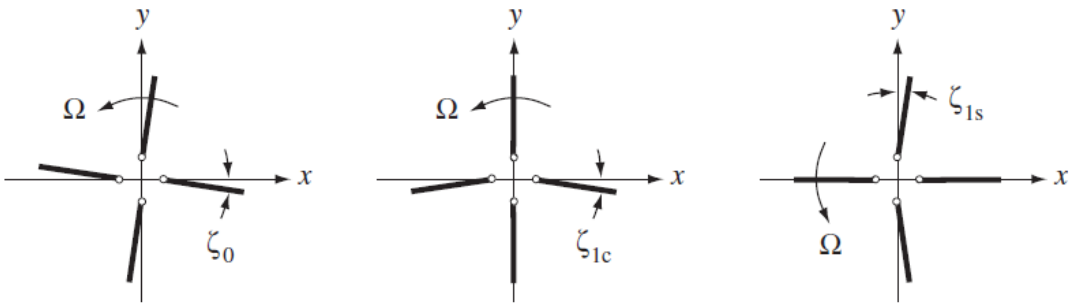

Figure 4.18. Rotor lag angle harmonics. ζ_0 mean lag, ζ_{1c} lateral lag, ζ_{1s} longitudinal lag (top view). [12]

In this work, since their influence on the aerodynamic loads are negligible, lag angle ζ and its effects are ignored.

4.9.3 Flapping Motion

In articulated rotors, a flapping hinge is introduced at the hub which adds an out-of-plane bending degree of freedom to the blade so that out-of-plane bending stress is decreased at the hub.

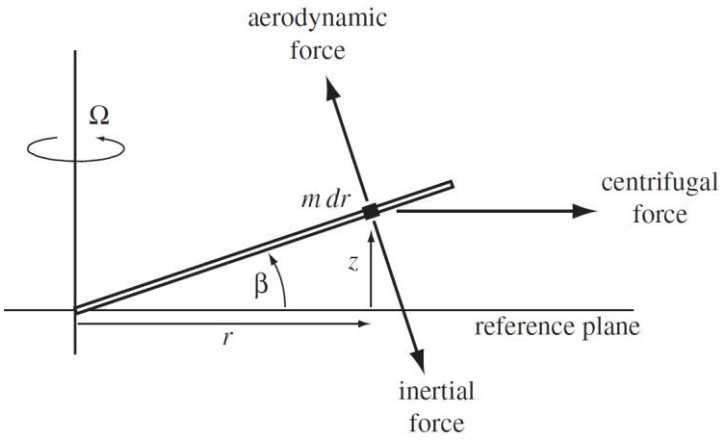

Figure 4.19. Flapping motion and forces on the blade. [12]

To analyze rotor behavior and trim conditions in forward flight, blade flapping motion is needed to be examined. Rotor flapping equation of motion is constructed for rigid blades having a flapping hinge at the root. In Figure 4.19, forces action on a mass element is shown. For small angle β, these forces are:

- Aerodynamic force: F_z in the normal direction of the blade. Moment arm of this force about the root is r.
- Centrifugal force: $m\Omega^2 r dr$ in the direction of radially outward. Moment arm of this force about the root is $z = r\beta$.
- Inertial force: $m\ddot{z}dr = mr\ddot{\beta}dr$ in the opposite direction of the flap motion. Moment arm of this force about the root is r.

By integrating these forces with their moments arm from root to the tip of the blade, we would obtain:

$$\int_0^R mr\ddot{\beta}rdr + \int_0^R m\Omega^2 r(r\beta)dr - \int_0^R F_z rdr = 0 \qquad (4.51)$$

Since the blade is assumed to be rigid, β is constant over the blade radius. By taking out β from the integral expressions, we obtain:

$$\left(\int_0^R r^2 m dr\right)\left(\ddot{\beta} + \Omega^2\beta\right) = \int_0^R F_z r dr \tag{4.52}$$

Let us define $I_b = \left(\int_0^R r^2 m dr\right)$ which is the moment of inertia of the blade about the flap hinge and re-write Eq. (4.52):

$$\left(\ddot{\beta} + \Omega^2\beta\right) = \frac{1}{I_b}\int_0^R F_z r dr \tag{4.53}$$

From Eq. (4.53), it is found that first flapping natural frequency of the blade is exactly equal to the rotor speed Ω if there is a flapping hinge at the root.

4.10 Forward Flight Aerodynamics

In this section, the details of the aerodynamic analyses and blade dynamics will be discussed for the forward flight condition. The assumptions made in this section are:

- Loads are steady, any unsteady effects are neglected.
- Inflow is assumed to be uniform over the main rotor.
- Shear center and aerodynamic center of the blade does not change with rotation and forward flight.
- Any interaction between the main rotor and the fuselage or the tail rotor is neglected.
- In references such as [4], [11], [12], [14], [19] rotor forces are calculated by taking integrals and assuming a linear twist. In this work, main aim is to obtain the twist field. Therefore, analytical expression of the elastic twist field must be found. As a result, all the calculations are done by using Blade Element Momentum Theory in which local forces, and local twists are combined to find the rotor forces instead of taking integrals analytically.

Tangential and radial velocity components experienced by the airfoil was given in Eq's. (4.41) and (4.42). Let us define the perpendicular component of the velocity u_P by combining with flapping effect:

$$u_P = v + r\dot{\beta} + u_R\beta \tag{4.54}$$

First term appearing in Eq. (4.54) is the inflow, second term is the flapping speed, and the last term is normal component of the radial velocity. Note that since β is small, it is assumed that $\sin\beta \cong \beta$.

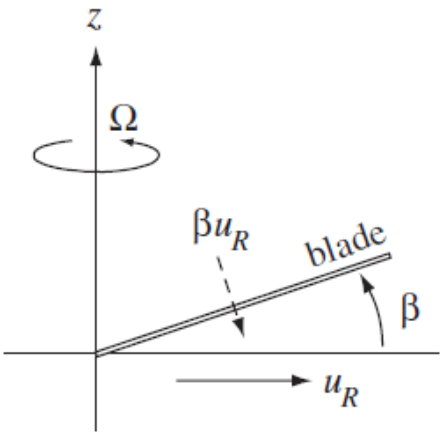

Figure 4.20. Normal component of the radial velocity to the blade. [12]

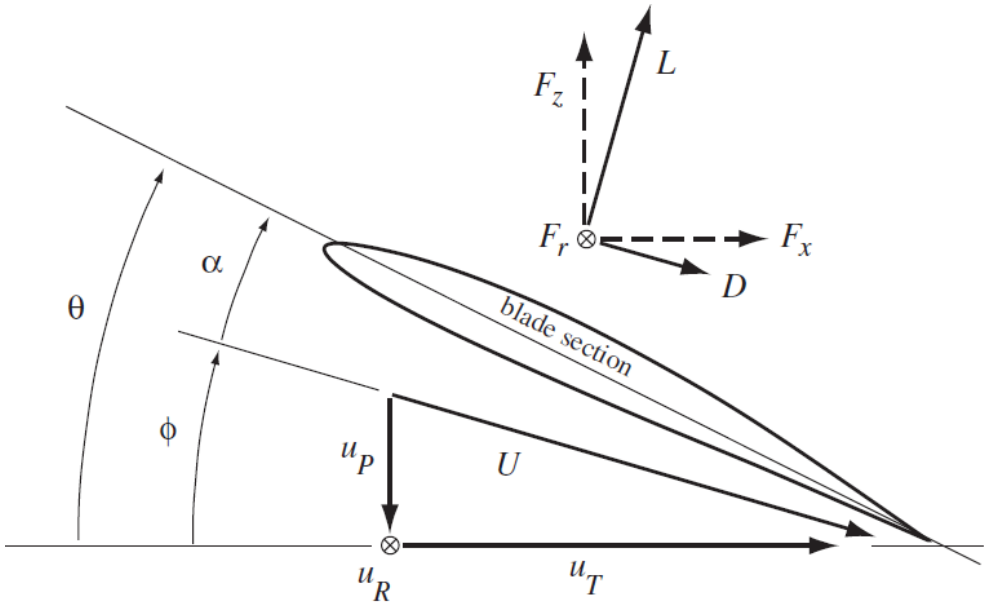

Figure 4.21. Blade section aerodynamics in forward flight. [12]

If the forward flight velocity is set to zero, the velocity components u_T, u_P and u_R in Eq's. (4.41), (4.54) and (4.42) become as given in Eq's. (4.18), (4.19) and zero respectively since time rate of change of flapping angle is zero due to the symmetrical load field in hover.

Inflow angle ϕ, angle of attack α, normal force F_z, in-plane force F_x, blade pitch angle θ, perpendicular velocity component of the blade u_P, tangential velocity component of the blade u_T, radial velocity component of the blade u_R were given in Eq's. (4.21), (4.22), (4.25), (4.26), (4.48), (4.54), (4.41) and (4.42) respectively.

Resultant velocity U, and radial force component is given as:

$$U = \sqrt{u_T^2 + u_P^2 + u_R^2} \cong u_T \tag{4.55}$$

$$F_r = -\beta F_z \tag{4.56}$$

Since main velocity component the blade experiences is the tangential velocity u_T and $u_T \gg u_P, u_R$, resultant velocity could be approximated as $U \cong u_T$. In Eq. (4.56), small angle is assumed and radial drag force is neglected.

4.11 Rotor Forces and Moments in Forward Flight

Rotor forces are defined relative to the reference plane described in Section 4.9.1. Thrust T is defined in normal direction to the plane, rotor longitudinal force H and lateral force Y are defined in the plane. Thrust T is given in Eq. (4.27). Let us obtain the rotor longitudinal force H and lateral force Y:

$$H = N_b \int_0^R (F_x \sin\psi + F_r \cos\psi) dr \tag{4.57}$$

$$Y = N_b \int_0^R (-F_x \cos\psi + F_r \sin\psi) dr \tag{4.58}$$

where F_x and F_r are given in Eq's. (4.26) and (4.56).

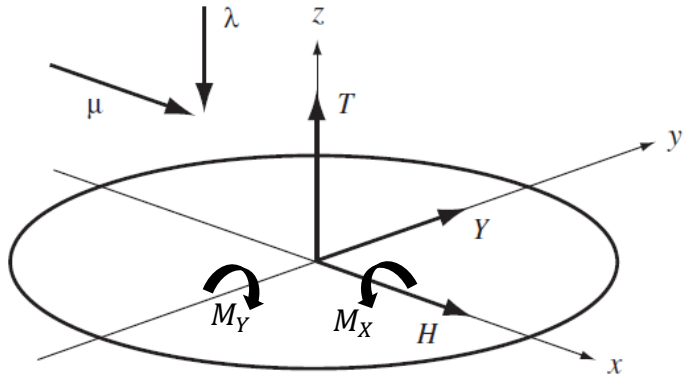

Figure 4.22. Rotor forces and moments in forward flight. [12]

In forward flight, due to control inputs, blade flapping and the dynamic pressure difference between advancing side and retreating side, rotor hub moments M_X and M_Y occur. Rotor hub moments are given as:

$$M_X = N_b \int_0^R F_z \sin\psi \, r dr \tag{4.59}$$

$$M_Y = -N_b \int_0^R F_z \cos\psi \, r dr \tag{4.60}$$

Note that integrating limits in Eq's. (4.59) and (4.60) should be updated as from aerodynamic root cutout r_R and to the tip loss BR.

Figure 4.22 shows the rotor forces and moments in the reference plane. Since tip-path plane and no-feathering plane are defined w.r.t the reference plane, the rotor forces, the inflow, and the rotor incidence i could be represented in these planes as well.

$$\lambda = \lambda_{TPP} - \mu\beta_{1c} = \lambda_{NFP} + \mu\theta_{1s} \tag{4.61}$$

$$i = i_{TPP} - \beta_{1c} = i_{NFP} + \theta_{1s} \tag{4.62}$$

$$H = H_{TPP} - T\beta_{1c} = H_{NFP} + T\theta_{1s} \tag{4.63}$$

$$Y = Y_{TPP} - T\beta_{1s} = Y_{NFP} - T\theta_{1c} \tag{4.64}$$

Cyclic controls and flapping angles are usually small; therefore, it is assumed that small angle assumption is valid for flapping angles and cyclic control inputs.

Thrust is the main rotor force component and most of the time it is much greater than the other rotor forces. Hence, it is adequate to assume that rotor thrust is independent of the reference plane.

4.11.1 Flapping Hinge Offset

Due to the flapping motion, air moves in the direction of inflow which is perpendicular to the tangential speed of the blade section. Therefore, flapping motion directly affects the aerodynamics of the blade by affecting the angle of attack of the blade. Since flapping motion occurs about the flapping hinge, flapping hinge offset is an important parameter. Flap hinge offset e is defined as the ratio of the distance of the hinge to the blade radius.

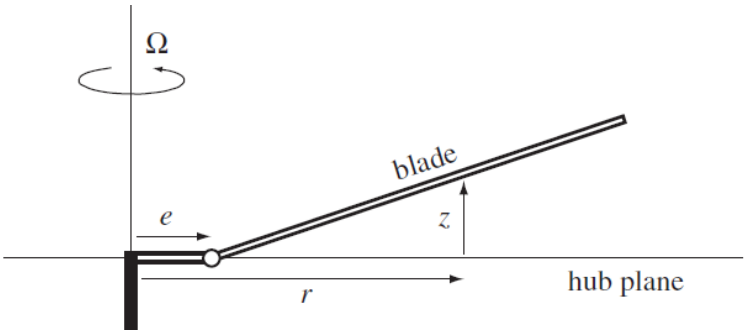

Figure 4.23. Flap hinge offset for an articulated rotor. [12]

By referring Ref. [12], define a piecewise function to describe the vertical displacement of the blade about a flap hinge offset,

$$\eta = \begin{cases} a(r - eR) & r \geq eR \\ 0 & r < eR \end{cases} \tag{4.65}$$

where a is constant to normalize the η. If η is normalized such that $\eta(R) = R$, then a becomes as $a = 1/(1 - e)$. If the flap-hinge offset is set to zero, then η becomes as r. Since the flapping motion is described w.r.t the flap-hinge, perpendicular velocity experienced by the blade section must be re-written as well:

$$u_P = v + \eta\dot{\beta} + u_R\eta'\beta \tag{4.66}$$

Re-consider the moment equilibrium in Section 4.9.3 by implementing flap hinge offset:

- Aerodynamic force: F_z in the normal direction of the blade. Moment arm of this force about the flap hinge is $(r - eR)$.
- Centrifugal force: $m\Omega^2 r dr$ in the direction of radially outward. Moment arm of this force about the flap hinge is $z = \eta\beta$.
- Inertial force: $m\ddot{z}dr = m\eta\ddot{\beta}dr$ in the opposite direction of the flap motion. Moment arm of this force about the flap hinge is $(r - eR)$.

By integrating these forces with their moments arm from the flap hinge to the tip of the blade, we would obtain:

$$\int_{eR}^{R} m\eta\ddot{\beta}(r - eR)dr + \int_{eR}^{R} m\Omega^2 r(\eta\beta)dr - \int_{eR}^{R} F_z(r - eR)dr = 0 \qquad (4.67)$$

From Eq. (4.65), replace $(r - eR)$ with η/a.

$$\int_{eR}^{R} m\frac{\eta^2}{a}\ddot{\beta}dr + \int_{eR}^{R} m\Omega^2 r(\eta\beta)dr = \int_{eR}^{R} F_z\frac{\eta}{a}dr = 0 \qquad (4.68)$$

$$\int_{eR}^{R} m\eta^2\ddot{\beta}dr + a\int_{eR}^{R} m\Omega^2 r(\eta\beta)dr = \int_{eR}^{R} F_z\eta dr = 0 \qquad (4.69)$$

In [18] a new flap frequency parameter ξ is defined to express Eq. (4.69). By using ξ, re-write Eq. (4.69):

$$\ddot{\beta} + (\xi\Omega)^2\beta = \frac{1}{\widehat{I_b}}\int_{eR}^{R} F_z\eta dr \qquad (4.70)$$

where $\widehat{I_b} = \int_{eR}^{R}\eta^2 m dr$. Note that if e is zero $\widehat{I_b} = I_b$ and $\xi = 1$.

For an articulated rotor having uniform blades and no flap hinge spring, flap frequency is given in [4]:

$$\xi^2 = 1 + \frac{3}{2}\frac{e}{1 - e} \qquad (4.71)$$

where e is typically around 0.04 for articulated rotors which gives ξ as about 1.06. [4]

On the other hand, hingeless rotors do not have any hinges as their name suggests. Johnson [12] suggests that first out-of-plane bending is mostly dominated by the rotor nominal speed as it is showed in Section 3.2.1 and discussed in Section 4.9.3. Therefore, by using Eq. (4.71) an equivalent flap hinge offset could be found:

$$e_{eq} = \frac{\frac{2}{3}(\xi^2 - 1)}{1 + \frac{2}{3}(\xi^2 - 1)} \tag{4.72}$$

For hingeless rotors, non-dimensional flap frequency ξ could be written as the ratio of the first out-of-plane bending natural frequency to the rotor speed.

$$\xi = \frac{\omega_h}{\Omega} \tag{4.73}$$

Natural frequencies and mode shapes of the reference blade is given in Section 3.2.1. From Table 3.3, non-dimensional flap frequency ξ of the reference blade could be found as 1.08.

Right-hand side of Eq. (4.70) could be written as:

$$\int_{eR}^{R} F_z \eta dr = \int_{eR}^{R} (L' \cos\phi - D' \sin\phi)\eta dr \tag{4.74}$$

From Figure 3.6, it could be seen that $c_l \gg c_d$ in the operating range of the reference helicopter. In addition, ϕ is given as u_P/u_T in Eq. (4.21) and it is known that $u_T \gg u_P$; therefore, $\cos\phi$ could be approximated as one. Hence, Eq. (4.74) could be approximated as:

$$\int_{eR}^{R} F_z \eta dr \cong \int_{eR}^{R} L' \eta dr = \int_{eR}^{R} \frac{1}{2} \rho U^2 c c_l \eta dr \tag{4.75}$$

To further simplify Eq. (4.75), resultant velocity U could be approximated as u_T, since $u_T \gg u_P, u_R$. Hence, Eq. (4.75) could be written as:

$$\int_{eR}^{R} F_z \eta dr \cong \int_{eR}^{R} \frac{1}{2} \rho c c_l (u_T^2 \theta - u_T u_P) \eta dr \tag{4.76}$$

If Eq. (4.76) is put into the flapping equation Eq. (4.70), we would obtain:

$$\ddot{\beta} + (\xi \Omega)^2 \beta \cong \frac{1}{\widehat{I_b}} \int_{eR}^{R} \frac{1}{2} \rho c c_l (u_T^2 \theta - u_T u_P) \eta dr \tag{4.77}$$

Note that the pitch angle θ term in Eq. (4.77) has a twist term $\theta_{tw}(r, \psi)$ which is still not known. To be able to solve Eq. (4.77), twist term $\theta_{tw}(r, \psi)$ must be found. Therefore, in the following section details of the $\theta_{tw}(r, \psi)$ is discussed.

4.12 Torsional Twist and Divergence Speed

As it is discussed in the very beginning of Ch. 4, static aeroelasticity studies the interaction between the structural deformation and steady aerodynamic forces. When the structure is loaded by an aerodynamic force, it will deform resulting a change in the aerodynamic loading. Therefore, there occurs a cycle between structural deformation and aerodynamic loads. It is needed that this cycle converges to a point where structural deformation is in an equilibrium with aerodynamic loads. If the convergence could not be achieved, the structure may fail eventually. Therefore, static aeroelasticity is mainly interested on two concepts. First one is the divergence, in order to prevent any structural failure. Second one is the equilibrium state to analyze aerodynamic loads and elastic deformation on the wing.

4.12.1 Divergence Speed

As it is discussed above, divergence speed is the speed where the interaction between structural deformations and aerodynamic loads are not in an equilibrium such that as the structure deforms, aerodynamic loads increases resulting a greater deformation on the structure.

To examine the divergence speed, Hodges [10] suggests a wind-tunnel model. In the wind-tunnel model, airfoil is supported with a rigid hinge and a torsional spring at its elastic axis which constrains the plunging motion pitching direction and add a torsional stiffness to the system in the pitching direction respectively.

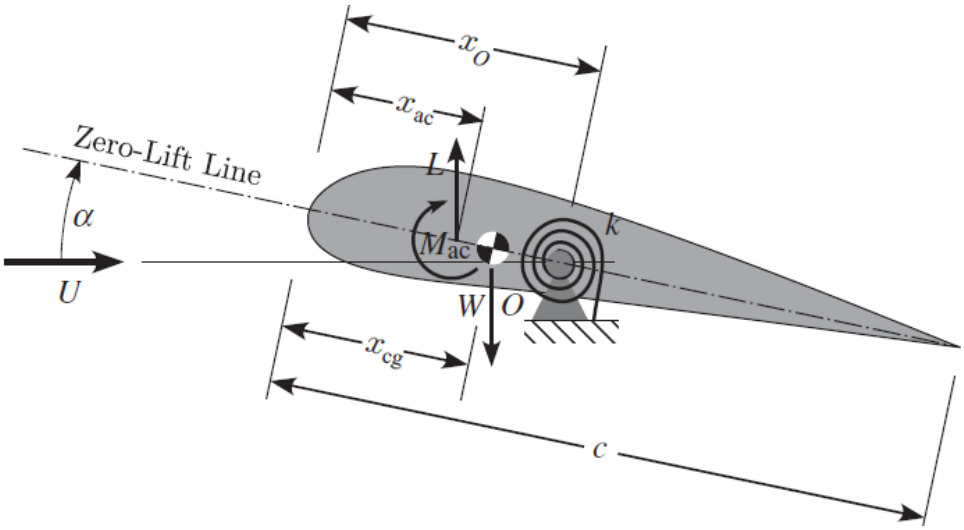

Figure 4.24. Wind-tunnel model of the airfoil. [10]

In Figure 4.24, x_O is the distance between the leading edge and elastic axis (shear center), x_{ac} is the distance between the leading edge and aerodynamic center, x_{cg} is the distance between the leading edge and center of gravity of the airfoil, c is the chord of the airfoil, k is the torsional spring stiffness.

By assuming thin airfoil theory is valid, sectional lift and aerodynamic moment are given as:

$$L = \frac{1}{2}\rho U^2 c c_{l_\alpha}(\alpha_r + \delta) \tag{4.78}$$

$$M_{ac} = \frac{1}{2}\rho U^2 c^2 c_m \tag{4.79}$$

α_r and δ in Eq. (4.78) are rigid angle of attack of the airfoil and elastic increment of the angle of attack respectively. c_m is the non-dimensional aerodynamic pitching moment coefficient and it could be assumed as constant.

If moment equilibrium is written for Figure 4.24 w.r.t connection point by using Eq's (4.78) and (4.79), we would obtain:

$$\frac{1}{2}\rho U^2 c^2 C_M + \frac{1}{2}\rho U^2 c C_{L_\alpha}(\alpha_r + \delta)(x_o - x_{ac}) - W\left(x_o - x_{cg}\right) = k\delta \tag{4.80}$$

Solve Eq. (4.80) for the elastic increment of the angle of attack δ:

$$\delta = \frac{\frac{1}{2}\rho U^2 c^2 C_M + \frac{1}{2}\rho U^2 c C_{L_\alpha}\alpha_r(x_o - x_{ac}) - W\left(x_o - x_{cg}\right)}{k - \frac{1}{2}\rho U^2 c C_{L_\alpha}(x_o - x_{ac})} \tag{4.81}$$

From Eq. (4.81), it could be observed that if the denominator of the equation becomes zero, elastic increment δ blows up i.e., δ diverges. Let us define the divergence velocity U_D which makes the denominator of Eq. (4.81) zero:

$$k - \frac{1}{2}\rho U_D^2 c C_{L_\alpha}(x_o - x_{ac}) = 0 \tag{4.82}$$

If Eq. (4.82) is solved for the divergence speed U_D:

$$U_D = \sqrt{\frac{2k}{\rho c C_{L_\alpha}(x_o - x_{ac})}} \tag{4.83}$$

If the aerodynamic center of the airfoil x_{ac} is coincident with the elastic axis location x_o i.e., $(x_o = x_{ac})$, divergence speed approaches to infinity $(U_D \to \infty)$. If the aerodynamic center is behind the elastic axis $(x_o < x_{ac})$, there is no real

solution for the divergence speed U_D; therefore, no divergence occurs in any speed. Hence, while designing a wing or a blade, it should be intended that $x_o - x_{ac}$ is minimized to increase the divergence speed and avoid any divergence related failure. For the reference blade whose properties are given in Ch. 3, shear center x_o is measured as 2.2 cm from the leading edge. Whereas, the aerodynamic center x_{ac} of the blade is at the quarter chord which is 2.25 cm from the leading edge. Since $x_o < x_{ac}$ is satisfied, it could be concluded that there exists no divergence speed for the reference blade. Note that for the static aeroelastic analyses it is assumed that shear center and aerodynamic center of the reference blade does not change.

4.12.2 Torsional Twist of the Helicopter Blades

As it is discussed in the very beginning of Section 4.12, torsional twist and the aerodynamic loads are related to each other. This coupling might be an important relation for the lifting surfaces since structural deformations cause aerodynamic loads to change.

In [15], torsional twist relation is given as:

$$M' = GJ\frac{d\theta_{tw}}{dr} \tag{4.84}$$

where M' is:

$$M' = F_z(x_o - x_{ac}) \tag{4.85}$$

If F_z in Eq. (4.85) is approximated as it is done in Eq. (4.75):

$$M' = \frac{1}{2}\rho c c_{l_\alpha}(u_T^2\theta - u_T u_P)(x_o - x_{ac}) \tag{4.86}$$

Blade pitch angle θ has a twist term as well. Therefore, Eq. (4.86) could be re-written as:

$$M' = \frac{1}{2}\rho c c_{l_\alpha}(u_T^2\theta_{con} + u_T^2\theta_{tw} - u_T u_P)(x_o - x_{ac}) \tag{4.87}$$

When Eq. (4.87) is put into Eq. (4.84):

$$GJ\frac{d\theta_{tw}}{dr}-\frac{1}{2}\rho u_T^2 cc_{l_\alpha}\theta_{tw}=\frac{1}{2}\rho cc_{l_\alpha}(u_T^2\theta_{con}-u_T u_P)(x_o-x_{ac}) \qquad (4.88)$$

In Eq. (4.88), tangential and perpendicular velocity component u_T, u_P are a function of radial distance r due to rotation and blade flapping respectively. In addition, lift curve slope c_{l_α} is a function of radial distance r as well due to the compressibility effect. Therefore, Eq. (4.88) is very hard to solve analytically. Therefore, a numerical solution should be implemented. An iterative solution procedure could be implemented from starting $(\theta_{tw})_0$ is zero as following:

$$(M')_n=\frac{1}{2}\rho cc_{l_\alpha}(u_T^2\theta_{con}+u_T^2(\theta_{tw})_{n-1}-u_T u_P)(x_o-x_{ac}) \qquad (4.89)$$

Where subscript n is the iteration step. When $(M')_n$ is solved by using Eq. (4.89), $(M')_n$ becomes a constant w.r.t radial position r. Therefore, $(\theta_{tw})_n$ could be found from Eq. (4.84):

$$(\theta_{tw})_n=\frac{(M')_n r}{GJ} \qquad (4.90)$$

After finding new elastic twist, n is incremented by 1. In order to stop the iterations, define a tolerance $\theta_{tw,err}$ such that iteration stops if the condition $\theta_{tw,err}\geq|(\theta_{tw})_n-(\theta_{tw})_{n-1}|$ is satisfied.

4.12.3 Superposition of the Torsional Twist

Solution procedure given in Section 4.12.2 is applicable for only a very specific case when there is a single load at a radial distance r. However, it is known that there is a loading field on the blade. In order to obtain twist field for the aerodynamic loading on the blade, superposition principle could be applied. In superposition method, if there exist several concentrated loads on a beam, these loads could be analyzed separately as if the beam was loaded by only one concentrated load. After finding the individual displacement fields due to the loads, displacement fields could be summed to find the resultant displacement field.

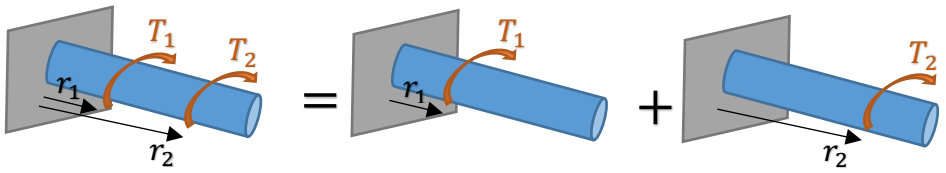

a) Actual Load b) First Load Case c) Second Load Case

Figure 4.25. Superposition principle illustration.

To find twist field for the actual load in Figure 4.25, twist field of first load case and second load case could be summed which are given as:

$$\theta_{tw,1} = \begin{cases} \frac{T_1 r}{GJ} & r \le r_1 \\ \frac{T_1 r_1}{GJ} & r > r_1 \end{cases}$$
$$\theta_{tw,2} = \begin{cases} \frac{T_2 r}{GJ} & r \le r_2 \\ \frac{T_2 r_2}{GJ} & r > r_2 \end{cases} \tag{4.91}$$

If these two twist fields are collected, actual twist field could be found.

$$\theta_{tw,act} = \begin{cases} \frac{T_1 r}{GJ} + \frac{T_2 r}{GJ} & r \le r_1 \\ \frac{T_1 r_1}{GJ} + \frac{T_2 r}{GJ} & r_2 \ge r > r_1 \\ \frac{T_1 r_1}{GJ} + \frac{T_2 r_2}{GJ} & r > r_2 \end{cases} \tag{4.92}$$

Same analogy could be used for the blade element analysis as well.

$$\theta_{tw} = \begin{cases} \frac{T_1 r}{GJ} + \frac{T_2 r}{GJ} + \frac{T_3 r}{GJ} + \cdots + \frac{T_n r}{GJ} & r_1 \ge r \\ \frac{T_1 r_1}{GJ} + \frac{T_2 r}{GJ} + \frac{T_3 r}{GJ} + \cdots + \frac{T_n r}{GJ} & r_2 \ge r > r_1 \\ \frac{T_1 r_1}{GJ} + \frac{T_2 r_2}{GJ} + \frac{T_3 r}{GJ} + \cdots + \frac{T_n r}{GJ} & r_3 \ge r > r_2 \\ \frac{T_1 r_1}{GJ} + \frac{T_2 r_2}{GJ} + \frac{T_3 r_3}{GJ} + \cdots + \frac{T_n r}{GJ} & r_n > r \ge r_{n-1} \end{cases} \tag{4.93}$$

4.13 Harmonic Solution of the Flapping with Hinge Offset

If Eq. (4.77) is expanded, it would be seen that lots of harmonic terms appear in the equation. These harmonics consist of not only the first harmonics $\sin\psi$ and $\cos\psi$ but also combined harmonics such as $\sin\psi\cos\psi$ and higher order harmonics such as $\sin^2\psi$ and $\cos^2\psi$. To solve Eq. (4.77) for steady-state condition, Johnson [12] suggests that operands given in Eq. (4.94) could be applied to both sides to obtain the mean and the first harmonics for blade pitch angle θ and flapping angle β.

$$\frac{1}{2\pi}\int_0^{2\pi}(\dots)d\psi\,,\quad \frac{1}{\pi}\int_0^{2\pi}(\dots)\cos\psi\,d\psi\,,\quad \frac{1}{\pi}\int_0^{2\pi}(\dots)\sin\psi\,d\psi \tag{4.94}$$

Since closed form of the twist is not known, operands given in Eq. (4.94) should be expressed in a discrete form. From [19], discrete form of the operands could be written as:

$$\frac{1}{N_{az}}\sum_{n=1}^{n=N_{az}}(\dots)\,,\quad \frac{2}{N_{az}}\sum_{n=1}^{n=N_{az}}(\dots)\cos\psi_n\,,\quad \frac{2}{N_{az}}\sum_{n=1}^{n=N_{az}}(\dots)\sin\psi_n \tag{4.95}$$

where $\psi_n = 2\pi\frac{n}{N_{az}}$. If operands in Eq. (4.95) are applied to the left-hand side of Eq. (4.77), we obtain:

$$\frac{1}{N_{az}}\sum_{n=1}^{n=N_{az}}(\ddot{\beta}_n + (\xi\Omega)^2\beta_n) = (\xi\Omega)^2\beta_0 \tag{4.96}$$

$$\frac{2}{N_{az}}\sum_{n=1}^{n=N_{az}}(\ddot{\beta}_n + (\xi\Omega)^2\beta_n)\cos\psi_n \cong \Omega^2(\xi^2-1)\beta_{1c} \tag{4.97}$$

$$\frac{2}{N_{az}}\sum_{n=1}^{n=N_{az}}(\ddot{\beta}_n + (\xi\Omega)^2\beta_n)\sin\psi_n \cong \Omega^2(\xi^2-1)\beta_{1s} \tag{4.98}$$

For the right-hand side of Eq. (4.77), it is needed to change the integral order such that operand integral is taken firstly then the integral over the blade span is taken.

In the moment expression of Eq. (4.77), only the term $\frac{1}{\sqrt{1-M^2}}(u_T^2\theta - u_T u_P)$ is a function of ψ, other terms are constant w.r.t the azimuth angle ψ. Therefore, the operands given in Eq. (4.95) applied to the periodic term in Eq. (4.77).

$$\begin{aligned}\frac{1}{N_{az}}\sum_{n=1}^{n=N_{az}}\frac{1}{\sqrt{1-M^2}}(u_T^2\theta - u_T u_P) \\ \cong \theta_0\{(\Omega r)^2 H^{0,0} + 2\Omega r V H^{1,0} + V^2 H^{2,0}\} \\ + \theta_{1s}\{(\Omega r)^2 H^{1,0} + 2\Omega r V H^{2,0} + V^2 H^{3,0}\} \\ + \beta_{1c}\{\Omega^2 r\eta H^{1,0} - \Omega r V\eta' H^{0,2} + \Omega V\eta H^{2,0} \\ - V^2\eta' H^{1,2}\} - \nu\{\Omega r H^{0,0} + V H^{1,0}\} \\ + \frac{1}{N_{az}}\sum_{n=1}^{n=N_{az}}\frac{1}{\sqrt{1-M_n^2}}u_{T_n}^2\theta_{tw_n}\end{aligned} \tag{4.99}$$

$$\begin{aligned}\frac{1}{N_{az}}\sum_{n=1}^{n=N_{az}}\frac{1}{\sqrt{1-M^2}}(u_T^2\theta - u_T u_P)\cos\psi_n \\ \cong \theta_{1c}\{(\Omega r)^2 H^{0,2} + 2\Omega r V H^{1,2} + V^2 H^{2,2}\} \\ - \beta_0\{\Omega r V\eta' H^{0,2} + V^2\eta' H^{1,2}\} \\ - \beta_{1s}\{\Omega^2 r\eta H^{0,2} + \Omega r V\eta' H^{1,2} + \Omega V\eta H^{1,2} \\ + V^2\eta' H^{2,2}\} + \frac{1}{N_{az}}\sum_{n=1}^{n=N_{az}}\frac{1}{\sqrt{1-M_n^2}}u_{T_n}^2\theta_{tw_n}\cos\psi_n\end{aligned} \tag{4.100}$$

$$\begin{aligned}\frac{1}{N_{az}}\sum_{n=1}^{n=N_{az}}\frac{1}{\sqrt{1-M^2}}(u_T^2\theta - u_T u_P)\sin\psi_n \\ \cong \theta_0\{(\Omega r)^2 H^{1,0} + 2\Omega r V H^{2,0} + V^2 H^{3,0}\} \\ + \theta_{1s}\{(\Omega r)^2 H^{2,0} + 2\Omega r V H^{3,0} + V^2 H^{4,0}\} \\ + \beta_{1c}\{\Omega^2 r\eta H^{2,0} - \Omega r V\eta' H^{1,2} + \Omega V\eta H^{3,0} \\ - V^2\eta' H^{2,2}\} - \nu\{\Omega r H^{1,0} + V H^{2,0}\} \\ + \frac{1}{N_{az}}\sum_{n=1}^{n=N_{az}}\frac{1}{\sqrt{1-M_n^2}}u_{T_n}^2\theta_{tw_n}\sin\psi_n\end{aligned} \tag{4.101}$$

where $H^{a,b}$ is harmonic solution parameter and given as:

$$H^{a,b} = \frac{1}{N_{az}} \sum_{n=1}^{n=N_{az}} \frac{sin^a \psi_n \, cos^b \psi_n}{\sqrt{1 - M_n^2}} \tag{4.102}$$

By combining Eq's. from (4.96) to (4.101) respectively:

$$\begin{aligned}(\xi\Omega)^2\beta_0 = \frac{1}{\widehat{I_b}} \int_{eR}^{R} \frac{1}{2} \rho c C_{L_\alpha} \Bigg(& \theta_0\{(\Omega r)^2 H^{0,0} + 2\Omega r V H^{1,0} + V^2 H^{2,0}\} \\ & + \theta_{1s}\{(\Omega r)^2 H^{1,0} + 2\Omega r V H^{2,0} + V^2 H^{3,0}\} \\ & + \beta_{1c}\{\Omega^2 r \eta H^{1,0} - \Omega r V \eta' H^{0,2} + \Omega V \eta H^{2,0} - V^2 \eta' H^{1,2}\} \\ & - \nu\{\Omega r H^{0,0} + V H^{1,0}\} + \frac{1}{N_{az}} \sum_{n=1}^{n=N_{az}} \frac{1}{\sqrt{1 - M_n^2}} u_{T_n}^2 \theta_{tw_n} \Bigg) \eta dr\end{aligned} \tag{4.103}$$

$$\begin{aligned}\Omega^2(\xi^2 - 1)\beta_{1c} = \frac{2}{\widehat{I_b}} \int_{eR}^{R} \frac{1}{2} \rho c C_{L_\alpha} \Bigg(& \theta_{1c}\{(\Omega r)^2 H^{0,2} \\ & + 2\Omega r V H^{1,2} + V^2 H^{2,2}\} - \beta_0\{\Omega r V \eta' H^{0,2} + V^2 \eta' H^{1,2}\} \\ & - \beta_{1s}\{\Omega^2 r \eta H^{0,2} + \Omega r V \eta' H^{1,2} + \Omega V \eta H^{1,2} + V^2 \eta' H^{2,2}\} \\ & + \frac{1}{N_{az}} \sum_{n=1}^{n=N_{az}} \frac{1}{\sqrt{1 - M_n^2}} u_{T_n}^2 \theta_{tw_n} \, cos \, \psi_n \Bigg) \eta dr\end{aligned} \tag{4.104}$$

$$\begin{aligned}\Omega^2(\xi^2 - 1)\beta_{1s} = \frac{2}{\widehat{I_b}} \int_{eR}^{R} \frac{1}{2} \rho c C_{L_\alpha} \Bigg(& \theta_0\{(\Omega r)^2 H^{1,0} \\ & + 2\Omega r V H^{2,0} + V^2 H^{3,0}\} + \theta_{1s}\{(\Omega r)^2 H^{2,0} + 2\Omega r V H^{3,0} + V^2 H^{4,0}\} \\ & + \beta_{1c}\{\Omega^2 r \eta H^{2,0} - \Omega r V \eta' H^{1,2} + \Omega V \eta H^{3,0} - V^2 \eta' H^{2,2}\} \\ & - \nu\{\Omega r H^{1,0} + V H^{2,0}\} + \frac{1}{N_{az}} \sum_{n=1}^{n=N_{az}} \frac{1}{\sqrt{1 - M_n^2}} u_{T_n}^2 \theta_{tw_n} \, sin \, \psi_n \Bigg) \eta dr\end{aligned} \tag{4.105}$$

Since closed form of θ_{tw} could not be obtained, integrals and infinitesimal length dr appearing in Eq's. (4.103), (4.104) and (4.105) should be replaced with a summation symbol and with a blade element length Δr.

Another critical point regarding Eq's. (4.103), (4.104) and (4.105) is that the integral lower limit should be updated if $r_R > e$ i.e., the aerodynamic root cutout is higher than flap hinge offset. In addition, upper limit of the integrals should be written as tip loss BR instead of blade tip.

$$
\begin{aligned}
(\xi\Omega)^2\beta_0 = \frac{1}{\widehat{I_b}}\sum_{m=1}^{N_{bem}}\frac{1}{2}\rho c C_{L_\alpha}\Bigg(&\theta_0\{(\Omega r_m)^2 H_m^{0,0} + 2\Omega r_m V H_m^{1,0} \\
&+ V^2 H_m^{2,0}\} + \theta_{1s}\{(\Omega r_m)^2 H_m^{1,0} + 2\Omega r_m V H_m^{2,0} + V^2 H_m^{3,0}\} \\
&+ \beta_{1c}\{\Omega^2 r_m \eta_m H_m^{1,0} - \Omega r_m V \eta'_m H_m^{0,2} + \Omega V \eta_m H_m^{2,0} - V^2 \eta'_m H_m^{1,2}\} \\
&- \nu\{\Omega r_m H_m^{0,0} + V H_m^{1,0}\} \\
&+ \frac{1}{N_{az}}\sum_{n=1}^{n=N_{az}}\frac{1}{\sqrt{1-M_{m,n}^2}} u_{T_{m,n}}^2 \theta_{tw_{m,n}}\Bigg)\eta_m \Delta r
\end{aligned}
\tag{4.106}
$$

$$
\begin{aligned}
\Omega^2(\xi^2-1)\beta_{1c} = \frac{2}{\widehat{I_b}}\sum_{m=1}^{N_{bem}}\frac{1}{2}\rho c C_{L_\alpha}\Bigg(&\theta_{1c}\{(\Omega r_m)^2 H_m^{0,2} \\
&+ 2\Omega r_m V H_m^{1,2} + V^2 H_m^{2,2}\} - \beta_0\{\Omega r_m V \eta'_m H_m^{0,2} + V^2 \eta'_m H_m^{1,2}\} \\
&- \beta_{1s}\{\Omega^2 r_m \eta_m H_m^{0,2} + \Omega r_m V \eta'_m H_m^{1,2} + \Omega V \eta_m H_m^{1,2} + V^2 \eta'_m H_m^{2,2}\} \\
&+ \frac{1}{N_{az}}\sum_{n=1}^{n=N_{az}}\frac{1}{\sqrt{1-M_{m,n}^2}} u_{T_{m,n}}^2 \theta_{tw_{m,n}} \cos\psi_n\Bigg)\eta_m \Delta r
\end{aligned}
\tag{4.107}
$$

$$
\begin{aligned}
\Omega^2(\xi^2-1)\beta_{1s} = \frac{2}{\widehat{I_b}}\sum_{m=1}^{N_{bem}}\frac{1}{2}\rho c C_{L_\alpha}\Bigg(&\theta_0\{(\Omega r)^2 H_m^{1,0} + 2\Omega r V H_m^{2,0} \\
&+ V^2 H_m^{3,0}\} + \theta_{1s}\{(\Omega r)^2 H_m^{2,0} + 2\Omega r V H_m^{3,0} + V^2 H_m^{4,0}\} \\
&+ \beta_{1c}\{\Omega^2 r \eta H_m^{2,0} - \Omega r V \eta' H_m^{1,2} + \Omega V \eta H_m^{3,0} - V^2 \eta' H_m^{2,2}\} \\
&- \nu\{\Omega r H_m^{1,0} + V H_m^{2,0}\} \\
&+ \frac{1}{N_{az}}\sum_{n=1}^{n=N_{az}}\frac{1}{\sqrt{1-M_{m,n}^2}} u_{T_{m,n}}^2 \theta_{tw_{m,n}} \sin\psi_n\Bigg)\eta_m \Delta r
\end{aligned}
\tag{4.108}
$$

where the summations are calculated for the blade elements between the aerodynamic root cutout and tip loss.

For a given set of θ_{con} flapping of the main rotor β could be found by using final flapping Eq's. (4.106), (4.107) and (4.108) or vice versa. For the trim analyses, β is found by using the force and moment equilibrium equations which is discussed in Section 4.14.2. By implementing obtained β harmonics, control inputs θ_{con} could be calculated by using Eq's. from (4.106) to (4.108).

Another point regarding the flapping equations is that as it could be seen from the equations, flapping harmonics are coupled with each other since blade aerodynamic forces depend on the perpendicular speed coming from the flap motion. Therefore, an iterative solution procedure is needed to solve the flapping harmonics.

Now let us re-write rotor hub moment. There are three components of the rotor hub moment:

- Aerodynamic force: F_z in the normal direction of the blade. Moment arm of this force about the hub is r.
- Centrifugal force: $m\Omega^2 r dr$ in the direction of radially outward. Moment arm of this force about the hub is $z = \eta\beta$.
- Inertial force: $m\ddot{z}dr = m\eta\ddot{\beta}dr$ in the opposite direction of the flap motion. Moment arm of this force about the root is r.

Therefore, rotor hub moment produced by one blade could be written as:

$$M_H = -\left(\ddot{\beta} + \Omega^2\beta\right)\int_{eR}^{R} m\eta r dr + \int_{r_R}^{BR} F_z r dr \qquad (4.109)$$

From the relation given in Eq. (4.70), Eq. (4.109) could be re-written:

$$
\begin{aligned}
M_H &= -\left(\frac{1}{\widehat{I_b}}\int_{r_R}^{BR} F_z \eta dr - (\xi\Omega)^2\beta + \Omega^2\beta\right)\int_{eR}^{R} m\eta r dr + \int_{r_R}^{BR} F_z r dr \\
&= \Omega^2(\xi^2-1)\beta\int_{eR}^{R} m\eta r dr - \frac{1}{\widehat{I_b}}\int_{r_R}^{BR} F_z\eta dr \int_{eR}^{R} m\eta r dr + \int_{r_R}^{BR} F_z r dr \\
&= \Omega^2(\xi^2-1)\beta\widehat{I_a} - \frac{\widehat{I_a}}{\widehat{I_b}}\int_{r_R}^{BR} F_z\eta dr + \int_{r_R}^{BR} F_z r dr \\
&= \Omega^2(\xi^2-1)\beta\widehat{I_a} + \int_{r_R}^{BR} F_z\left(r - \frac{\widehat{I_a}}{\widehat{I_b}}\eta\right) dr
\end{aligned}
\tag{4.110}
$$

where $\widehat{I_b}$ is given as $\int_{eR}^{R}\eta^2 m dr$ in Section 4.11.1 and $\widehat{I_a}$ is main rotor blade second-order inertia and defined as $\int_{eR}^{R} m\eta r dr$.

To find steady-state solution of the main rotor hub, second and third operands given in Eq. (4.95) should be used.

$$
\begin{aligned}
M_Y &= -N_b\frac{2}{N_{az}}\sum_{n=1}^{n=N_{az}} M_H \cos\psi_n \\
&= -N_b\Omega^2(\xi^2-1)\beta_{1c}\widehat{I_a} \\
&\quad + N_b\frac{2}{N_{az}}\int_{r_R}^{BR}\left(\sum_{n=1}^{n=N_{az}} F_{z,n}\cos\psi_n\right)\left(\frac{\widehat{I_a}}{\widehat{I_b}}\eta - r\right) dr
\end{aligned}
\tag{4.111}
$$

$$
\begin{aligned}
M_X &= N_b\frac{2}{N_{az}}\sum_{n=1}^{n=N_{az}} M_H \sin\psi_n \\
&= N_b\Omega^2(\xi^2-1)\beta_{1s}\widehat{I_a} \\
&\quad + N_b\frac{2}{N_{az}}\int_{r_R}^{BR}\left(\sum_{n=1}^{n=N_{az}} F_{z,n}\sin\psi_n\right)\left(r - \frac{\widehat{I_a}}{\widehat{I_b}}\eta\right) dr
\end{aligned}
\tag{4.112}
$$

Integrals given in Eq's. (4.111) and (4.112) could be replaced by summation symbols such that:

$$M_Y = -N_b\Omega^2(\xi^2-1)\beta_{1c}\widehat{I_a} + N_b\frac{2}{N_{az}}\left(\sum_{m=1}^{N_{bem}}\left\{\sum_{n=1}^{n=N_{az}}F_{z_{m,n}}\cos\psi_n\right\}_m\left(\frac{\widehat{I_a}}{\widehat{I_b}}\eta_m - r_m\right)\Delta r\right) \quad (4.113)$$

$$M_X = N_b\Omega^2(\xi^2-1)\beta_{1s}\widehat{I_a} + N_b\frac{2}{N_{az}}\left(\sum_{m=1}^{N_{bem}}\left\{\sum_{n=1}^{n=N_{az}}F_{z_{m,n}}\sin\psi_n\right\}_m\left(r_m - \frac{\widehat{I_a}}{\widehat{I_b}}\eta_m\right)\Delta r\right) \quad (4.114)$$

Note that blade element summations are done for the elements between the aerodynamic root cutout and tip loss.

4.14 Force and Moment Equilibrium in Forward Flight

In this section, force, and moment equilibrium of the aircraft in forward flight will be discussed in detail. The flight condition where all forces and moments are in equilibrium is called as **trim** or **trim points.** Trim points are one of the key parameters in helicopter flight analyses power calculations for the helicopters are done according to the trim points.

4.14.1 Force Equilibrium

Force equilibrium calculations are done w.r.t the two sets of forces. First one is **longitudinal forces** which consist of rotor longitudinal force H, fuselage aerodynamic drag D. Second set of forces is defined by fuselage side force Y_F, rotor lateral force Y. Latter set of forces is called as **lateral forces**. Rotor thrust T and the weight of the aircraft W contribute both longitudinal and lateral forces.

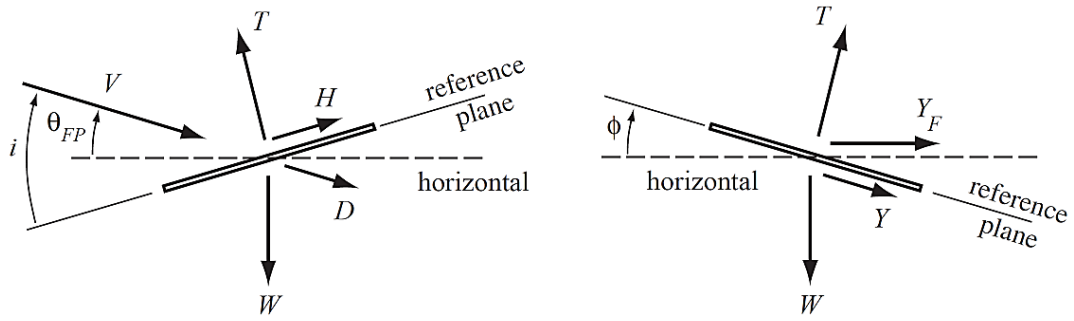

a) Longitudinal forces b) Lateral force (aft view)

Figure 4.26. Forces on the main rotor in forward flight. [12]

θ_{FP} is called flight path angle which is the angle between the speed of the aircraft and the horizontal plane. If the helicopter flies in the horizontal plane; in other words, does not change its altitude, θ_{FP} is zero. i is called as tilt angle or angle of attack of the rotor. i is defined between the speed of the aircraft and reference plane. Φ is the roll angle of the reference plane. Φ is also called as lateral tilt.

By using Figure 4.26, longitudinal force equilibrium could be written for both in vertical and horizontal axis, respectively.

$$W = T\,cos(i - \theta_{FP}) - D\,sin\,\theta_{FP} + H\,sin(i - \theta_{FP}) \tag{4.115}$$

$$D\,cos\,\theta_{FP} + H\,cos(i - \theta_{FP}) = T\,sin(i - \theta_{FP}) \tag{4.116}$$

For small angles and flight in horizontal plane, Eq's. (4.115) and (4.116) could be written as:

$$W = T \tag{4.117}$$

$$D + H = Ti \tag{4.118}$$

In Eq. (4.63), H is given as $H_{TPP} - \beta_{1c}T$ for small angle β_{1c}. Therefore, Eq. (4.118) becomes:

$$D + H_{TPP} - \beta_{1c}T = Ti \tag{4.119}$$

From Eq. (4.119) incidence of the reference plane could be found as:

$$i = \frac{D}{T} + \frac{H_{TPP}}{T} - \beta_{1c} \tag{4.120}$$

For the lateral force equilibrium:

$$Y_F + Y\cos\Phi + T\sin\Phi = 0 \tag{4.121}$$

$$W = T\cos\Phi - Y\sin\Phi \tag{4.122}$$

From Eq's. (4.121) and (4.122), roll angle of the rotor disk could be found as by implementing Eq. (4.64):

$$\Phi = -\frac{Y_F}{W} - \frac{Y_{TPP}}{T} + \beta_{1s} \tag{4.123}$$

4.14.2 Moment Equilibrium

Rotor hub moments could be divided into two sub-sets as forces are divided. First moment set is called as **pitch moments**. M_Y is rotor hub pitch moment, M_{YF} is fuselage aerodynamic pitching moment, h is the vertical distance between the rotor hub and center of gravity of the aircraft in body-fixed frame, i_s is the longitudinal tilt of the rotor shaft and is equal to $(i - \theta_{FP})$, X_{CG} is the horizontal distance between the rotor hub and center of gravity of the aircraft in the x-axis of body-fixed frame. Second set is **rolling moments**. M_X is the rotor hub rolling moment, M_{XF} is the fuselage aerodynamic moment in rolling direction, Y_F is the fuselage aerodynamic side force, Φ_s is the shaft roll angle which is equal to the Φ, Y_{CG} is the horizontal distance between the rotor hub and center of gravity of the aircraft in the y-axis of body-fixed frame.

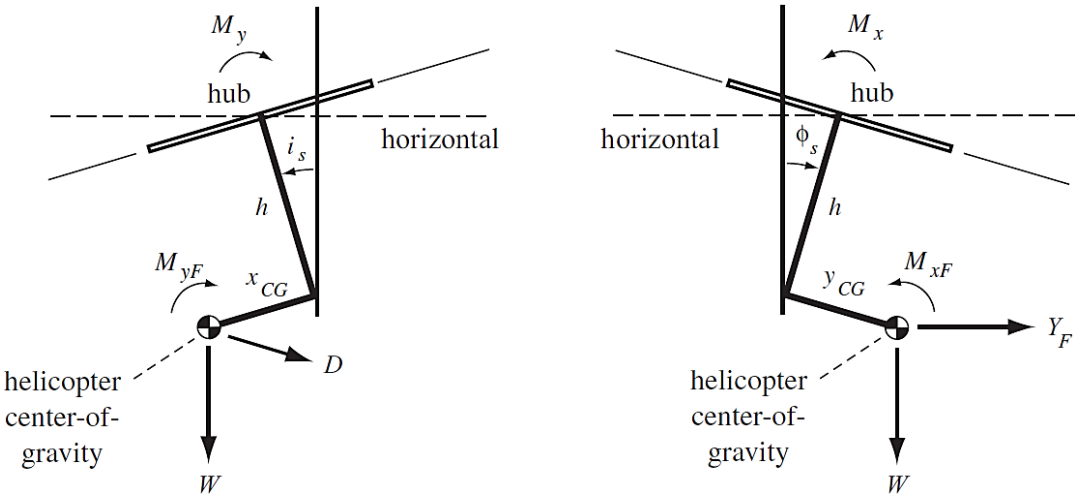

a) Pitch moments b) Roll moments

Figure 4.27. Moments on the main rotor in forward flight. [12]

From Figure 4.27, moment equilibrium w.r.t rotor hub could be written for pitch moments assuming small angles:

$$M_Y + M_{YF} + W(hi_s - X_{CG}) - hD = 0 \tag{4.124}$$

From Eq. (4.124) i_s could be solved:

$$i_s = i - \theta_{FP} = \frac{X_{CG}}{h} + \frac{D}{W} - \frac{M_{YF}}{Wh} - \frac{M_Y}{Wh} \tag{4.125}$$

Note that for the flights in the horizontal plane θ_{FP} is zero which results $i_s = i$.

Roll moment equilibrium is written by making small angle assumption:

$$M_X + M_{XF} + W(h\Phi_s - Y_{CG}) + hY_F = 0 \tag{4.126}$$

Φ_s could be written as from Eq. (4.126):

$$\Phi_s = \Phi = \frac{Y_{CG}}{h} - \frac{Y_F}{W} - \frac{M_{XF}}{Wh} - \frac{M_X}{Wh} \tag{4.127}$$

By combining Eq. (4.120) with Eq. (4.125) and Eq. (4.123) with Eq. (4.127), β_{1c} and β_{1s} for the trimmed flight could be written as:

$$\beta_{1c} = \frac{D}{T} + \frac{H_{TPP}}{T} - \left(\frac{X_{CG}}{h} + \frac{D}{W} - \frac{M_{YF}}{Wh} - \frac{M_Y}{Wh}\right) \tag{4.128}$$

$$\beta_{1s} = \frac{Y_F}{W} + \frac{Y_{TPP}}{T} + \left(\frac{Y_{CG}}{h} - \frac{Y_F}{W} - \frac{M_{XF}}{Wh} - \frac{M_X}{Wh}\right) \tag{4.129}$$

If Eq's. (4.113) and (4.114) are put into Eq's. (4.128) and (4.129) respectively, flapping harmonics in trim flight is found as:

$$\beta_{1c} = \frac{\frac{D}{T} + \frac{H_{TPP}}{T} - \frac{X_{CG}}{h} - \frac{D}{W} + \frac{M_{YF}}{Wh} + \frac{M_{YY}}{Wh}}{1 + \frac{N_b \Omega^2 (\xi^2 - 1)\widehat{I_a}}{Wh}} \tag{4.130}$$

$$\beta_{1s} = \frac{\frac{Y_F}{W} + \frac{Y_{TPP}}{T} + \frac{Y_{CG}}{h} - \frac{Y_F}{W} - \frac{M_{XF}}{Wh} - \frac{M_{XX}}{Wh}}{1 + \frac{N_b \Omega^2 (\xi^2 - 1)\widehat{I_a}}{Wh}} \tag{4.131}$$

where, M_{YY} and M_{XX} are longitudinal and lateral component of the rotor hub pitching and rolling moment respectively. M_{YY} and M_{XX} are given as:

$$\begin{aligned} M_{YY} &= N_b \frac{2}{N_{az}} \left(\sum_{m=1}^{N_{bem}} \left\{ \sum_{n=1}^{n=N_{az}} F_{z_{m,n}} \cos\psi_n \right\}_m \left(\frac{\widehat{I_a}}{\widehat{I_b}} \eta_m - r_m \right) \Delta r \right) \\ M_{XX} &= N_b \frac{2}{N_{az}} \left(\sum_{m=1}^{N_{bem}} \left\{ \sum_{n=1}^{n=N_{az}} F_{z_{m,n}} \sin\psi_n \right\}_m \left(r_m - \frac{\widehat{I_a}}{\widehat{I_b}} \eta_m \right) \Delta r \right) \end{aligned} \tag{4.132}$$

4.15 Performance in Forward Flight

The term performance is used for calculation of the required power and comparing the required power with the power available. Performance calculations are usually done for over a range of forward flight speed. In this section, details of the power calculations for the forward flight will be discussed.

Power required for the main rotor in a flight could be described as sum of the four parts. First one is called as **induced power**. Induced power describes the power needed to lift the aircraft. Induced power is directly related to thrust and induced flow. Second one is the **profile power** which describes the power needed to turn the blades in air. As it could be understood from the description, profile power is calculated by the rotor torque which is mainly determined by the aerodynamic drag forces acting on the blade. Third part is called as **parasite power**. Parasite power is the power needed to move the aircraft in air medium and it is related to the helicopter's forward flight speed and aerodynamic drag force of the fuselage. Last one is the **climb power**. As its name suggests, climb power is the power needed to change the aircraft's altitude. Induced power, profile power, parasite power and climb power relations are given respectively as:

$$P_i = T v_i, \quad P_o = \Omega Q, \quad P_p = DV, \quad P_c = TV_c \tag{4.133}$$

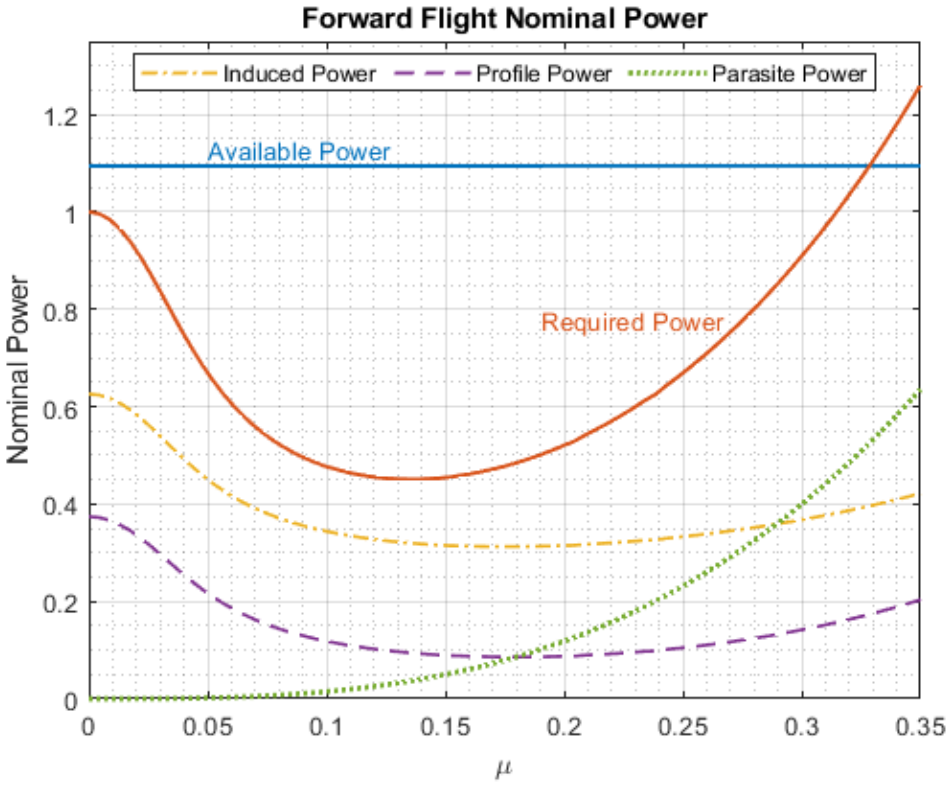

Figure 4.28. Typical required power graph for helicopters in trimmed forward flight.

In Figure 4.28, it is seen that required power decreases as the forward flight speed increases up to some point, then required power starts to increase. There are two main reasons of this decrease in the required power. First one is that as the forward flight speed increases, inflow decreases as discussed in Section 4.2. A decrease in inflow results a decrease in induced power for constant thrust as well. Second one is that as the inflow angle ϕ decreases with forward flight speed, sectional lift contribution to the horizontal force decreases which dampens the required profile power since horizontal force of the blade depends on not only drag force but also sectional lift force as given in Eq. (4.26). Although parasite power increases with the forward flight speed, decrease in the induced and profile power dominates the overall performance up to a certain level. After some point, parasite power starts to dominate the performance; hence, the required power increases.

4.16 Trimmed Forward Flight Analysis

As it is discussed in the very beginning of Section 0, performance calculations of a helicopter are conducted in trim points. Therefore, trim analysis must be done carefully to obtain trim points adequately. In this section, details of the trim analysis of the reference helicopter and effects of the torsional twist experienced by the blade to the trim points and performance characteristics will be discussed.

4.16.1 Trim Analysis

In the very end of Section 0, a closed form of the flapping harmonics is given. Therefore, necessary flapping harmonics for a forward flight could be found by using Eq's. (4.128) and (4.129). By putting the necessary flapping harmonics into Eq's. (4.106), (4.107) and (4.108), coning angle β_0 and harmonic inputs θ_{1c} and θ_{1s} could be solved. However, a closed form solution of collective input θ_0 is not given yet. In Eq. (4.40), thrust is given as:

$$T = N_b \sum_{m=1}^{N_{bem}} (F_z)_m \tag{4.134}$$

where the summation starts from the aerodynamic root cutout and ends at where the tip loss effect starts. In an explicit form, Eq. (4.134) could be written as:

$$T = N_b \sum_{m=1}^{N_{bem}} \frac{1}{2} \rho c \frac{c_{l_\alpha}}{\sqrt{1 - M_m^2}} \left(u_{T_m}^2 \theta_m - u_{T_m} u_{P_m} \right) \tag{4.135}$$

If right hand side of Eq. (4.135) is written explicitly there will be lots of higher order harmonic terms. On the other hand, thrust T is independent of any harmonics. To obtain a steady-state solution, first operand given in Eq. (4.95) could be used. If the operand applied to the right-hand side of Eq. (4.135) a similar expression will be obtained given in Eq. (4.106):

$$T = N_b \sum_{m=1}^{N_{bem}} \frac{1}{2}\rho c C_{L_\alpha} \Bigg(\theta_0 \left\{ (\Omega r_m)^2 H_m^{0,0} + 2\Omega r_m V H_m^{1,0} + V^2 H_m^{2,0} \right\} + \theta_{1s} \left\{ (\Omega r_m)^2 H_m^{1,0} + 2\Omega r_m V H_m^{2,0} + V^2 H_m^{3,0} \right\} + \beta_{1c} \left\{ \Omega^2 r_m \eta_m H_m^{1,0} - \Omega r_m V \eta'_m H_m^{0,2} + \Omega V \eta_m H_m^{2,0} - V^2 \eta'_m H_m^{1,2} \right\} - \nu \left\{ \Omega r_m H_m^{0,0} + V H_m^{1,0} \right\} + \frac{1}{N_{az}} \sum_{n=1}^{n=N_{az}} \frac{1}{\sqrt{1 - M_{m,n}^2}} u_{T\,m,n}^2 \theta_{tw\,m,n} \Bigg) \Delta r \quad (4.136)$$

In trim analysis, thrust T is equated to the aircraft's weight W in the first iteration step. Therefore, from Eq. (4.136), collective input θ_0 could be solved. However, as it could be seen that there are θ_{1s} and θ_{tw} terms in Eq. (4.136). If torsional twist θ_{tw} expression given in Section 4.12.3 and Eq. (4.105) which gives longitudinal cyclic input θ_{1s} are inspected in detail, it is seen that the control inputs, torsional twist, flapping harmonics, rotor forces are all coupled. Therefore, an iterative solution is needed to be implemented. In Figure 4.29, iterative solution procedure for trim analysis is given as a flowchart then trim analysis solution procedure is explained step-by-step in detail.

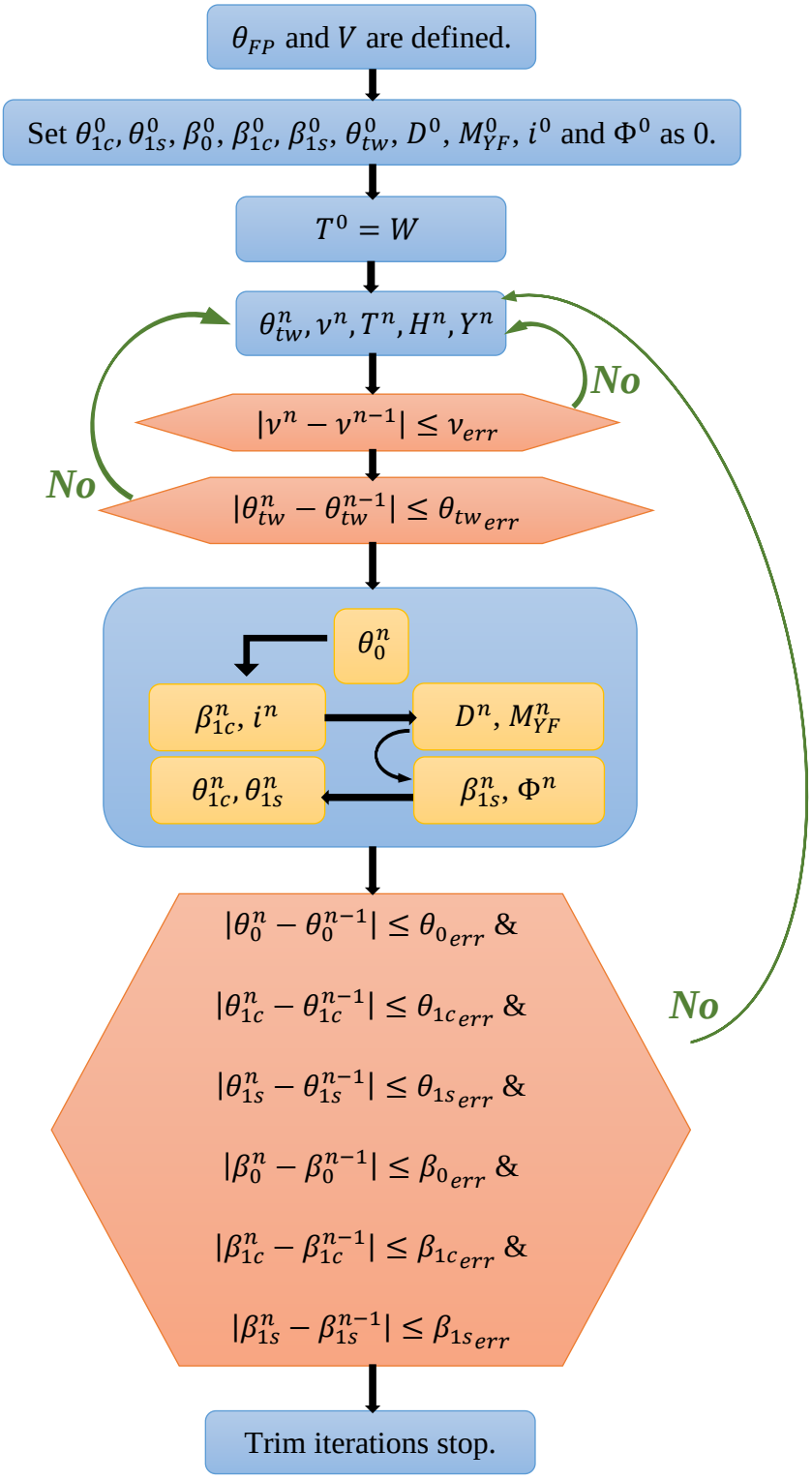

Figure 4.29. Trim iterations flowchart.

Steps of the trim iterations given in Figure 4.29:

1. Define a flight path angle θ_{FP} and a forward flight velocity of the helicopter V.
2. Assume that cyclic inputs θ_{1c}, θ_{1s}, flapping angles β_0, β_{1c}, β_{1s}, torsional twist field of the blade θ_{tw}, fuselage aerodynamic loads D, M_{YF}, pitching and rolling angles i and Φ are all zero for the first step of the iterations.
3. From Eq. (4.136) calculate the collective input θ_0 by assuming $v = \sqrt{W/2\rho A}$ from Eq. (4.1) and $T = W$.
4. Set the azimuth angle as 0°.
5. Calculate tangential and perpendicular velocities of the blade section from Eq's. (4.41) and (4.54) respectively then obtain inflow angle ϕ.
6. Calculate aerodynamic lift and drag forces of the blade elements and obtain torsional twist for each blade element.
7. Increment the azimuth angle and repeat the steps from 5 to 9 for all azimuth angles.
8. After completing one revolution, calculate the rotor forces T, H, Y and uniform inflow from Eq's. (4.40), (4.57), (4.58) and (4.1) respectively.
9. Go to the step-4 and continue the iterations until inflow and twist of the blade is converged.
10. Calculate the new collective input from the relation given in Eq. (4.136).
11. From the relation in Eq's. (4.125) and (4.127), calculate pitching and rolling angle of the aircraft respectively. After finding pitching angle of the aircraft, fuselage aerodynamic drag force and pitching moment are calculated.
12. Since all the aerodynamic loads are calculated, necessary flapping harmonics β_{1c} and β_{1s} could be found from Eq's. (4.128) and (4.129).
13. From the harmonic solutions given in Eq's. (4.106), (4.107) and (4.108), coning angle β_0 and necessary cyclic inputs θ_{1c} and θ_{1s} could be solved for the flight condition defined in step-1.
14. Return to step-4 and continue the iterations until control input θ and flapping angle β are converged.

4.17 Results of the Trim Analysis

4.17.1 Elastic Twist in Trim

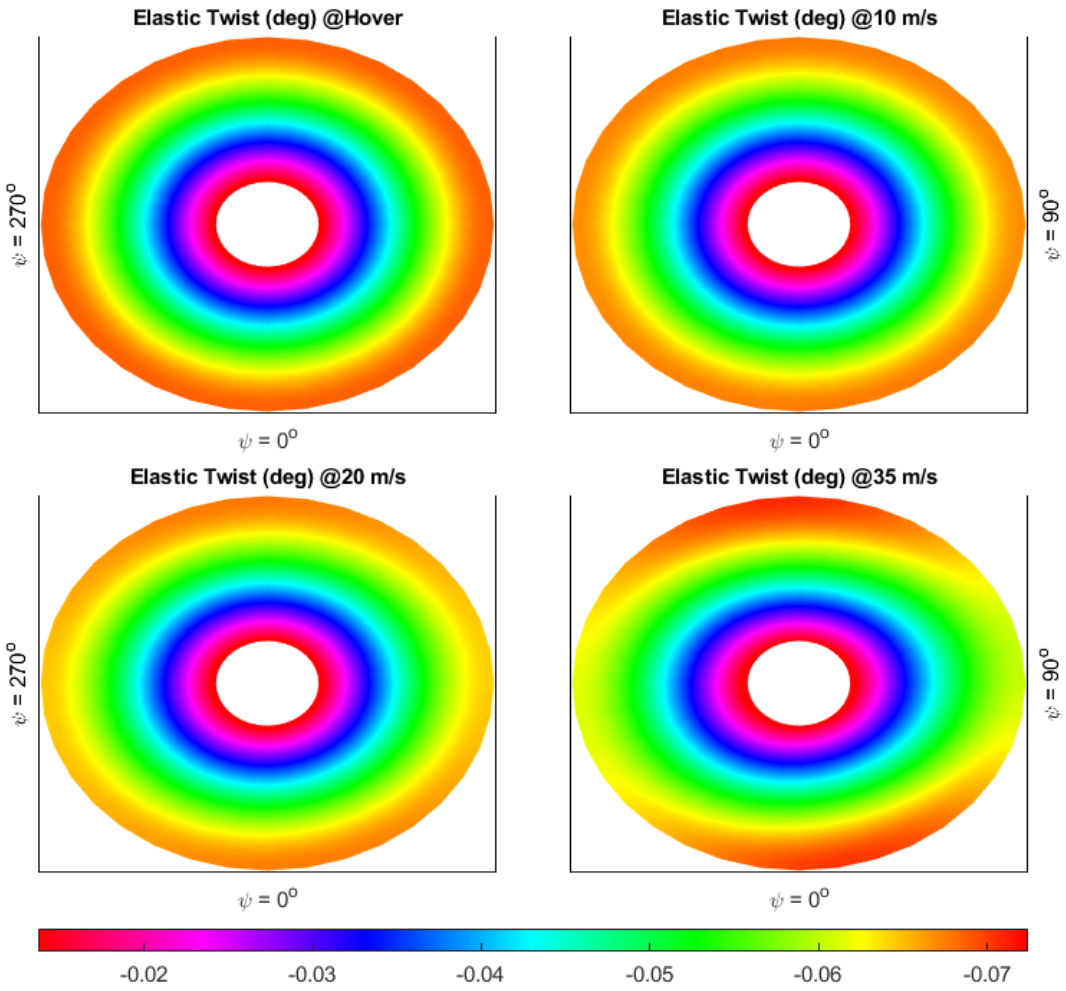

Figure 4.30. Elastic twist field on the rotor for different forward flight speeds.

Figure 4.30 illustrates the elastic twist field of the blade. In Figure 4.30, it is seen that elastic twist field is axially symmetric in both lateral and longitudinal direction in hover flight since aerodynamic loads are axially symmetric in hover condition. However, as the forward flight speed increases elastic twist field becomes unsymmetrical in both fore-aft and left-right direction. The main reason behind this situation is that as the forward flight speed increases helicopter gets both a pitching and a rolling angle. Therefore, thrust vector tilts both in longitudinal and lateral

axes which decreases the vertical component of the thrust vector; however, main purpose of the thrust vector is balancing the weight. To balance the weight of the helicopter, inputs are given such that thrust of the rotor would balance the weight. As a result, an unsymmetrical load distribution occurs which creates an unsymmetrical twist field.

Another important result observed from Figure 4.30 is that the elastic twist is in the order of 0.05 degrees. Although the magnitude of the elastic twist could be considered as very small, to be able to make any comment about the magnitude and the effects of the twist, collective and cyclic inputs should be inspected as well.

4.17.2 Collective Input in Trim

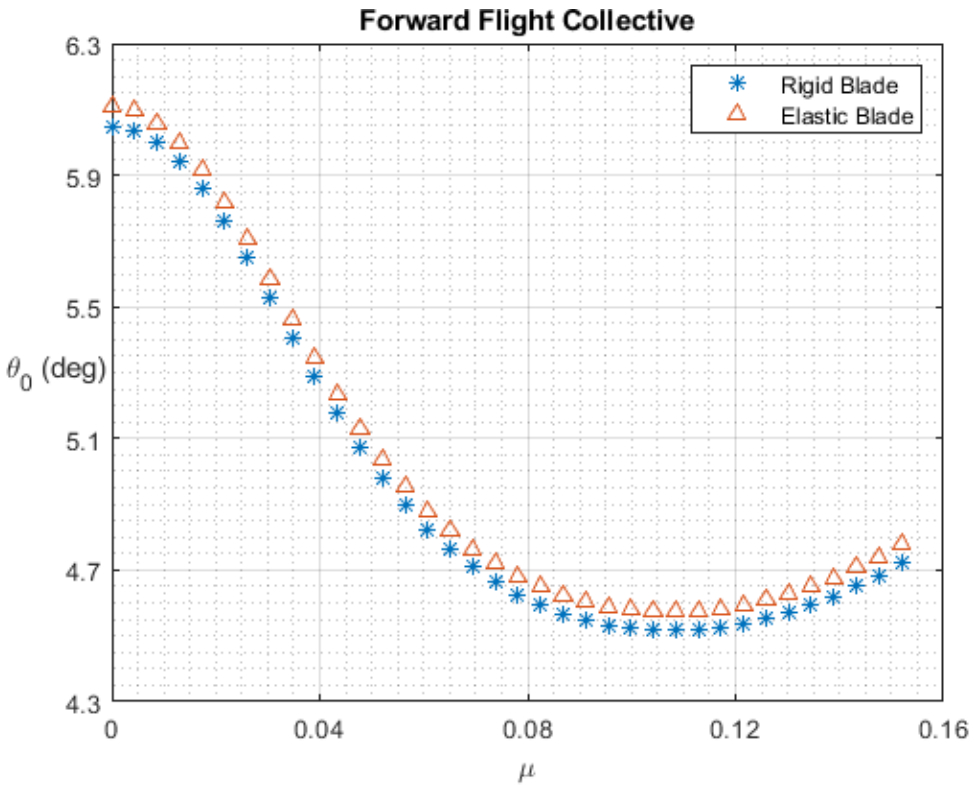

Figure 4.31. Collective input in forward flight.

As it could be seen from Figure 4.31, collective input θ_0 is in the order of 4 to 6 degrees. If the twist is compared with the collective input, the effect of the twist is observed very small. The collective input difference between the rigid and elastic

blade is about 0.05 degrees. Therefore, it could be stated that the effect of the elastic twist is negligible in terms of collective input.

A typical characteristic of the collective input in trimmed forward flight obtained in Figure 4.31 which is the decreasing trend in collective input as the forward flight speed increases. The main reason behind this phenomenon is that as the inflow decreases with forward flight up to some forward flight speed, negative effect of the inflow on the angle of attack decreases as well. Hence, necessary collective input to produce same thrust decreases.

4.17.3 Cyclic Inputs in Trim

Now let us examine the effect of the torsional twist to the cyclic inputs θ_{1c} and θ_{1s}.

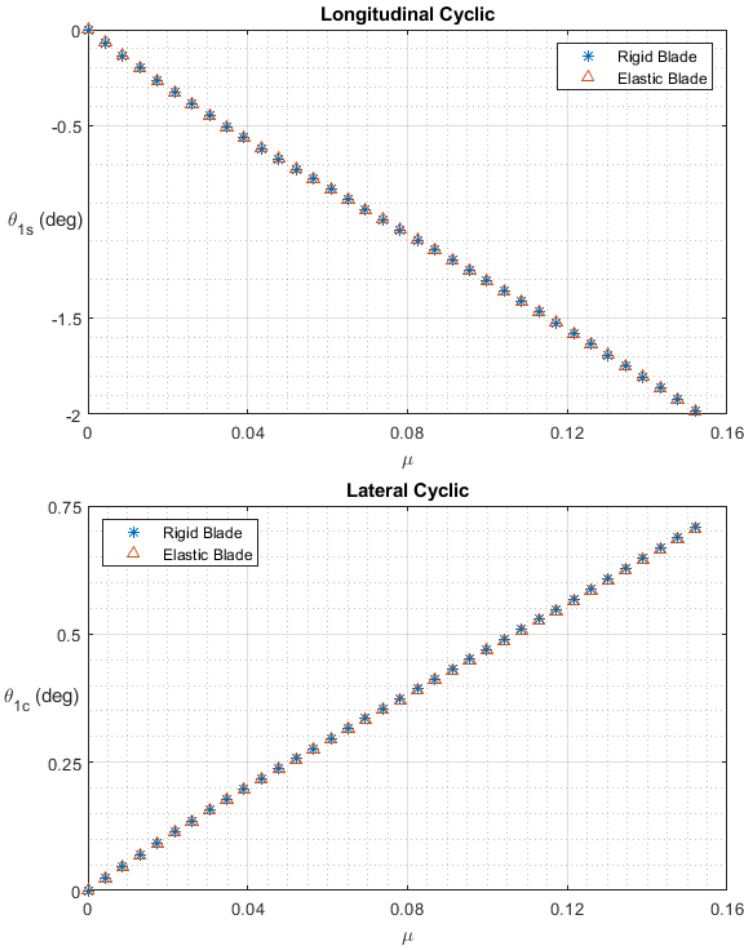

Figure 4.32. Longitudinal and lateral cyclic input in forward flight.

To balance the lift distribution between the advancing and retreating side, longitudinal cyclic is given negative. So that the lift balance is obtained by increasing the angle of attack in the retreating side where the dynamic pressure is lower than the advancing side and decreasing the angle of attack in the advancing side.

As the forward flight speed increases, fuselage aerodynamic drag force increases as well. To overcome fuselage aerodynamic drag force, θ_{1c} increases as the forward flight speed increases as it could be seen from Figure 4.32.

Figure 4.32 also shows that the cyclic inputs for elastic and rigid blade are almost identical. Therefore, it could be stated that rigid blade assumption is valid for the reference blade and reference helicopter in terms of control inputs.

4.17.4 Required Power in Trim

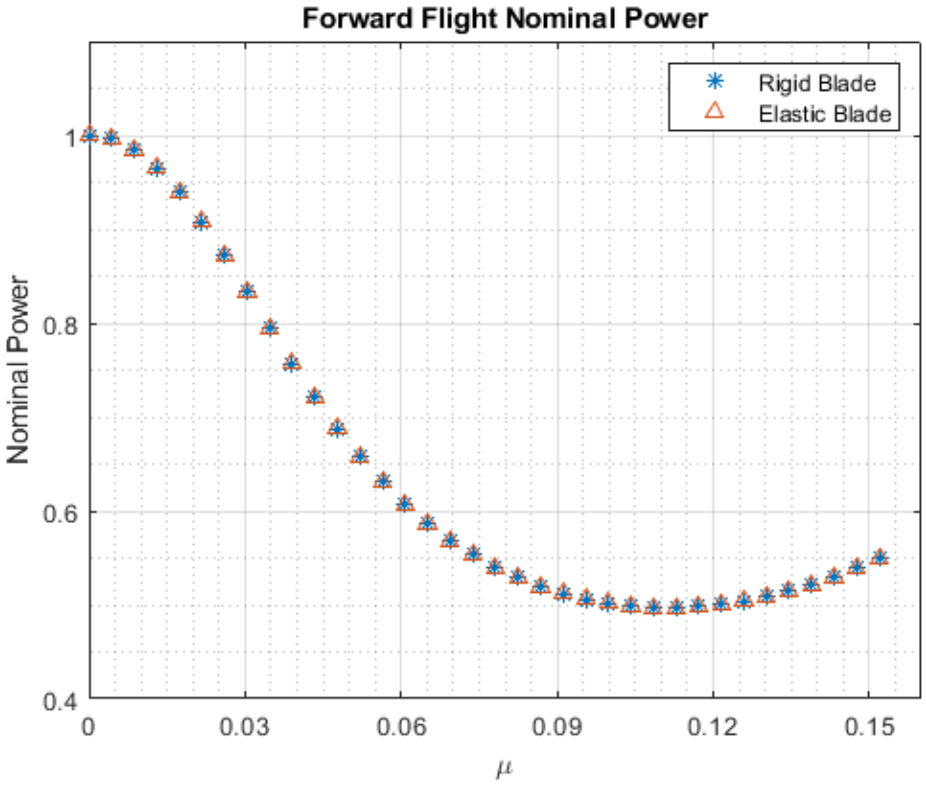

Figure 4.33. Required power in trimmed forward flight.

Another important performance outcome of the trimmed forward flight is the required power curve. In Figure 4.33, it is observed that required power decreases about %55 w.r.t hover as forward flight speed increases. As it is discussed in Section 0, during the decreasing phase of the required power, dominating power terms are induced and profile powers. Since the induced power is related with thrust and torsional twist is very low, the difference between induced and profile power terms are almost zero for rigid and elastic blade in Figure 4.33.

4.17.5 Incidence (Pitch) and Roll Angle in Trim

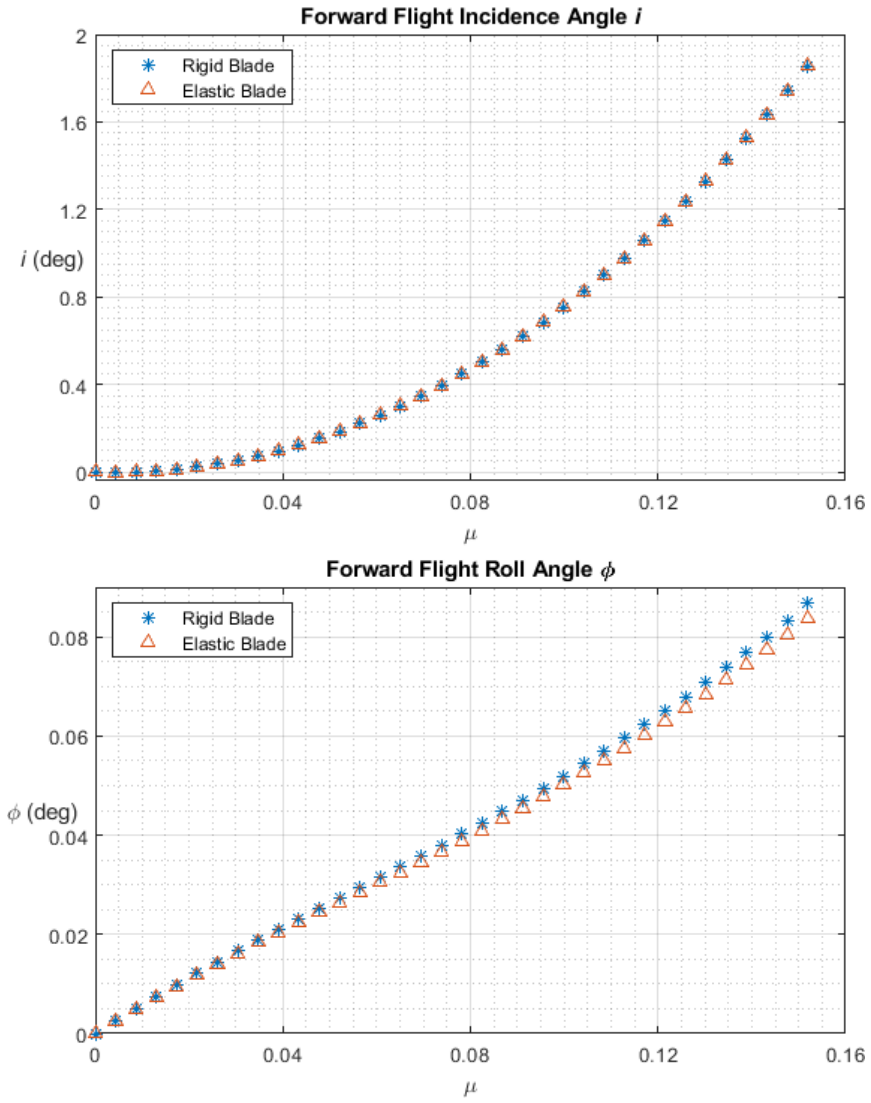

Figure 4.34. Forward flight incidence (pitch) and rolling angle of the helicopter.

In Figure 4.34, it is observed that incidence angle increases as the forward flight speed increases which is an expected result from a general sense. It is also observed that incidence angle increases up to 2 degrees. Although 2 degrees could be considered as small tilt, maximum incidence angle of the reference helicopter in maximum forward flight could be stated as considerably high compared to the rotor longitudinal flapping angle shown in Figure 4.36. If the rotor design of the reference helicopter is chosen as articulated rather than hingeless, it could be expected that this big difference between rotor longitudinal angle and helicopter tilt angle would be smaller since rotor hub moment will decrease and required rotor thrust tilt could be achieved by longitudinal flapping instead of tilting whole helicopter.

It is also observed that roll angle increases with the forward flight speed. However, it might not be easy to expect any roll angle during forward flight. Although the magnitude of the rolling angle is small, roll angle occurs due to the rotor hub moment M_X which occurs with asymmetrical lift distribution of the rotor in forward flight. It is also observed that there is a slight difference in the rolling angle between elastic and rigid blade. The main reason behind this is that magnitude of the rolling angle is in the order of elastic twist of the blades which makes the difference between elastic and rigid blade results could be seen clearly.

4.17.6 Main Rotor Forces and Moments in Trim

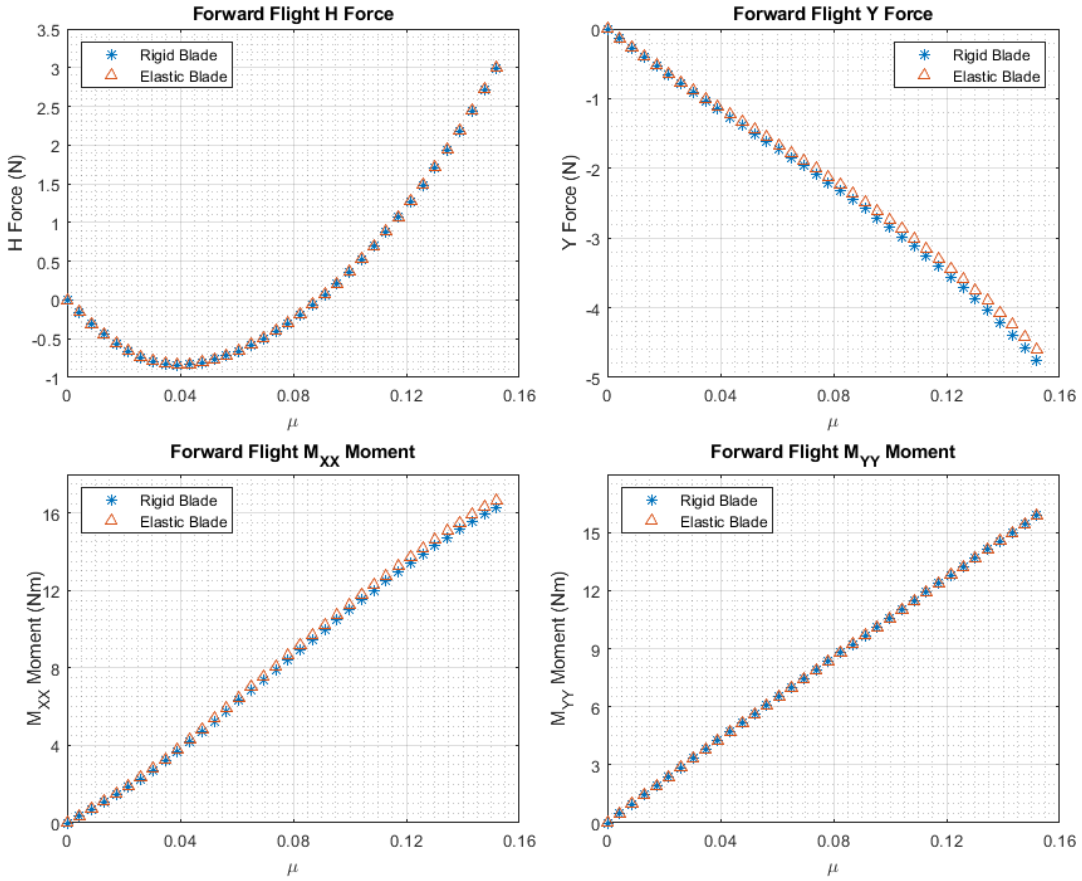

Figure 4.35. Rotor force and moment components in forward flight.

As a general sense, main expectation is that as the forward flight speed increases rotor longitudinal force increases as well; however, it is seen that rotor longitudinal force decreases up to some forward flight speed then starts to increase. In Eq. (4.63), rotor longitudinal force H consists of two parts. First one is the TPP component of the force which increases as the forward flight speed. Second one is the $-T\beta_{1c}$ term. For the low forward flight speeds, $-T\beta_{1c}$ dominates the rotor longitudinal force negatively; therefore, rotor H force decreases up to some forward flight speeds then it starts to increase.

If rotor lateral force is inspected from Figure 4.35, it is observed that rotor lateral force increases as the forward flight speed increases. Although it could be expected

that magnitude of the rotor lateral force Y would increase, making a comment about the sign of the rotor lateral force Y at the first sight may be hard since it depends on both flapping angles and cyclic inputs. However, if Eq. (4.64) is considered, it could be expected that rotor lateral force Y will increase in the negative direction since thrust is much greater than the Y_{TPP}.

In Figure 4.35, rotor M_{XX} and M_{YY} moment components are given as well. From the figure it is seen that they increase as the forward flight speed since aerodynamic forces experienced by the blades become asymmetrical as forward flight speed increases. Hence, this asymmetrical aerodynamic load profile increases the rotor hub moment components M_{XX} and M_{YY}.

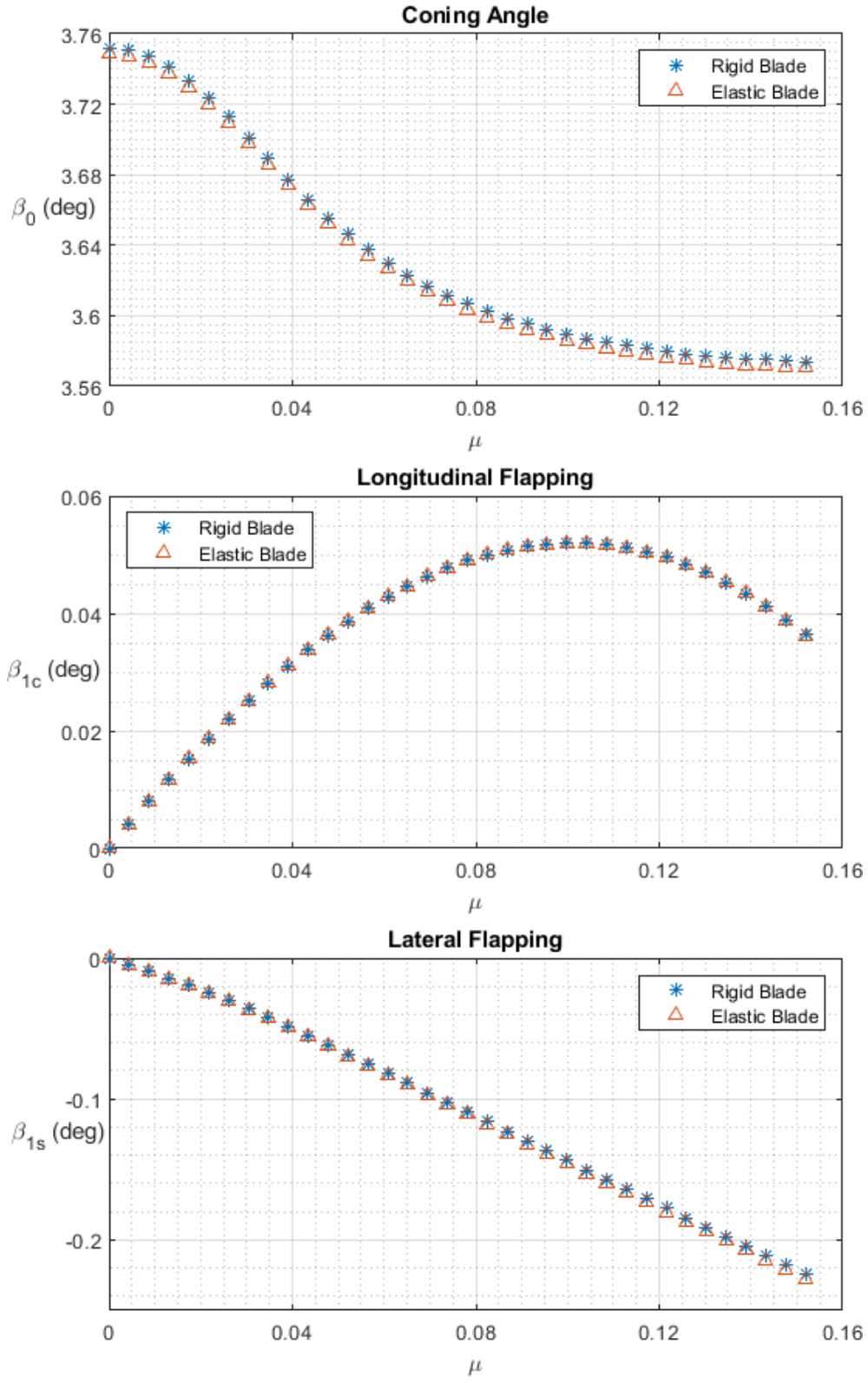

Figure 4.36. Coning angle, longitudinal and lateral flapping in forward flight.

From Figure 4.36, it is observed that coning angle β_0 has a similar characteristic to the collective input in the given forward flight speed range. If Eq. (4.106) is inspected in detail, it is seen that collective angle θ_0 and inflow ν are the main contributing parameters to the coning angle β_0. In Section 4.2 and in Figure 4.31, it is shown that inflow and collective input decreases as forward flight speed increases. Although, the inflow term appearing in Eq. (4.106) has an opposing effect on coning angle β_0, decrease in the collective input is more dominant than the inflow. Hence, coning angle β_0 decreases as the forward flight speed increases. In addition, it is observed that there is a slight difference between the rigid and elastic blade in terms of coning angle. Collective input and torsional twist are the only differentiating terms between the rigid and elastic blade contributing the coning angle. Collective input difference between rigid and elastic blade is about 0.01 degrees and the torsional deformation is in the order of 0.05 degrees averagely. When these differences are combined, it is seen that coning angle is slightly lower for the elastic blade than the rigid blade.

In Figure 4.36, longitudinal flapping β_{1c} increases up to some point then starts to decrease as the forward flight increases. In Eq. (4.130), it is seen that longitudinal flapping angle β_{1c} depends on rotor longitudinal force, fuselage aerodynamic pitching moment and rotor hub moment since fuselage drag force terms cancels each other for the reference helicopter. In the increasing region, rotor hub moment and rotor longitudinal force dominates the longitudinal flapping angle. As forward flight speed increases, fuselage aerodynamic pitching moment starts to dominating longitudinal flapping angle negatively. Hence, longitudinal flapping starts to decrease after some point as the forward flight speed increases.

Lateral flapping β_{1s} decreases as the forward flight speed increases as it could be seen from Figure 4.36. In Eq. (4.131), lateral flapping is affected by only rotor Y force and rotor hub moment in rolling direction since other terms are zero for the reference helicopter. Rotor hub moment component M_{XX} increases as the forward flight speed increases. However, rotor hub moment component M_{XX} is given with

negative sign in Eq. (4.131). Therefore, as the forward flight speed increases rotor hub moment component M_{XX} decreases the lateral flapping angle. Whereas rotor lateral force Y is given same sign with lateral flapping angle such that lateral flapping angle would have same tendency with rotor lateral force Y. In Figure 4.35, it is observed that Y force decreases. Hence, lateral flapping angle β_{1s} decreases as well.

CHAPTER 5

DYNAMIC AEROELASTICITY

Dynamic aeroelasticity is a brand of the aeroelasticity in which aerodynamic loads are unsteady and inertial forces are considered in contrast to static aeroelasticity in which unsteady effects in the aerodynamic loads and inertial forces are neglected.

As it is discussed in detail in Ch. 4, helicopter blades are experiencing a time dependent load profile. Although one of the main assumptions made in Ch. 4 is assuming the aerodynamic loads to be steady, the aerodynamics loads are not steady but time dependent actually. Therefore, dynamic aeroelastic analyses should be carried as well for the helicopter blades.

There are many dynamic aeroelastic phenomena for helicopter blades; however, in this work main focus is a phenomenon called as **flutter**. Flutter is a dynamic aeroelastic instability in which all inertial, elastic, and aerodynamic forces are interacting with each other. Since inertial forces are important in terms of the flutter, equations of motion should be revisited.

5.1 Lagrange's Equation of Motion

To be able to analyze a system by writing the equations using the Newton's laws, all the forces must be carefully included to the equations. On the other hand, in Lagrange's equations of motion, forces which do not do any work are ignored. Therefore, using Lagrangian form of equations of motion has an advantage over using Newton's laws.

5.1.1 Degrees of Freedom (Independent Coordinates)

Before developing Lagrangian form of the equations of motion, it should be stated that one of the most important concepts in Lagrangian form is degrees of freedom or number of independent coordinates. Degrees of freedom or number of independent coordinates of a system are needed to know an object's both location and orientation completely. For example, a particle's location in space could be defined completely by knowing the three coordinates of the particle i.e. its x, y, z coordinates. Therefore, a particle in space has three degrees of freedom or three independent coordinates.

Another example could be given is a wheel moving by rolling without any slippage. To define the exact location of the wheel, either total angle rotated or the distance from the starting point must be known. If one of them is known, exact location of the wheel could be expressed. Therefore, it could be said that the wheel has only one degree of freedom.

5.1.2 Generalized Coordinates

As it is discussed in the previous section, in order to define a location and orientation of a system, its independent coordinates must be known. Generalized coordinates are set of these independent coordinates which enable us to locate a system. For example, a pendulum has three sets of degrees of freedom each of which has two elements. First set is the angle and the horizontal position of the pendulum, (Θ, x). Second set is both horizontal and vertical position of the pendulum (x, y). Last set is the angle and the vertical position of the pendulum (Θ, y). In this case generalized coordinates are x, y, and Θ. Note that since the system has two degrees of freedom, all three coordinates could not be independent; therefore, one of them will be dependent.

5.1.3 Lagrange's Equation of Motion

Since details of derivation of Lagrange's equation of motion is out of scope of this work, it is directly given as by referring [10]:

$$\frac{d}{dt}\left(\frac{\partial K}{\partial \dot{q}_i}\right) - \frac{\partial K}{\partial q_i} + \frac{\partial P}{\partial q_i} = Q_i \qquad i = 1, 2, \dots, n \tag{5.1}$$

where K is the kinetic energy, P is the potential energy, q_i is the generalized coordinates, Q_i is the generalized forces acting on the system.

5.1.4 Lagrangian of a Typical Wing Section

To analyze the flutter phenomenon of a linear aeroelastic system, a spring-restrained rigid wing model called as typical section model could be used. In the typical section, bending stiffness of the wing is modeled as a linear spring and torsional stiffness of the wing is modeled as a torsional spring. Both springs are attached to the elastic axis. The attachment point is called as refence point.

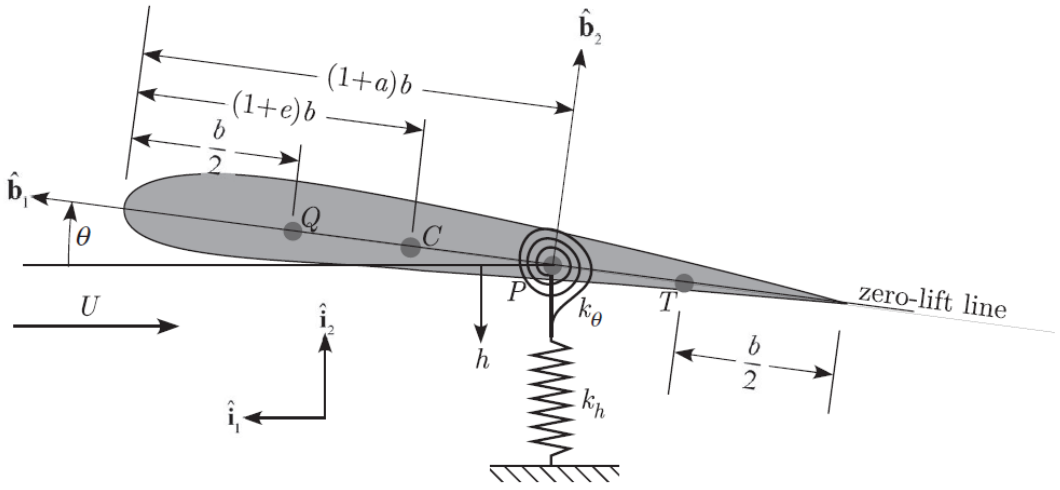

Figure 5.1. Typical wing section having stiffness in pitching and plunging directions. [10]

In Figure 5.1, the point Q represents the quarter chord which is the aerodynamic center presuming subsonic thin airfoil theory, C is the center of gravity of the

section, P is the reference point located at the elastic axis of the wing, T is the three-quarter chord point. k_h is the stiffness of the linear spring, k_θ represents the torsional spring's stiffness. To locate Q, C, P and T points, half chord b and non-dimensional constants e and a are used. U is the tangential airspeed airfoil experiences. θ is the pitch angle of the airfoil and one of the degrees of freedom of the section. h is the second degree of freedom representing the vertical displacement of the wing. Motion occurs in the θ direction called as **pitching**, whereas **plunging** is defined as the motion in the direction of h. $\hat{b}_i$ is the unit vector defining a right-handed coordinate system which is fixed to the airfoil section. $\hat{\imath}_i$ is the unit vector defining a reference frame.

Let us write the Lagrangian of the typical section. Potential energy of the system could be written as:

$$P = \frac{1}{2}k_h h^2 + \frac{1}{2}k_\theta \theta^2 \tag{5.2}$$

To write the kinetic energy expression, it is necessary to find the velocity of the center of gravity which is:

$$V_C = V_P + \dot{\theta}\hat{b}_3 \times b[(1+a) - (1+e)]\hat{b}_1 \tag{5.3}$$

V_P is the velocity of the reference point P in the inertial frame and it is given as:

$$V_P = -\dot{h}\hat{\imath}_2 \tag{5.4}$$

Negative sign in Eq. (5.4) is coming from the definition of the plunging direction. When Figure 5.1 is inspected, it is seen that plunging motion is defined in the negative direction of the $\hat{\imath}_2$. Hence, velocity of the mass center becomes:

$$V_C = -\dot{h}\hat{\imath}_2 + b\dot{\theta}(a-e)\hat{b}_2 \tag{5.5}$$

Kinetic energy of the section is:

$$K = \frac{1}{2}mV_C \cdot V_C + \frac{1}{2}I_C\,\dot{\theta}\cdot\dot{\theta} \tag{5.6}$$

where I_C is the mass moment of inertia of the airfoil about the center of gravity C. By putting Eq. (5.5) into Eq. (5.6), kinetic energy of the airfoil is obtained as:

$$\begin{aligned} K &= \frac{1}{2}m\left(\dot{h}^2 + 2b(e-a)\dot{h}\dot{\theta} + b^2(a-e)^2\dot{\theta}^2\right) + \frac{1}{2}I_C\,\dot{\theta}^2 \\ &= \frac{1}{2}m\left(\dot{h}^2 + 2bx_\theta\dot{h}\dot{\theta}\right) + \frac{1}{2}I_P\dot{\theta}^2 \end{aligned} \tag{5.7}$$

where x_θ is defined as $e-a$ and I_P is defined as $I_C + mb^2x_\theta^2$.

To complete the Lagrangian of the airfoil section, it is needed to write the generalized forces w.r.t the θ and h coordinates. In [10], generalized forces are given as:

$$Q_h = -L' \tag{5.8}$$

$$Q_\theta = M' = b\left(\frac{1}{2} + a\right)L' + M_{1/4} \tag{5.9}$$

where L' is the sectional aerodynamic lift, $M_{1/4}$ is the aerodynamic moment at the aerodynamic center Q. Note that, the reason of negative sign of L' is that L' is in the direction of $\hat{\imath}_2$ which is opposite direction of the generalized coordinate h.

Letting $q_1 = h$, and $q_2 = \theta$ and putting Eq's (5.2), (5.7), (5.8) and (5.9) into Eq. (5.1), equations of motion of the airfoil system could be written as:

$$\begin{aligned} \frac{d}{dt}\left(\frac{\partial K}{\partial \dot{h}}\right) - \frac{\partial K}{\partial h} + \frac{\partial P}{\partial h} &= Q_h \\ \frac{d}{dt}\left(\frac{\partial K}{\partial \dot{\theta}}\right) - \frac{\partial K}{\partial \theta} + \frac{\partial P}{\partial \theta} &= Q_\theta \end{aligned} \tag{5.10}$$

$$\begin{aligned} m\ddot{h} + mbx_\theta\ddot{\theta} + k_h h &= -L' \\ I_P\ddot{\theta} + mbx_\theta\ddot{h} + k_\theta h &= M' = b\left(\frac{1}{2} + a\right)L' + M_{1/4} \end{aligned} \tag{5.11}$$

Eq. (5.11) could be written in matrix form:

$$\begin{bmatrix} m & mbx_\theta \\ mbx_\theta & I_P \end{bmatrix} \begin{Bmatrix} \ddot{h} \\ \ddot{\theta} \end{Bmatrix} + \begin{bmatrix} k_h & 0 \\ 0 & k_\theta \end{bmatrix} \begin{Bmatrix} h \\ \theta \end{Bmatrix} = \begin{Bmatrix} -L' \\ M' \end{Bmatrix} \tag{5.12}$$

To simplify Eq. (5.12), introduce uncoupled natural frequencies of the airfoil section:

$$\omega_h = \sqrt{\frac{k_h}{m}} \qquad \omega_\theta = \sqrt{\frac{k_\theta}{I_P}} \tag{5.13}$$

If Eq. (5.13) is put into Eq. (5.12) and plunging motion h is non-dimensionalized by dividing by half chord b, we obtain:

$$\begin{bmatrix} mb^2 & mb^2x_\theta \\ mb^2x_\theta & I_P \end{bmatrix} \begin{Bmatrix} \ddot{h}/b \\ \ddot{\theta} \end{Bmatrix} + \begin{bmatrix} mb^2\omega_h^2 & 0 \\ 0 & I_P\omega_\theta^2 \end{bmatrix} \begin{Bmatrix} h/b \\ \theta \end{Bmatrix} = \begin{Bmatrix} -L'b \\ M' \end{Bmatrix} \tag{5.14}$$

5.2 Steady Loads Flutter

To understand general behavior of the system given in Eq. (5.14), let us assume that aerodynamic loads are steady such that:

$$L' = F_f 2\pi\rho b U^2 \theta \qquad M_{1/4} = 0 \tag{5.15}$$

where F_f is the ratio of lift-curve slope c_{l_α} to 2π such that $F_f = c_{l_\alpha}/2\pi$. Although the thin-airfoil theory suggests that 2π should be used for the lift-curve slope, [3] and [10] state that if c_{l_α} value is available of a wing then c_{l_α} should be used to obtain aerodynamic loads. By putting Eq. (5.15) into Eq. (5.14), and collecting all terms on one side, we obtain:

$$\begin{bmatrix} mb^2 & mb^2x_\theta \\ mb^2x_\theta & I_P \end{bmatrix} \begin{Bmatrix} \ddot{h}/b \\ \ddot{\theta} \end{Bmatrix} + \begin{bmatrix} mb^2\omega_h^2 & F_f 2\pi\rho b^2 U^2 \\ 0 & I_P\omega_\theta^2 - (1+2a)F_f\pi\rho b^2U^2 \end{bmatrix} \begin{Bmatrix} h/b \\ \theta \end{Bmatrix} = \begin{Bmatrix} 0 \\ 0 \end{Bmatrix} \tag{5.16}$$

Now let us assume that pitching and plunging motion could be defined as:

$$h = \bar{h}e^{st} \qquad \theta = \bar{\theta}e^{st} \tag{5.17}$$

By combining Eq. (5.17) with Eq. (5.16), we obtain:

$$\begin{bmatrix} mb^2s^2 + mb^2\omega_h^2 & mb^2s^2x_\theta + F_f 2\pi\rho b^2U^2 \\ mb^2s^2x_\theta & I_P\omega_\theta^2 + I_Ps^2 - (1+2a)F_f\pi\rho b^2U^2 \end{bmatrix} \begin{Bmatrix} \frac{\bar{h}}{b} \\ \bar{\theta} \end{Bmatrix} = \begin{Bmatrix} 0 \\ 0 \end{Bmatrix} \tag{5.18}$$

To simplify Eq. (5.18), let us define some non-dimensional parameters:

$$\begin{aligned} r_a^2 &= \frac{I_P}{mb^2} & \varphi &= \frac{\omega_h}{\omega_\theta} \\ \mu_m &= \frac{m}{\rho\pi b^2} & V_w &= \frac{U}{b\omega_\theta} \end{aligned} \tag{5.19}$$

r_a^2 is non-dimensional radius of gyration, φ is the ratio of the uncoupled plunging natural frequency to the pitching natural frequency of the airfoil, μ_m is the mass ratio parameter, V_w is non-dimensional airspeed.

After defining these non-dimensional parameters, let us s is defined as pU/b to solve Eq. (5.18), where p is a non-dimensional complex parameter and U is the tangential velocity of the section which consists of two parts: first one is the velocity due to rotational speed and second one is the helicopter forward flight speed, i.e. $U = \Omega r + V$. To be on the safe side, U is calculated at $\psi = \pi/2$ where U is maximum. Therefore, Eq. (5.18) becomes as:

$$\begin{bmatrix} p^2 + \frac{\varphi^2}{V_w^2} & x_\theta p^2 + \frac{2F_f}{\mu_m} \\ x_\theta p^2 & r_a^2 p^2 + \frac{r_a^2}{V_w^2} - \frac{F_f}{\mu_m}(1+2a) \end{bmatrix} \begin{Bmatrix} \frac{\bar{h}}{b} \\ \bar{\theta} \end{Bmatrix} = \begin{Bmatrix} 0 \\ 0 \end{Bmatrix} \tag{5.20}$$

To have a non-trivial solution for Eq. (5.20),

$$\begin{vmatrix} p^2 + \dfrac{\varphi^2}{V_w^2} & x_\theta p^2 + \dfrac{2F_f}{\mu_m} \\ x_\theta p^2 & r_a^2 p^2 + \dfrac{r_a^2}{V_w^2} - \dfrac{F_f}{\mu_m}(1+2a) \end{vmatrix} = 0 \tag{5.21}$$

must be satisfied. As it could be observed form Eq. (5.21), roots change with V_w. Therefore, the determinant should be solved separately for changing V_w values.

In general, two complex conjugate roots will be obtained from the determinant for different V_w values and the roots will be in the form of:

$$p_n = \frac{b}{U}(\Gamma_n \pm i\Omega_n) \qquad n = 1,2 \tag{5.22}$$

If the roots are multiplied by V_w:

$$V_w p_n = \frac{U}{b\omega_\theta}\frac{b}{U}(\Gamma_n \pm i\Omega_n) = \frac{\Gamma_n}{\omega_\theta} \pm i\frac{\Omega_n}{\omega_\theta} \qquad n = 1,2 \tag{5.23}$$

So that the roots are connected to a known parameter ω_θ. If the relation s and p is used and Eq. (5.23) is combined with Eq. (5.17), plunging and pitching motion will be:

$$\begin{aligned} h &= \bar{h}e^{p\frac{U}{b}t} & \theta &= \bar{\theta}e^{p\frac{U}{b}t} \\ h_n &= \bar{h}_n e^{(\Gamma_n \pm i\Omega_n)t} & \theta_n &= \bar{\theta}_n e^{(\Gamma_n \pm i\Omega_n)t} \end{aligned} \tag{5.24}$$

where $\bar{h}_n$ and $\bar{\theta}_n$ are the finite magnitudes of the motion. The exponential part of the motions $e^{(\Gamma_n \pm i\Omega_n)t}$ defines the motion characteristics such that whether the motion is oscillatory or not, or the motion is divergent or convergent. $e^{\pm i\Omega_n t}$ is the oscillation part. If $\Omega_n \neq 0$ then the motion will be oscillatory. The other part $e^{\Gamma_n t}$ is called as the damping. If $\Gamma_n > 0$ for a V_w value, then the steady solution of the motion ($t \to \infty$) blows up. Therefore, the lowest V_w value which satisfies the condition $\Gamma_n > 0$ is called as flutter speed.

Let us inspect the reference blade whose $x_\theta = 0.056$, $\mu_m = 35.86$, $r_a^2 = 0.223$ are given. In [12], a general approach is modeling the blade characteristics based on %75 radius. Therefore, in this work, a section of the blade is inspected instead of full three-dimensional blade model. To see how flutter speed prediction changes with if the section is taken from %95 radius of the blade, a section taken from %95 radius of the reference blade is also considered in the flutter calculations. Hence, flutter speed analyses are conducted for two sections. If the section is taken %75 radius of the reference blade non-dimensional natural frequency ratio becomes $\varphi_{0.75} = 0.146$, whereas if the section is taken from %95 radius of the reference blade $\varphi_{0.95} = 0.114$.

When damping curve in Figure 5.2 is inspected, it is seen that damping is zero which makes the motions pure oscillatory up to a certain tangential velocity. However, one of the damping Γ value becomes greater than zero after a certain value tangential speed which makes the system oscillatory divergent. Therefore, the V_w at which Γ becomes positive is called as flutter speed and showed as V_F. If the section is taken from the blade's %75 radius, flutter speed is found as approximately 459 m/s which is well beyond the experienced tangential velocity not only in hover but also at maximum forward flight speed 35 m/s. Therefore, it could be said that the blade does not experience flutter in the flight envelope under steady load assumption.

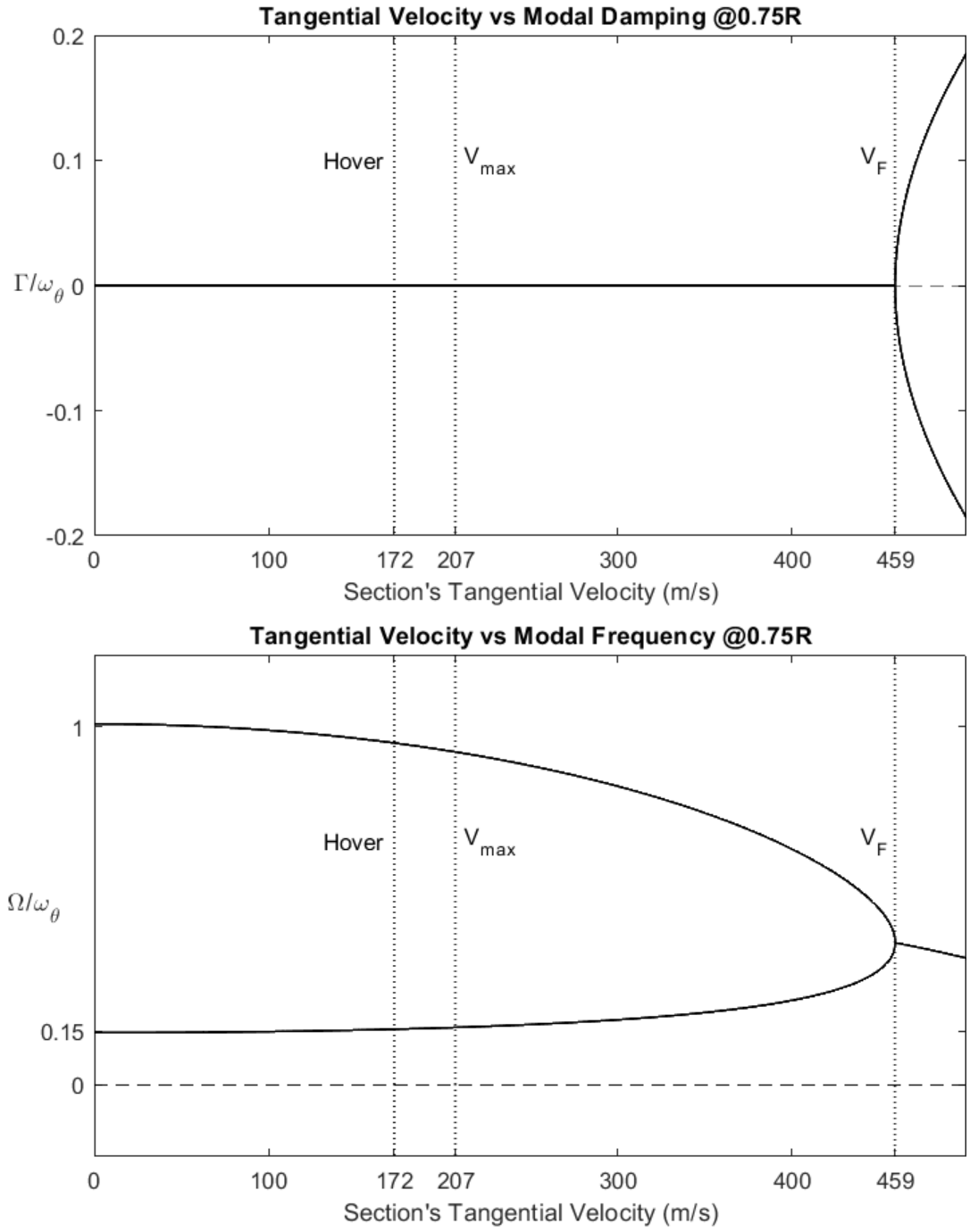

Figure 5.2. Section's tangential velocity versus damping and modal frequency at %75 radius of the reference blade under steady loads.

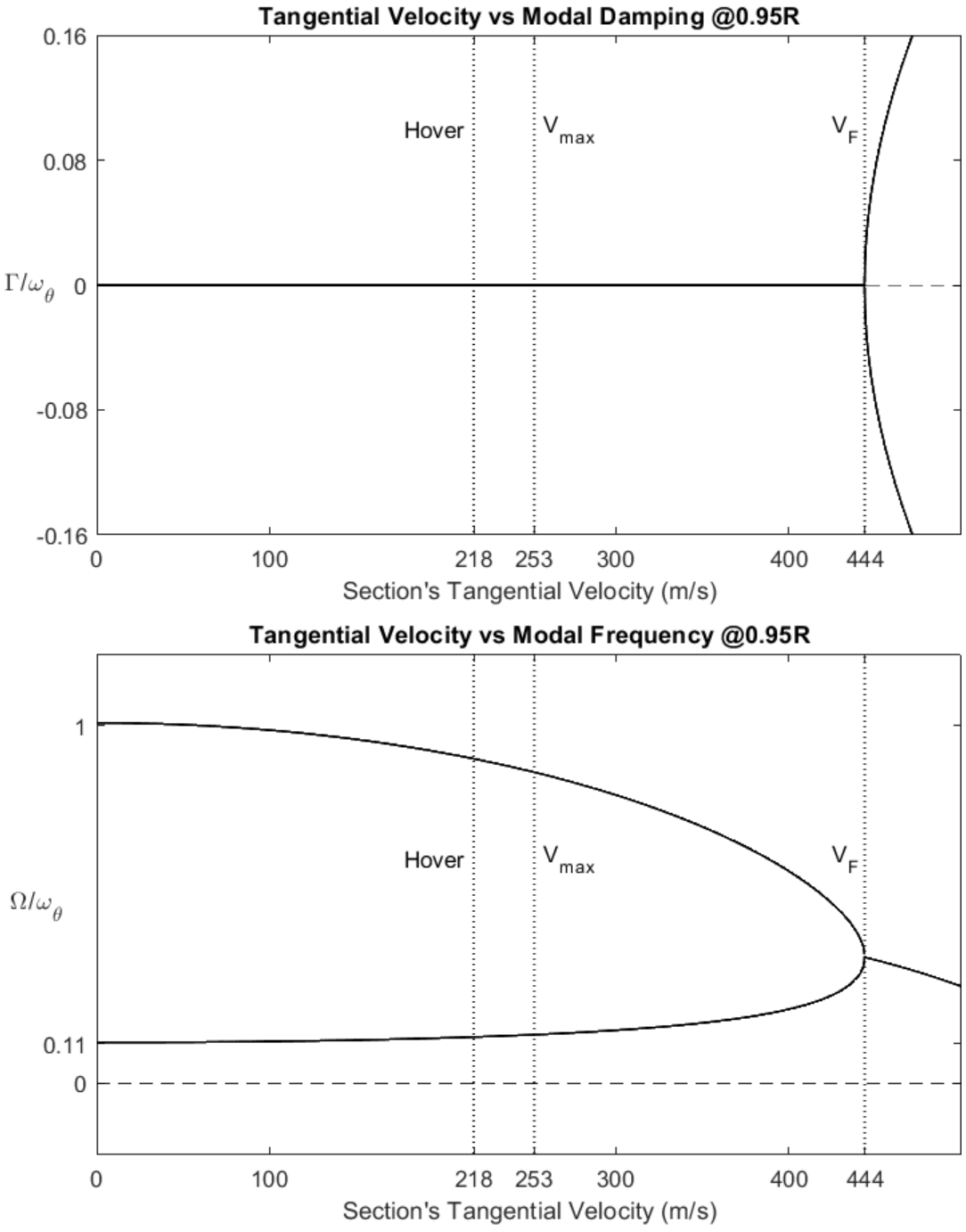

Figure 5.3. Section's tangential velocity versus damping and modal frequency at %95 radius of the reference blade under steady loads.

If the section is taken from the %95 radius of the reference blade, flutter speed is found as about 444 m/s which is again beyond the flight envelope. Therefore, it could be concluded that by assuming steady loads the reference helicopter does not experience any flutter.

If the flutter speeds obtained for %75 radius and %95 radius are compared, it will be seen that flutter speed of first one is greater than the latter one as expected although all non-dimensional parameters defined in Eq. (5.19) are same except the non-dimensional natural frequency ratio φ for both sections. Flutter determinant in Eq. (5.21) is a fourth-order polynomial in terms of p whose solution depends on the natural frequency ratio φ; hence, flutter determinant should be solved for each designed φ.

In Figure 5.2 and Figure 5.3, another interesting phenomenon occurs for the given system. Modal frequencies coalescence at the flutter speed V_F. This situation occurs if the loads are assumed to be steady. If the loads are not steady, the modal frequencies may not intersect at the flutter speed, but it will be observed that general tendency of the systems is that modal frequencies are getting closer to each other as the tangential velocity getting closer to the flutter speed in the following sections.

5.3 Theodorsen's Unsteady Aerodynamics

In Section 5.2, flutter analysis is done by assuming the aerodynamic loads are steady. Loads are given for the angle of attack θ only. However, it is easy to see that angle of attack is not only depending θ but also depending on the plunging motion. During the plunging motion, a vertical speed is experienced by the airfoil which creates an increment to the pitching angle θ. Therefore, the angle of attack could be written as:

$$\alpha_{eff} = \theta + \frac{\dot{h}}{U} \tag{5.25}$$

Another term which contributes to the angle of attack is pitching rate $\dot{\theta}$ of the airfoil. While writing the Lagrangian of the airfoil, it is shown that a perpendicular speed occurs due to $\dot{\theta}$. Perpendicular speed of the aerodynamic center due to the pitching rate is given as $b\left(\frac{1}{2}-a\right)\dot{\theta}$. Adding pitch rate effect to Eq. (5.25):

$$\alpha_{eff} = \theta + \frac{\dot{h}}{U} + \frac{b\left(\frac{1}{2}-a\right)\dot{\theta}}{U} \tag{5.26}$$

Therefore, sectional lift of the airfoil L' becomes as:

$$L' = F_f 2\pi\rho U b\left(\dot{h} + U\theta + b\left(\frac{1}{2}-a\right)\dot{\theta}\right) \tag{5.27}$$

where F_f is defined as $c_{l_\alpha}/2\pi$ in Section 5.2. By using effective angle of attack expression given in Eq. (5.26), Theodorsen derived an unsteady aerodynamic theory for thin airfoils undergoing small amplitude simple harmonic motions in an incompressible medium. Since details of the derivation is out of scope of this work, derivation is left to the [8]. Theodorsen's unsteady aerodynamic lift and pitching moment is given directly:

$$\begin{aligned} L' &= F_f 2\pi\rho U b C(k)\left[\dot{h} + U\theta + b\left(\frac{1}{2}-a\right)\dot{\theta}\right] + \pi\rho b^2\left(\ddot{h} + U\dot{\theta} - ba\ddot{\theta}\right) \\ M_{1/4} &= -\pi\rho b^3\left[\frac{1}{2}\ddot{h} + U\dot{\theta} + b\left(\frac{1}{8}-\frac{a}{2}\right)\ddot{\theta}\right] \end{aligned} \tag{5.28}$$

First term appearing in the Theodorsen's lift expression is called as **circulatory load**. The other term is called as **non-circulatory load**. Whereas, the pitching moment expression does not have any circulatory term, it is purely non-circulatory. Since the Theodorsen's theory assumes that simple harmonic motion, pitching and plunging motions could be expressed as:

$$h = \bar{h}e^{i\omega t} \qquad \theta = \bar{\theta}e^{i\omega t} \tag{5.29}$$

where ω is the oscillation frequency of the states.

$C(k)$ in Eq. (5.28) is called as **Theodorsen's lift deficiency function** and it is given as [8]:

$$C(k) = \frac{H_1^{(2)}(k)}{H_1^{(2)}(k) + iH_0^{(2)}(k)} \tag{5.30}$$

where $H_n^{(2)}(k)$ are the Hankel functions of the second kind and k is called as **reduced frequency** which is given as:

$$k = \frac{\omega b}{U} \tag{5.31}$$

b is the half-chord of the blade and U is the tangential velocity of the blade section in Eq. (5.31).

As it could be seen from Eq. (5.30), the lift deficiency function $C(k)$ is a complex function. Therefore, $C(k)$ could be written as $C(k) = F(k) + iG(k)$ where $F(k)$ and $G(k)$ are real and imaginary parts of the $C(k)$ respectively. Theodorsen's lift deficiency function $C(k)$, its real and imaginary parts w.r.t the reduced frequency are given in Figure 5.4 and Figure 5.5 respectively.

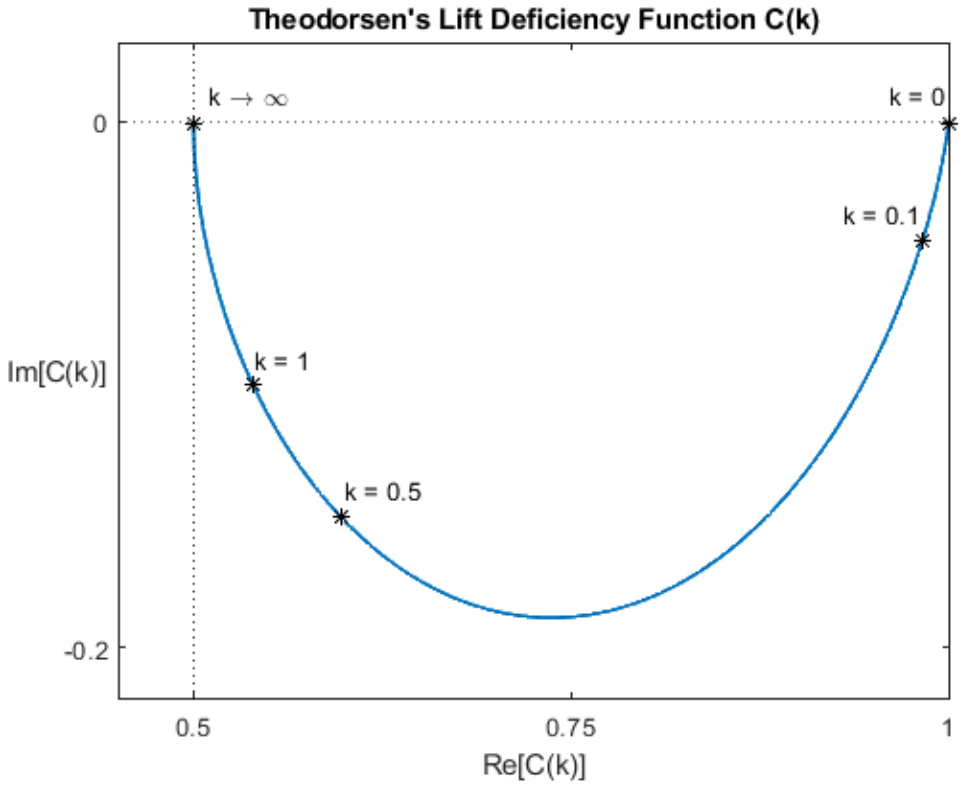

Figure 5.4. Theodorsen's lift deficiency function C(k) w.r.t the reduced frequency k.

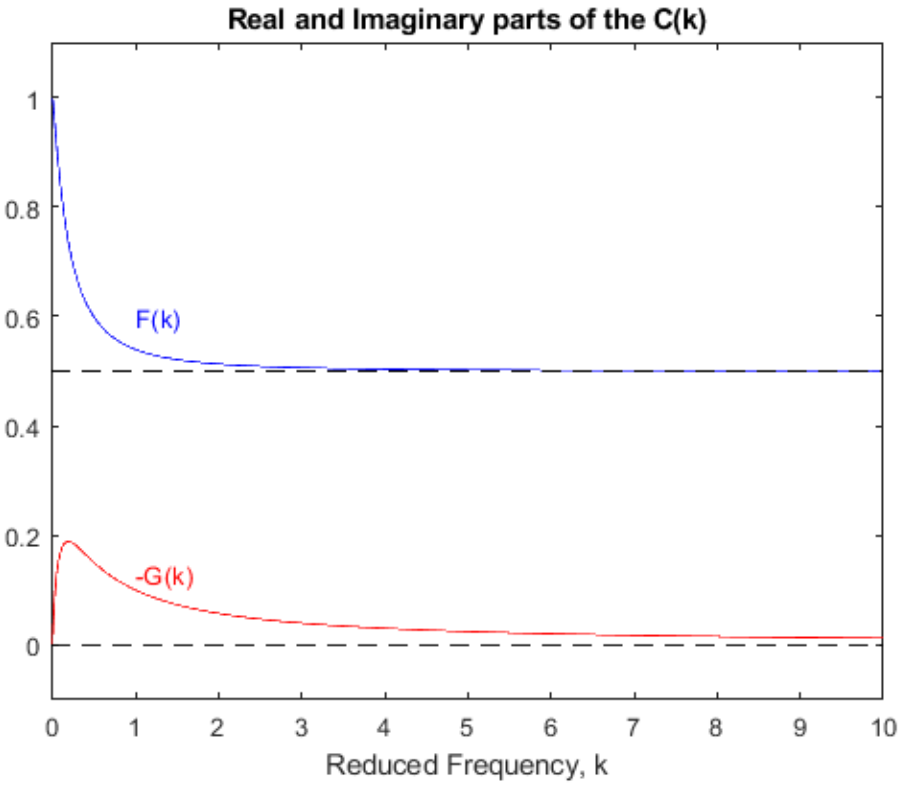

Figure 5.5. Real and imaginary parts of the C(k) w.r.t the reduced frequency k.

After defining L' and $M_{1/4}$ according to the Theodorsen's theory, let us re-write the unsteady lift and pitching moment given in Eq. (5.28) by using the plunging and pitching motion given in Eq. (5.29) recalling $M' = b\left(\frac{1}{2}+a\right)L' + M_{1/4}$:

$$L' = \left\{F_f 2\pi\rho UbC(k)\left[i\omega\bar{h} + U\bar{\theta} + i\omega b\left(\frac{1}{2}-a\right)\bar{\theta}\right] + \pi\rho b^2\left(-\omega^2\bar{h} + i\omega U\bar{\theta} + \omega^2 ba\bar{\theta}\right)\right\}e^{i\omega t} \tag{5.32}$$

$$M' = b\left(\frac{1}{2}+a\right)L' + \left\{-\pi\rho b^3\left[\frac{1}{2}\omega^2\bar{h} + i\omega U\bar{\theta} - \omega^2 b\left(\frac{1}{8}-\frac{a}{2}\right)\bar{\theta}\right]\right\}e^{i\omega t} \tag{5.33}$$

Multiply the circulatory lift term by $^{b\omega}/_{b\omega}$, non-circulatory lift term by $^{-b\omega^2}/_{-b\omega^2}$ in Eq. (5.32) and use the reduced frequency definition to replace U by $\omega b/k$:

$$L' = -\pi\rho b^3\omega^2\left\{\left[1-\frac{2iF_fC(k)}{k}\right]\frac{\bar{h}}{b} + \left[-a-\frac{i\left(1+(1-2a)F_fC(k)\right)}{k}-\frac{2F_fC(k)}{k^2}\right]\bar{\theta}\right\}e^{i\omega t} \tag{5.34}$$

By applying similar approach, multiply the lift contribution part by $^{b^2\omega^2}/_{b^2\omega^2}$, multiply the non-circulatory part by $^{b\omega}/_{b\omega}$ in Eq. (5.33) and replace the velocity term U by $\omega b/k$:

$$M' = \pi\rho b^4\omega^2\left\{\left[-a+\frac{i(2a+1)F_fC(k)}{k}\right]\frac{\bar{h}}{b} + \left[\frac{1}{8}+a^2 - \frac{i\left(\frac{1}{2}-a\right)\left(1-(2a+1)F_fC(k)\right)}{k}+\frac{(2a+1)F_fC(k)}{k^2}\right]\bar{\theta}\right\}e^{i\omega t} \tag{5.35}$$

To shorten the lengthy expressions in Eq's. (5.34) and (5.35), let us define some non-dimensional complex aerodynamic coefficients:

$$\begin{aligned} L_h(k) &= 1-\frac{2iF_fC(k)}{k} \\ L_\theta(k) &= -a-\frac{2i\left(\frac{1}{2}-a\right)F_fC(k)+i}{k}-\frac{2F_fC(k)}{k^2} \\ M_h(k) &= -a+\frac{2i\left(\frac{1}{2}+a\right)F_fC(k)}{k} \\ M_\theta(k) &= \frac{1}{8}+a^2+\frac{2i\left(\frac{1}{4}-a^2\right)F_fC(k)-i\left(\frac{1}{2}-a\right)}{k}+\frac{2\left(\frac{1}{2}+a\right)F_fC(k)}{k^2} \end{aligned} \tag{5.36}$$

Therefore, Eq's. (5.34) and (5.35) could be expressed by using the non-dimensional aerodynamic coefficients given in Eq. (5.36):

$$L' = -\pi\rho b^3\omega^2\left(L_h(k)\frac{\bar{h}}{b} + L_\theta(k)\bar{\theta}\right)e^{i\omega t}$$
$$M' = \pi\rho b^4\omega^2\left(M_h(k)\frac{\bar{h}}{b} + M_\theta(k)\bar{\theta}\right)e^{i\omega t} \tag{5.37}$$

If these unsteady aerodynamic loads are put into the Lagrangian of a typical wing section given in Eq. (5.12):

$$\begin{bmatrix} mb & mbx_\theta \\ mbx_\theta & \frac{I_P}{b} \end{bmatrix}\begin{Bmatrix}\ddot{h}\\ \ddot{\theta}\end{Bmatrix} + \begin{bmatrix} bk_h & 0 \\ 0 & \frac{k_\theta}{b} \end{bmatrix}\begin{Bmatrix}h\\ \theta\end{Bmatrix} - \pi\rho b^3\omega^2\begin{bmatrix} L_h(k) & L_\theta(k) \\ M_h(k) & M_\theta(k)\end{bmatrix}\begin{Bmatrix}\frac{\bar{h}}{b}\\ \bar{\theta}\end{Bmatrix}e^{i\omega t} = \begin{Bmatrix}0\\0\end{Bmatrix} \tag{5.38}$$

Substitute the harmonic motion assumption from Eq. (5.29) and non-dimensional parameters defined in Eq. (5.19):

$$\begin{bmatrix} \mu_m\left(1-\varphi^2\left(\frac{\omega_\theta}{\omega}\right)^2\right)+L_h(k) & \mu_m x_\theta + L_\theta(k) \\ \mu_m x_\theta + M_h(k) & \mu_m r_a^2\left(1-\left(\frac{\omega_\theta}{\omega}\right)^2\right)+M_\theta(k)\end{bmatrix}\begin{Bmatrix}\frac{\bar{h}}{b}\\ \bar{\theta}\end{Bmatrix} = \begin{Bmatrix}0\\0\end{Bmatrix} \tag{5.39}$$

To have a non-trivial solution, determinant of the matrix given in Eq. (5.39) must be zero.

$$\begin{vmatrix} \mu_m\left(1-\varphi^2\left(\frac{\omega_\theta}{\omega}\right)^2\right)+L_h(k) & \mu_m x_\theta + L_\theta(k) \\ \mu_m x_\theta + M_h(k) & \mu_m r_a^2\left(1-\left(\frac{\omega_\theta}{\omega}\right)^2\right)+M_\theta(k)\end{vmatrix} = 0 \tag{5.40}$$

The only unknown term in Eq. (5.40) is ω for a given reduced frequency k. Therefore, ω should be solved by varying reduced frequency k. In general, ω will be a complex number such that:

$$\omega = \omega_R + i\omega_i \tag{5.41}$$

If ω is put into Eq. (5.29) plunging and pitching motion will be:

$$h = \bar{h}e^{i\omega t} = \bar{h}e^{i\omega_R t}e^{-\omega_i t} \qquad \theta = \bar{\theta}e^{i\omega t} = \bar{\theta}e^{i\omega_R t}e^{-\omega_i t} \tag{5.42}$$

where $e^{i\omega_R t}$ is the oscillatory part and $e^{-\omega_i t}$ is the damping part. If $\omega_i < 0$, a divergent motion will occur. Hence, the k value which satisfies $\omega_i < 0$ becomes the flutter reduced frequency from which flutter speed could be found by the relation $V_F = \omega_R b/k$.

Normalized damping coefficient and non-dimensional modal frequency results are given in Figure 5.6 and Figure 5.7 for %75 and %95 radius of the blade respectively. In Figure 5.6, flutter speed is found as 481 m/s if the section is taken from the %75 radius of the blade. If the airfoil section is taken from the %95 radius of the blade, flutter speed is found as 457 m/s in Figure 5.7.

If predicted flutter speeds are compared, it is seen that flutter speed of the section taken from %75 radius is higher than the section taken from %95 radius as observed in Section 5.2; however, non-dimensional modal frequencies do not coalescence if Theodorsen's unsteady aerodynamic theory is implemented contrast to the situation obtained in Section 5.2 since aerodynamic damping terms coming from Theodorsen's unsteady aerodynamic theory affect the modal frequencies.

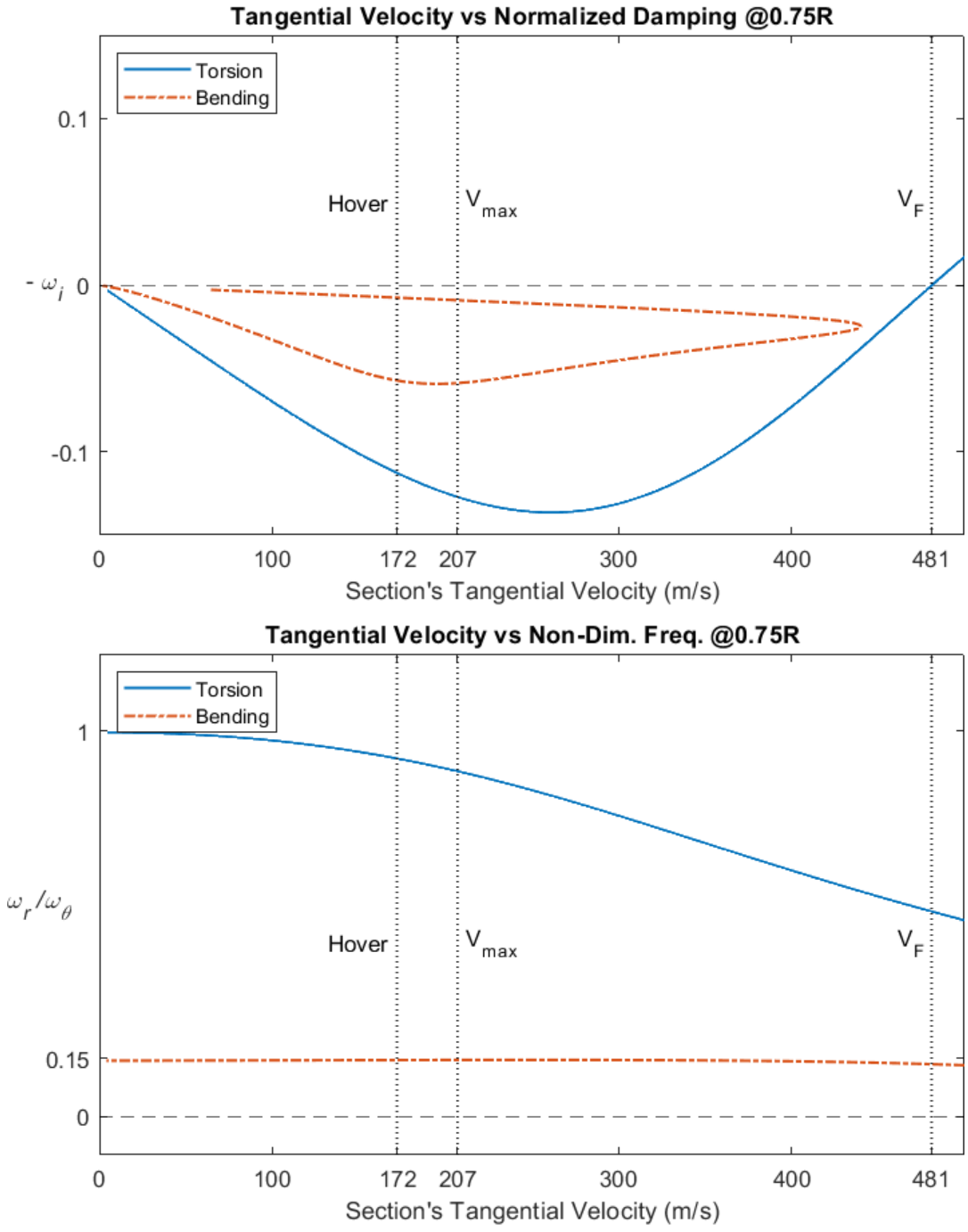

Figure 5.6. Section's tangential velocity versus damping and modal frequency at %75 of the radius of the reference blade under Theodorsen's unsteady aerodynamic loads.

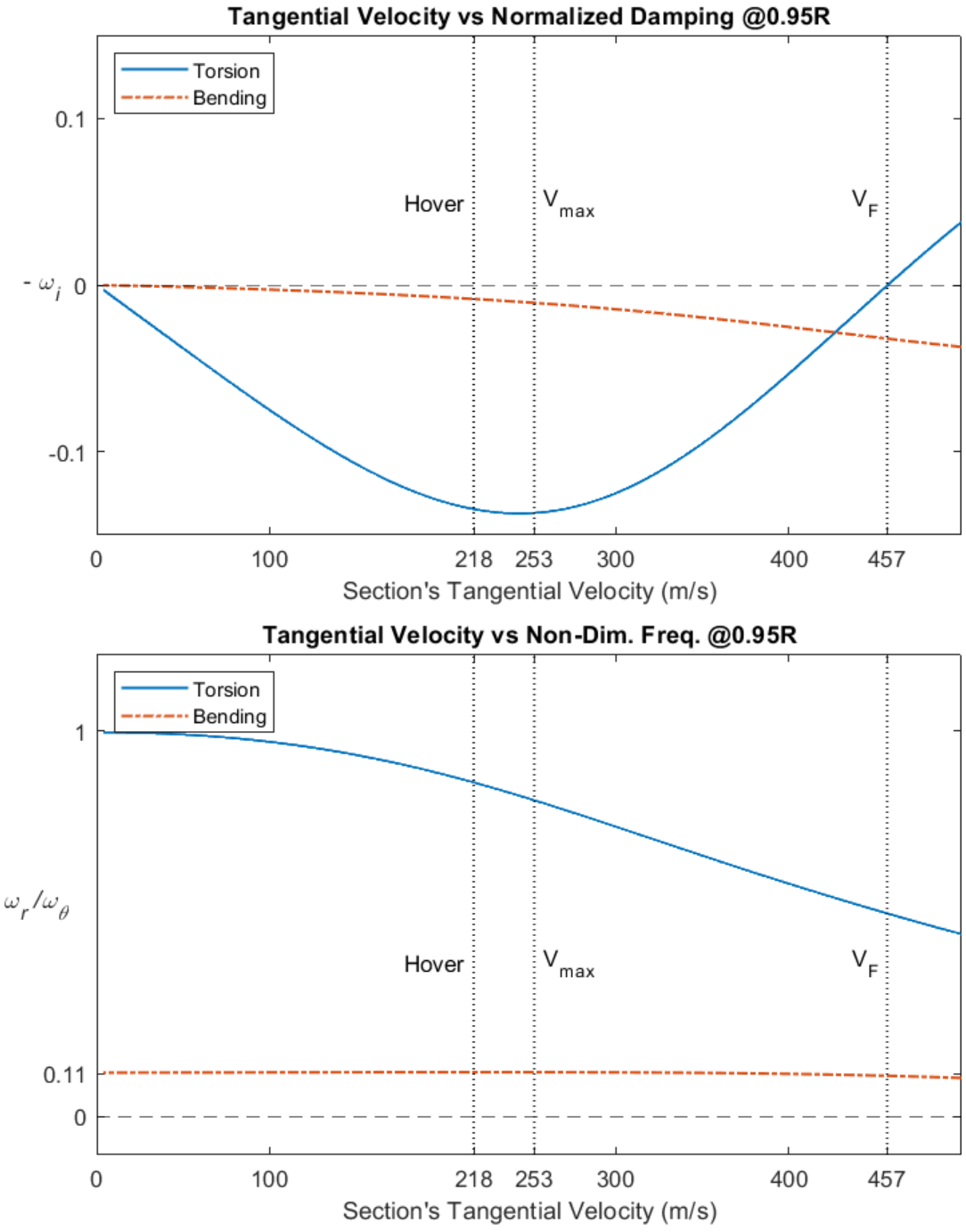

Figure 5.7. Section's tangential velocity versus damping and modal frequency at %95 of the radius of the reference blade under Theodorsen's unsteady aerodynamic loads.

5.4 K-Method

In Sections 5.2 and 5.3, flutter determinants are solved according to the Lagrangian of the system given in Eq. (5.12) without modeling the structural damping of the airfoil. In this section, structural damping of the airfoil will be modeled as well.

Structural experiments showed that during a simple harmonic motion, structural damping dissipates energy from the system which is independent of frequency; however, proportional to the square of the amplitude. Therefore, the structural damping could be modeled as damping force which is proportional to the displacement and in phase with the velocity.

To include the structural damping terms to the Lagrangian Eq. (5.12), let us define the structural damping terms D_h and D_θ which are defined as:

$$D_h = -ig_h k_h h \qquad D_\theta = -ig_\theta k_\theta h \tag{5.43}$$

where g_h and g_θ are the damping coefficients.

By including Eq. (5.43), Lagrangian of the wing section Eq. (5.12) could be written as:

$$\begin{bmatrix} m & mbx_\theta \\ mbx_\theta & I_P \end{bmatrix} \begin{Bmatrix} \ddot{h} \\ \ddot{\theta} \end{Bmatrix} + \begin{bmatrix} k_h & 0 \\ 0 & k_\theta \end{bmatrix} \begin{Bmatrix} h \\ \theta \end{Bmatrix} = \begin{Bmatrix} -L' + D_h \\ M' + D_\theta \end{Bmatrix} \tag{5.44}$$

Re-arrange Eq. (5.44):

$$\begin{bmatrix} m & mbx_\theta \\ mbx_\theta & I_P \end{bmatrix} \begin{Bmatrix} \ddot{h} \\ \ddot{\theta} \end{Bmatrix} + \begin{bmatrix} (1+ig_h)k_h & 0 \\ 0 & (1+ig\theta)k_\theta \end{bmatrix} \begin{Bmatrix} h \\ \theta \end{Bmatrix} = \begin{Bmatrix} -L' \\ M' \end{Bmatrix} \tag{5.45}$$

Scanlan and Rosenbaum (1948) [10] suggests that g_h and g_θ could be treated as if they were equal to an unknown g. Now introduce a new eigenvalue for the flutter determinant given in Eq. (5.40).

$$Z = \left(\frac{\omega_\theta}{\omega}\right)^2 (1+ig) \tag{5.46}$$

The flutter determinant becomes as:

$$\begin{vmatrix} \mu_m(1-\varphi^2 Z)+L_h(k) & \mu_m x_\theta + L_\theta(k) \\ \mu_m x_\theta + M_h(k) & \mu_m r_a^2(1-Z)+M_\theta(k) \end{vmatrix} = 0 \tag{5.47}$$

from which Z could be solved for a given reduced frequency k. Since Eq. (5.47) is a quadratic equation in terms of Z, there will two complex roots of Z which could be written as:

$$Z_n = \left(\frac{\omega_\theta}{\omega_n}\right)^2 (1+ig_n) \qquad n = 1,2 \tag{5.48}$$

After solving the eigenvalue Z, frequency of the states ω_n and structural damping coefficient g_n could be obtained from the real and imaginary part of the Z_n respectively.

$$\left(\frac{\omega_\theta}{\omega_n}\right)^2 = Re(Z_n)$$
$$\omega_n = \frac{\omega_\theta}{\sqrt{Re(Z_n)}} \tag{5.49}$$

$$Re(Z_n)g_n = Im(Z_n)$$
$$g_n = \frac{Im(Z_n)}{Re(Z_n)} \tag{5.50}$$

Note that flutter determinant in Eq. (5.47) should be solved for a varying reduced frequency k. The flutter speed is obtained where $g_n = 0$ is satisfied.

By using K-Method, flutter speed at %75 radius of the blade is found as about 481 m/s in Figure 5.8 which is beyond the flight envelope; hence, no flutter will be experienced during a flight. Another point should be emphasized is that at the flutter speed, natural frequencies do not coalescence since there are both structural and aerodynamic damping terms; however, they get close to each other.

Flutter analysis is done for the section at %95 radius as well. It is found that flutter speed is 457 m/s. It is seen that predicted flutter speed is higher if the section is taken from the %75 radius of the blade as obtained in Sections 5.2 and 5.3.

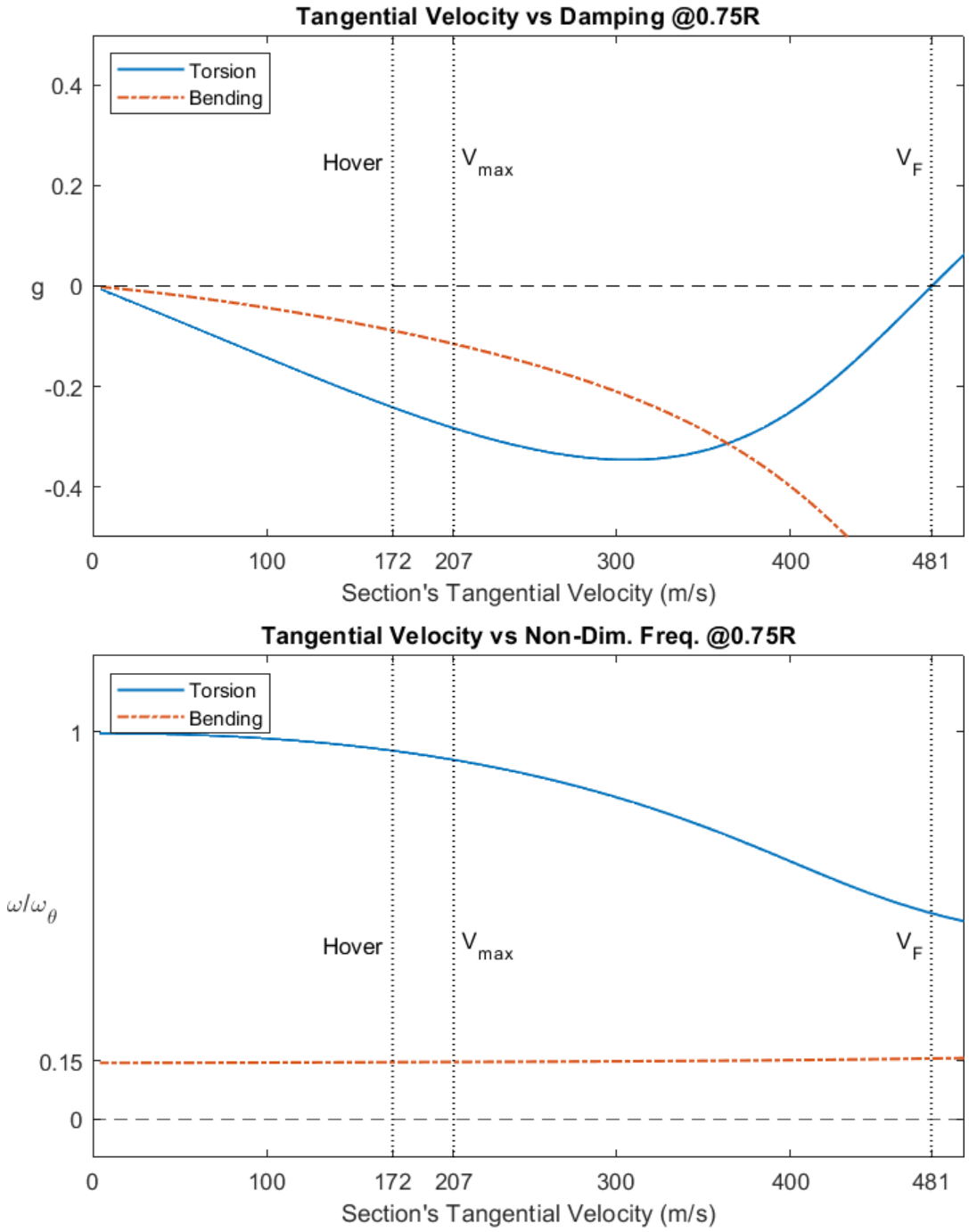

Figure 5.8. Section's tangential velocity versus damping and modal frequency at %75 of the radius of the reference blade under Theodorsen's unsteady aerodynamic loads with structural damping (K-Method).

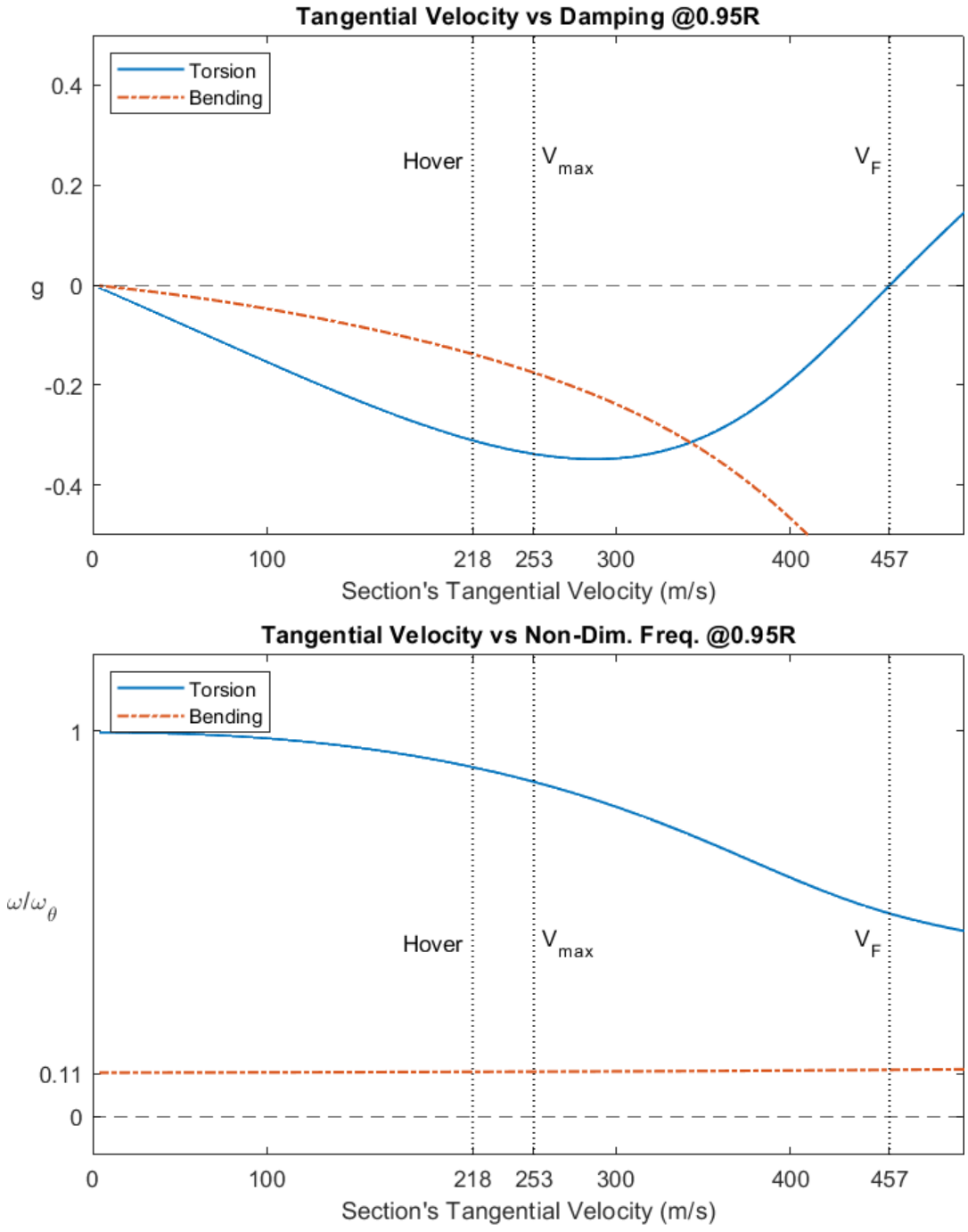

Figure 5.9. Section's tangential velocity versus damping and modal frequency at %95 of the radius of the reference blade under Theodorsen's unsteady aerodynamic loads with structural damping (K-Method).

5.5 Loewy's Unsteady Aerodynamics

As it is discussed in Section 4.1, helicopter rotors create an inflow and blades' wake interact with other blades which makes the unsteady aerodynamic studies more complex for the helicopters than the fixed wing aircrafts. In 1957, Loewy developed an unsteady aerodynamic theory for a rotor near hovering by accounting the wake returning from the blades of rotor. [14]

Leaving the derivation of Loewy's unsteady aerodynamic theory to Ref. [11], lift deficiency function for Loewy's unsteady theory is given as [11]:

$$C'(k) = \frac{H_1^{(2)}(k) + 2J_1(k)W'(k,\lambda,\sigma,m)}{H_1^{(2)}(k) + iH_0^{(2)}(k) + 2[J_1(k) + iJ_0(k)]W'(k,\lambda,\sigma,m)} \tag{5.51}$$

where $J_n(k)$ are the Bessel function of the first kind, $H_n^{(2)}(k)$ are the Hankel functions of the second kind and W' is called as returning wake effect and it could be expressed as from [14]:

$$W'(k,\lambda,\sigma,m) = \frac{1}{e^{4k\lambda/\sigma}e^{i2\pi m} - 1} \tag{5.52}$$

where k is the reduced frequency, λ is the non-dimensional inflow ratio, σ is the rotor solidity which is given as $\sigma = N_b c/\pi R$ and m is the non-dimensional frequency ratio of oscillatory frequency to rotational frequency and given as $m = \omega/\Omega$. Note that in [12] it is stated that if same wake spacing and proper m is used, $C'(k)$ of multi-bladed case is identical to single-bladed $C'(k)$. Therefore, in this work single-bladed case of the W′ is used to find lift deficiency function.

If the velocity of the inflow is too high i.e., $\lambda \to \infty$ blades do not interact with the returning wakes which makes W' approaches to zero. Hence, $\lim_{\lambda\to\infty} C'(k) = C(k)$. Another condition to satisfy the $C'(k) = C(k)$ is increasing the reduced frequency k. Denominator of the returning wake effect approaches to infinity as $k \to \infty$ which makes $W' \to 0$. Therefore, $\lim_{k\to\infty} C'(k) = C(k)$.

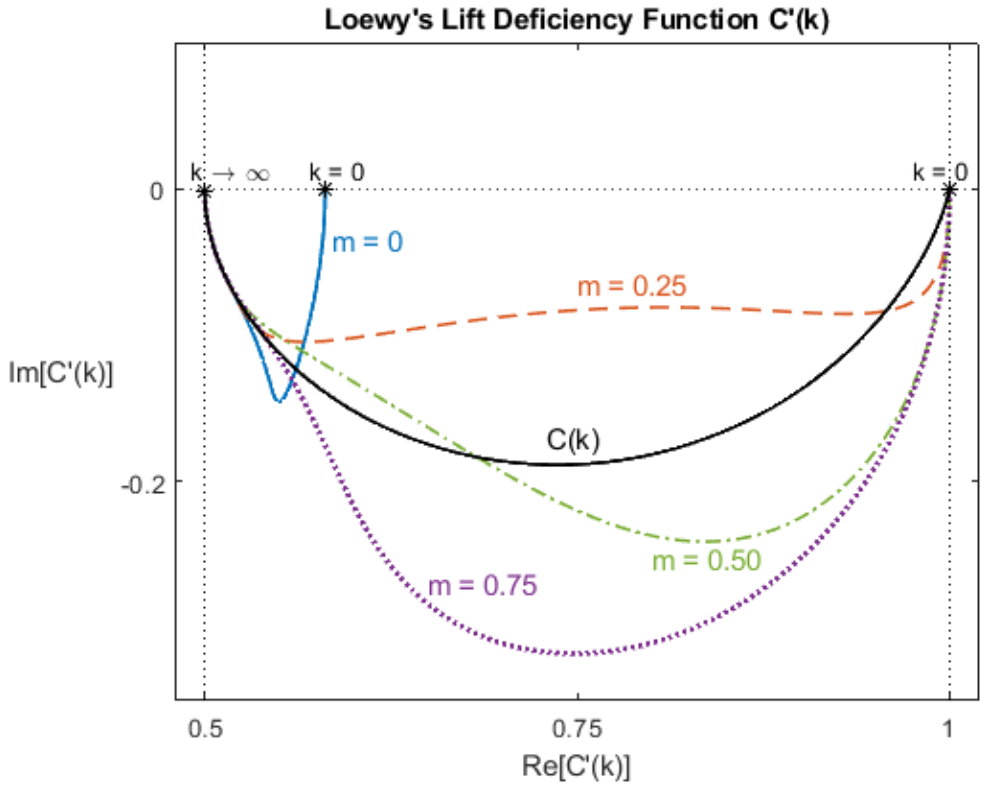

Figure 5.10. Comparison of Loewy's lift deficiency functions of the reference blade for different wake phasing with Theodorsen's lift deficiency function w.r.t the reduced frequency k.

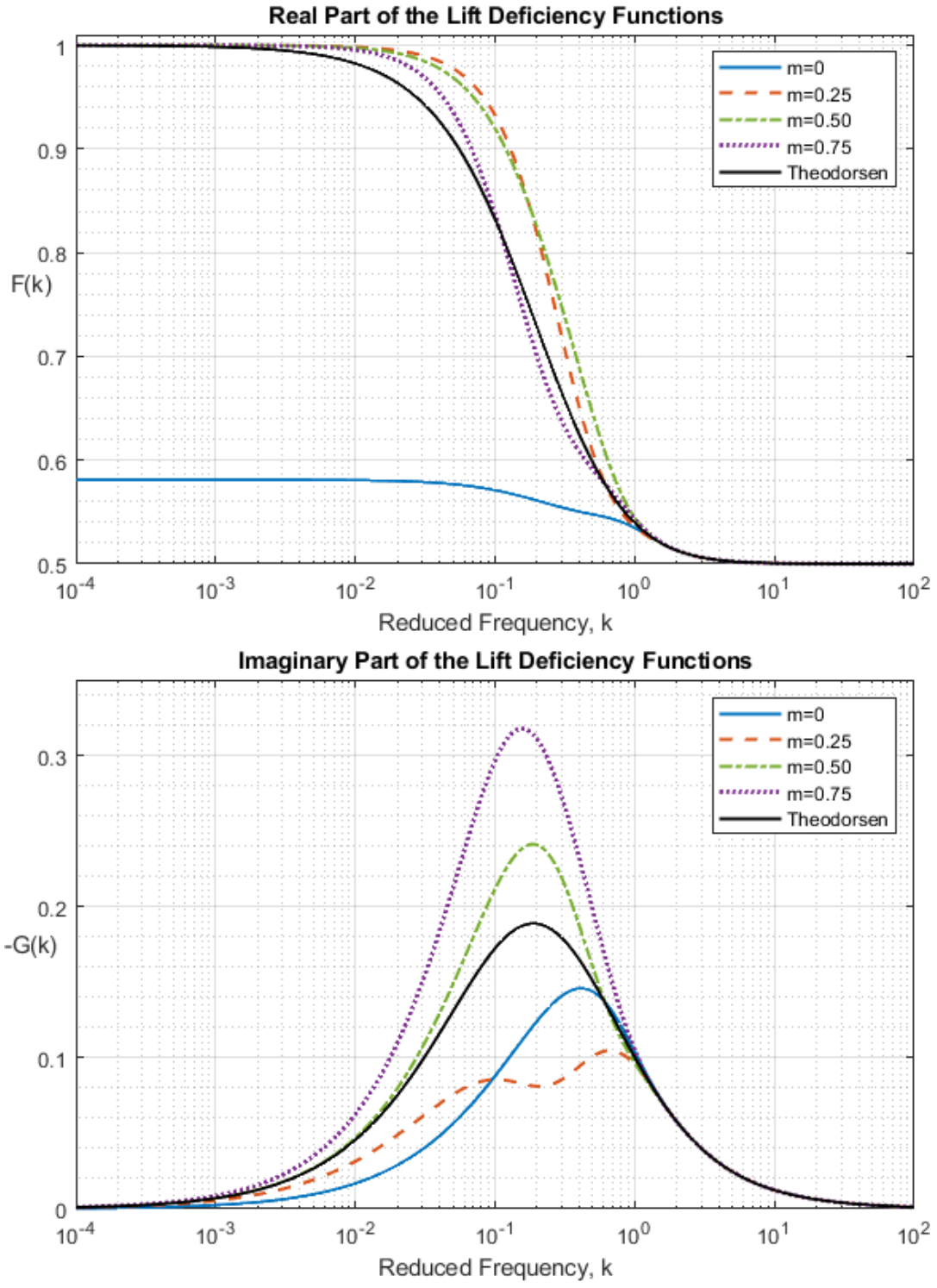

Figure 5.11. Comparison of real and imaginary parts of Loewy's lift deficiency functions of the reference blade for different wake phasing ratios with Theodorsen's lift deficiency function w.r.t the reduced frequency k.

If W' is inspected in detail, it would be seen that there is a $e^{i2\pi m}$ term in the denominator of the returning wake effect W'. Since $e^{i2\pi m}$ term is a periodic function being as same for every integer of m, rational part of m is interested. Hence, Figure 5.10 and Figure 5.11 are drawn for $m = 0, 0.25, 0.5, 0.75$ which are equal to $m = N, N + \frac{1}{4}, N + \frac{1}{2}, N + \frac{3}{4}$ respectively where N is an integer.

In Figure 5.10 and Figure 5.11, it is observed that for $k > 1$ Theodorsen's and Loewy's lift deficiency functions becomes identical for given frequency ratios as expected. However, for frequency ratio $m = N$ and $k < 1$, the difference between Loewy's and Theodorsen's lift deficiency function is significant. In fact, the main difference occurs in the real part of the $C'(k)$ since wake returning effect W' becomes purely real for $m = N$.

If the non-dimensional complex aerodynamic coefficients $L_h(k)$, $L_\theta(k)$, $M_h(k)$ and $M_\theta(k)$ are updated with $C'(k)$ for selected frequency ratio m, flutter determinant given in Eq. (5.47) could be solved by implementing Loewy's unsteady aerodynamic theory. Damping and non-dimensional frequency analyses of the reference blade by using $C'(k)$ are given in Figure 5.12 and Figure 5.13.

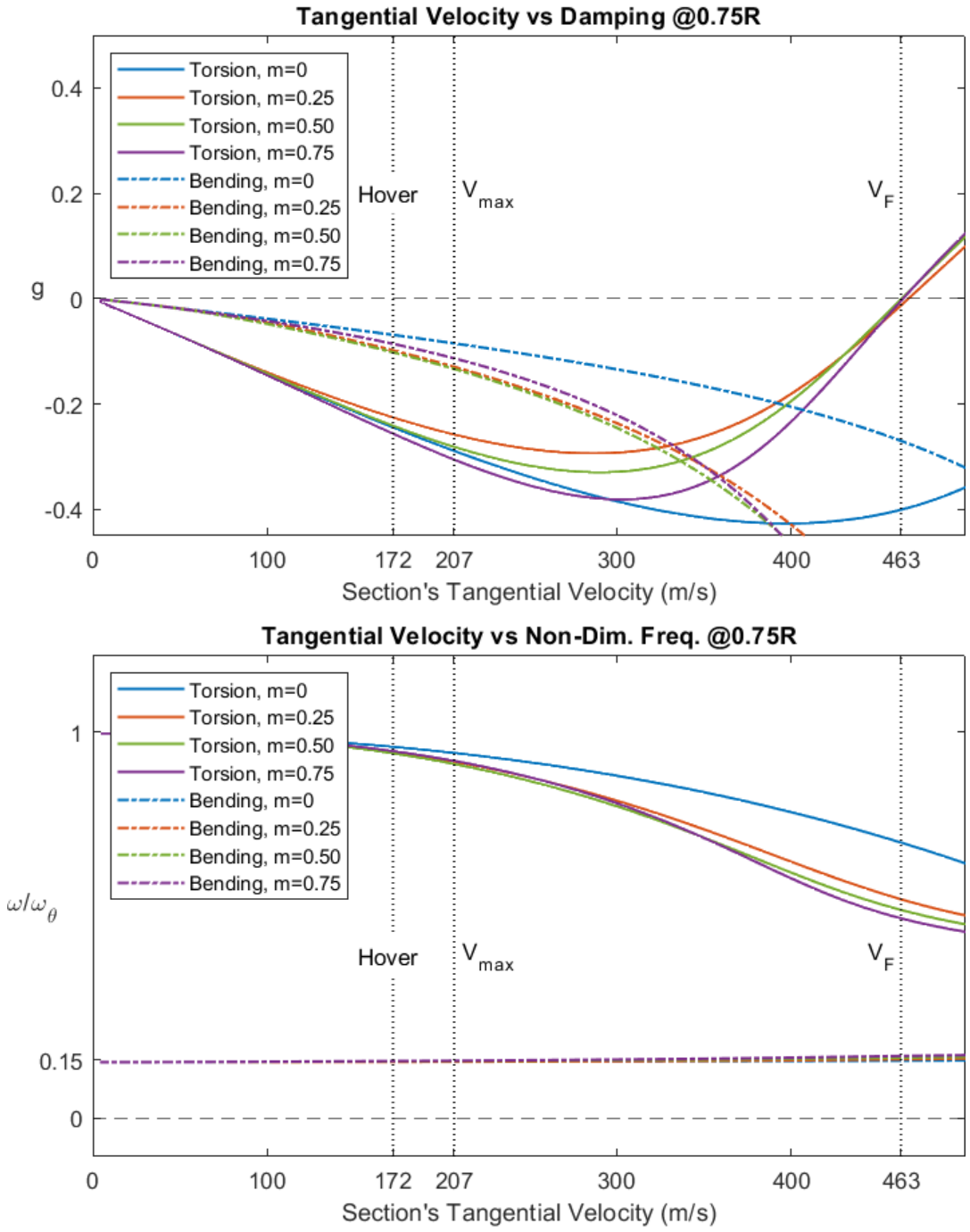

Figure 5.12. Section's tangential velocity versus damping and modal frequency at %75 of the radius of the reference blade under Loewy's unsteady aerodynamic loads with structural damping (K-Method).

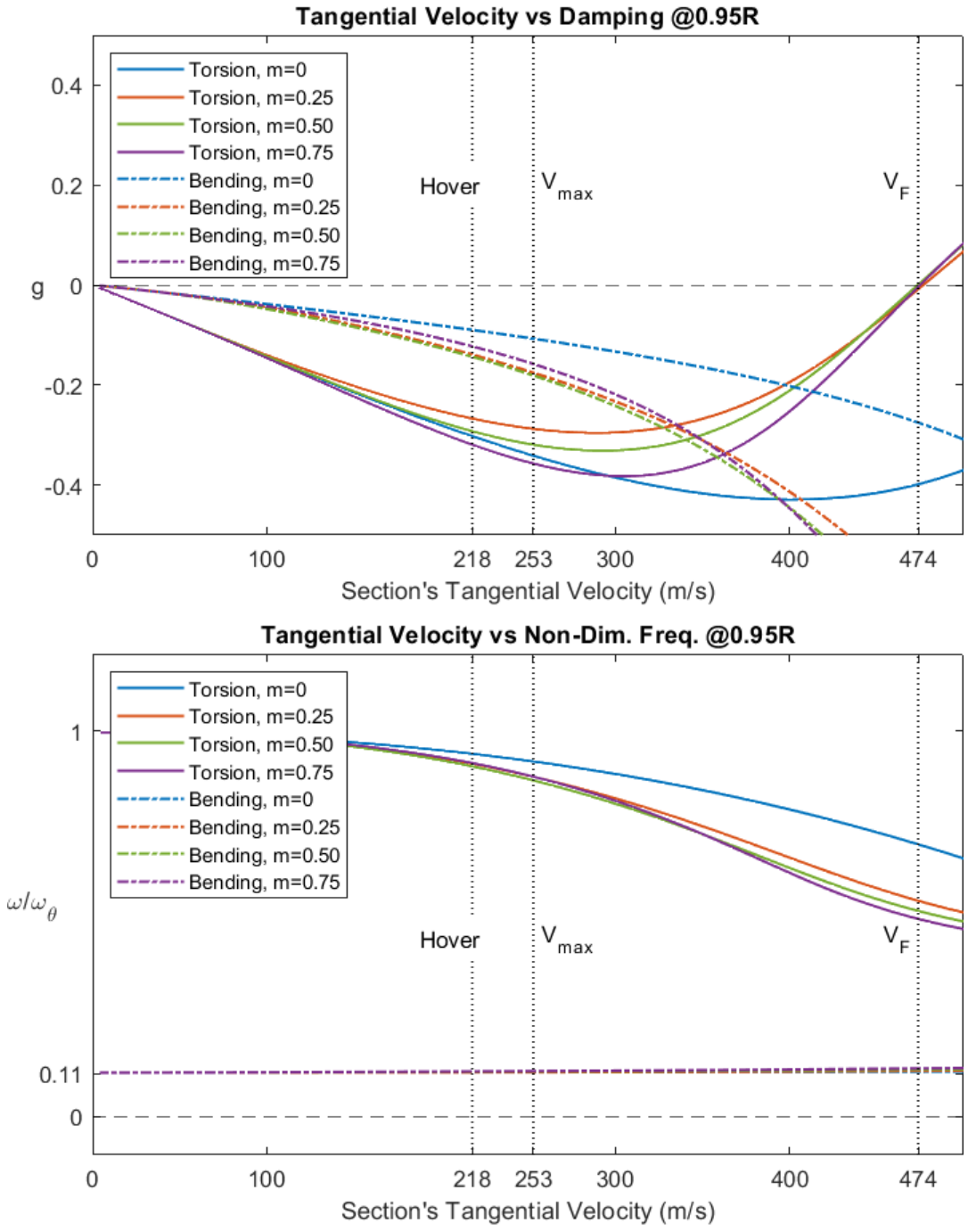

Figure 5.13. Section's tangential velocity versus damping and modal frequency at %95 of the radius of the reference blade under Loewy's unsteady aerodynamic loads with structural damping (K-Method).

Predicted flutter speed of the reference blade is found as 463 m/s if the frequency ratio is assumed to be as a non-integer, i.e., $m \neq 0$ and the section is taken from the blade's %75 radius, whereas if the section is taken from %95 radius of the blade, flutter speed is found as 474 m/s for $m \neq 0$.

In Figure 5.12 and Figure 5.13, it is observed that all damping and modal frequency curves are similar to each other and zero-damping boundaries are crossed at speeds which are close to each other if the frequency ratios are different than an integer, i.e., $m \neq 0$. Main reason behind this situation is that aerodynamic damping in pitching direction is higher for $m = 0$ than other frequency ratios. Therefore, flutter prediction is the highest for $m = 0$.

5.6 Modified Loewy's (Finite Wake) Lift Deficiency Function

If the derivation of Eq. (5.51) is inspected, it would be seen that Loewy used an infinite series solution while calculating the downwash. If the infinite number of revolutions changed with a finite number of revolutions, a new lift deficiency function will be obtained which is given in the [6] as:

$$C'_N(k) = \frac{H_1^{(2)}(k) + 2J_1(k)W'_N(k, m, \hat{h})}{H_1^{(2)}(k) + iH_0^{(2)}(k) + 2[J_1(k) + iJ_0(k)]W'_N(k, m, \hat{h})} \qquad (5.53)$$

where W_N is returning finite wake effect and given as in [6]:

$$W'_N(k, m, \hat{h}) = \sum_{n=1}^{N} e^{-nk\hat{h}} e^{-i2\pi mn} \qquad (5.54)$$

where m is the non-dimensional frequency ratio, $\hat{h}$ is the vertical distance between the wakes and it is given as $\hat{h} = \frac{4\lambda}{\sigma}$, N is the finite number of the wakes. It is observed that after 1000 wakes W'_N converges. Therefore, in this work finite wake lift deficiency function is calculated by using 1000 wakes. The comparison of $C'_N(k)$ with $C(k)$ and comparison of their real and imaginary parts are given in Figure 5.14 and Figure 5.15 respectively.

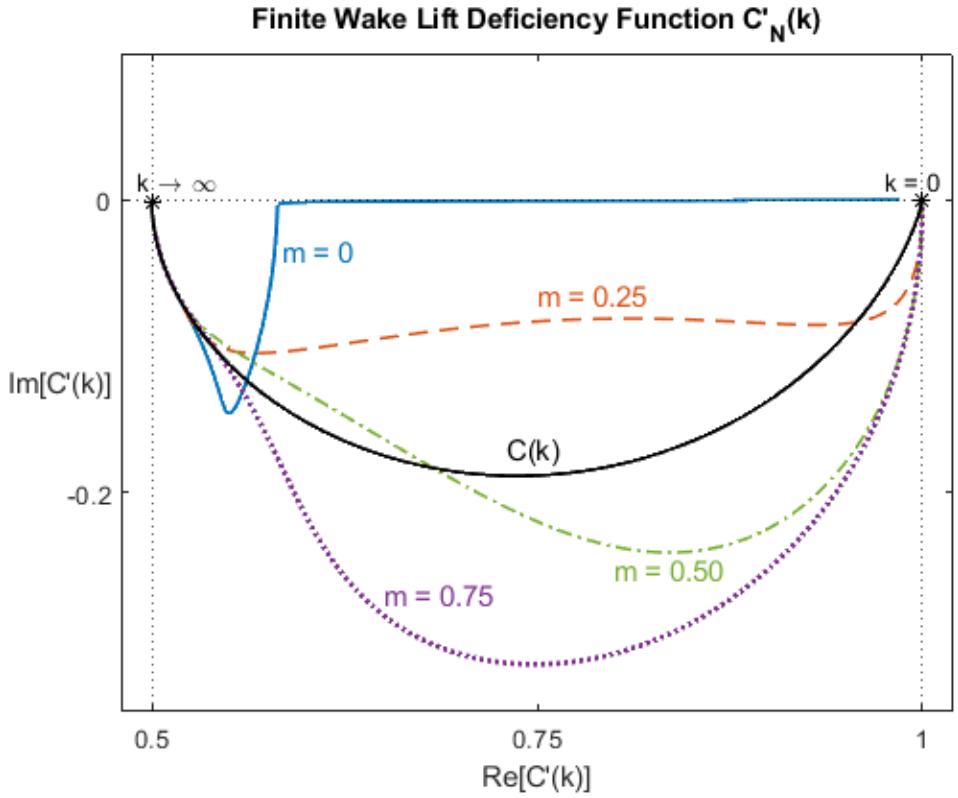

Figure 5.14. Comparison of finite wake lift deficiency functions of the reference blade for different non-dimensional frequency ratios with Theodorsen's lift deficiency function w.r.t the reduced frequency k.

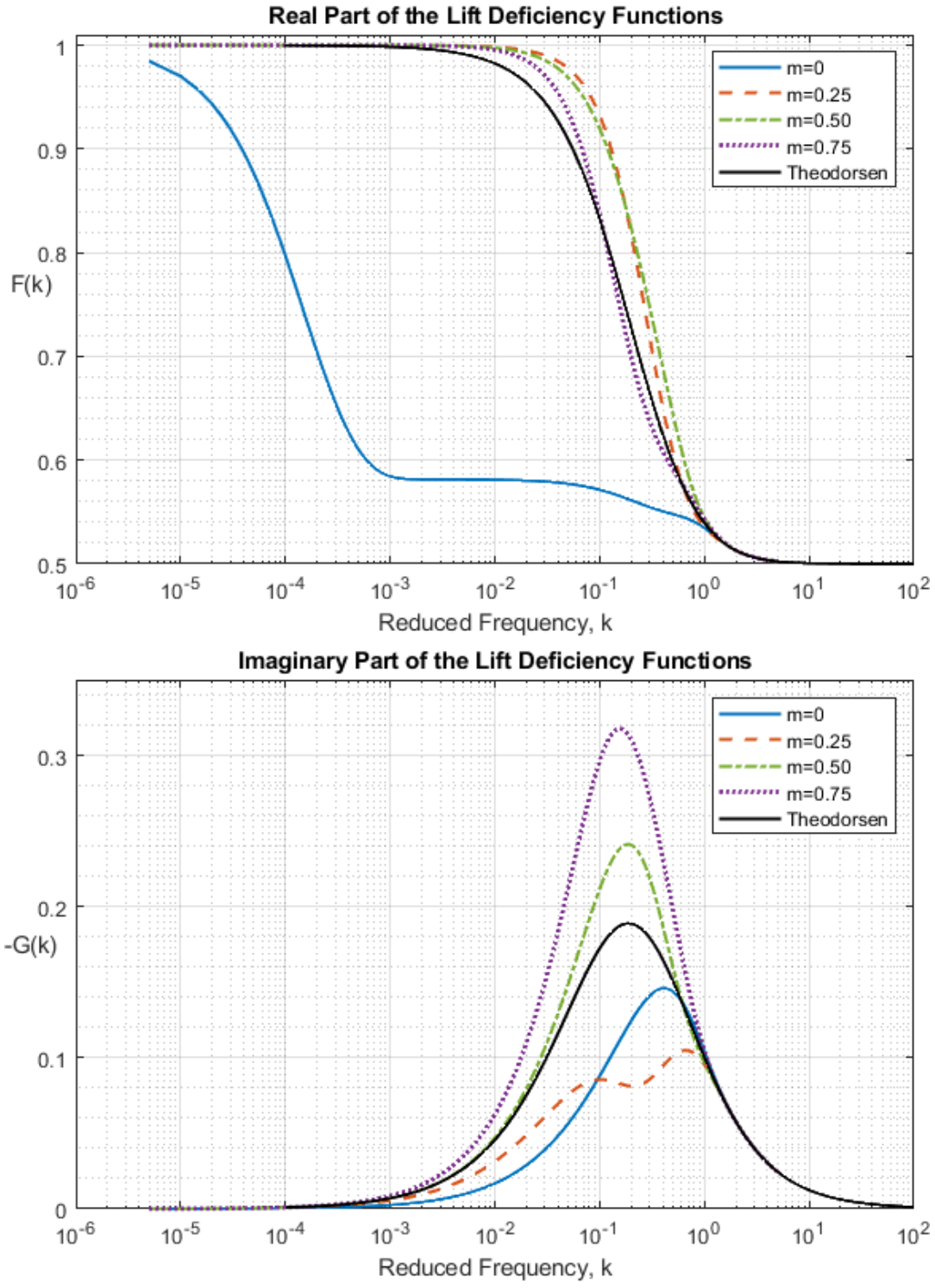

Figure 5.15. Comparison of real and imaginary parts of finite wake lift deficiency functions of the reference blade for different non-dimensional frequency ratios with Theodorsen's lift deficiency function w.r.t the reduced frequency k.

In Figure 5.14, it is observed that finite wake lift deficiency function has a similar characteristic as Loewy's lift deficiency function for all m's except $m = 0$. Although $C_N'(k)$ for $m = 0$ curve is also similar to $C'(k)$, $C_N'(k)$ approaches zero if k approaches to zero i.e., $\lim_{k\to 0} C_N'(k) = 1$, whereas $\lim_{k\to 0} C'(k) \cong 0.58$ for the reference blade. Therefore, finite wake lift deficiency function gives different results than Loewy's lift deficiency function for lower k values and $m = 0$.

In Figure 5.15, different characteristic of the $C_N'(k)$ for $m = 0$ could be observed in detail. As k approaches to zero real part of $C_N'(k)$ approaches to 1. It is also seen that real and imaginary parts of $C(k)$ and $C_N'(k)$ are identical for $k > 1$ which is an expected outcome since finite wake lift deficiency function is based on Loewy's unsteady aerodynamic theory and Loewy's lift deficiency function is identical to Theodorsen's lift deficiency function for $k > 1$.

As it is done in Section 5.5, by updating the non-dimensional complex aerodynamic coefficients with $C_N'(k)$, the flutter determinant in Eq. (5.47) could be solved to find the flutter speed. By implementing finite wake lift deficiency function into the flutter determinant in Eq. (5.47), flutter speed is found as 463 m/s if airfoil section is taken from %75 radius of the blade. If the section is taken from %95 radius of the blade, the flutter speed is found as 474 m/s.

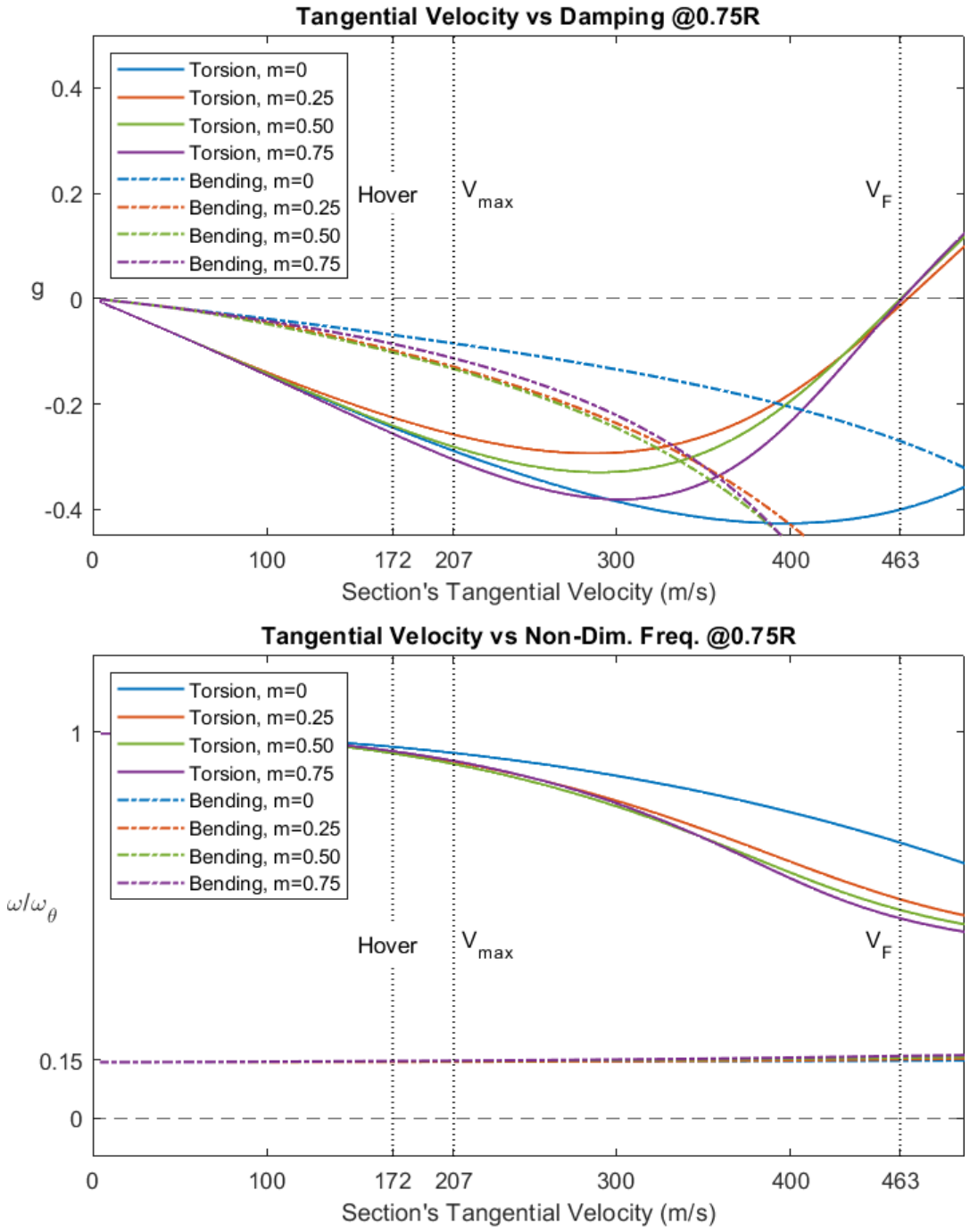

Figure 5.16. Section's tangential velocity versus damping and modal frequency at %75 of the radius of the reference blade under finite wake unsteady aerodynamic loads with structural damping (K-Method).

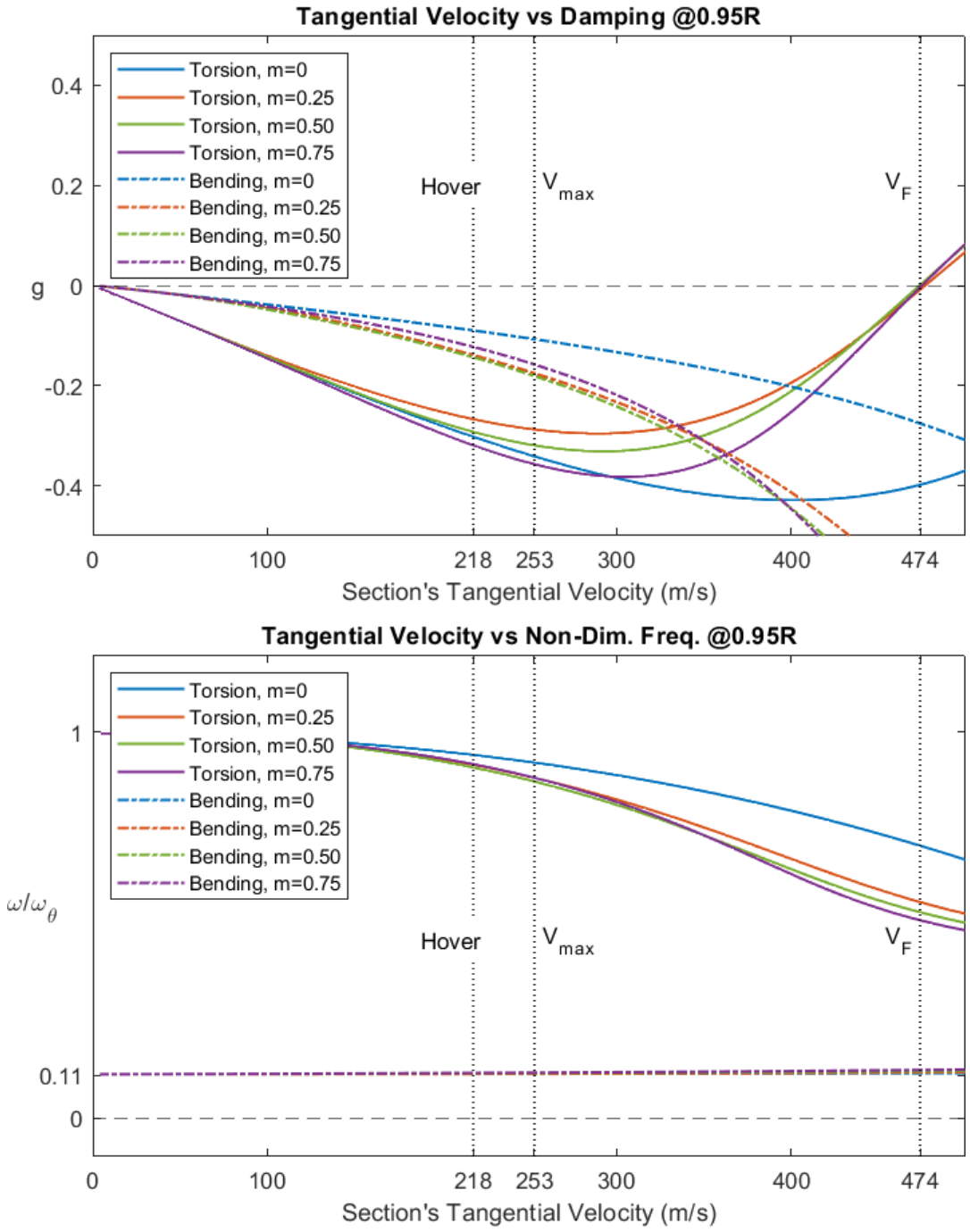

Figure 5.17. Section's tangential velocity versus damping and modal frequency at %95 of the radius of the reference blade under finite wake unsteady aerodynamic loads with structural damping (K-Method).

5.7 Comparison of K-Method with Finite Element Analysis

In this section, comparisons of presented K-Method results with finite element analyses results are going to be discussed. To compare the results, finite element analyses results from Ref. [21] are going to be taken. In [21] flutter analyses are conducted by using MSC FlightLoads for a symmetrical Wortmann FX 76-120 airfoil. Dimensions and structural design of the symmetrical wing for which flutter analysis is conducted in [21] are given in Figure 5.18 and Figure 5.19 respectively.

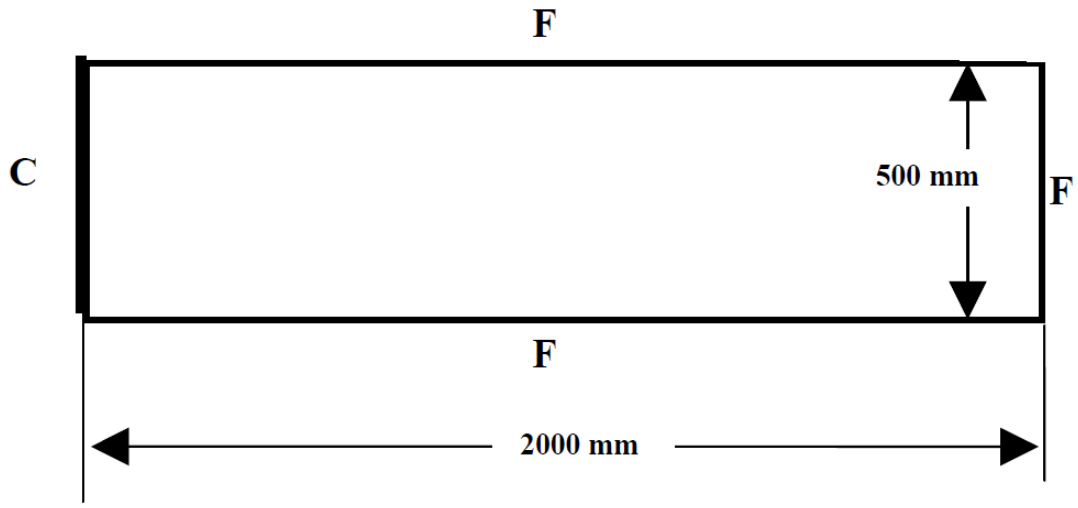

Figure 5.18. Dimensions of the Wortmann FX 76-120 symmetrical wing. [21]

In Figure 5.18, C and F represent clamped and free boundary conditions of the wing respectively. According to Figure 5.18, reference wing has 0.5 m chord and 2 m span. Aluminum 6061-76 is chosen for the material of the reference Wortmann FX 76-120 wing whose Young's Modulus is 70 GPa, Poisson's ratio is 0.3 and density is 2710 kg/m^3. Ribs of the wing have 1.5 mm thickness and skin thickness of the wing is 1 mm.

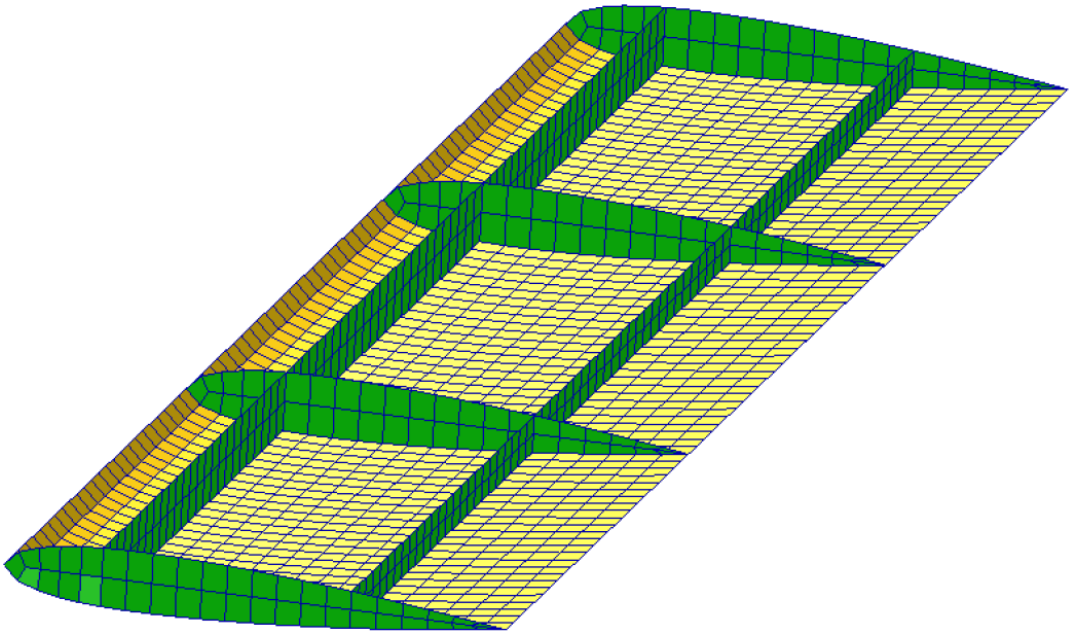

Figure 5.19. Structural design and finite element mesh of the reference Wortmann FX 76-120 symmetrical wing. [21]

In [21], flutter speed of the Wortmann FX 76-120 wing is found as about 368 m/s in sea level altitude. Let us compare the finite element result with the K-Method discussed in Section 5.4. To be able to predict the flutter speed, non-dimensional parameters of the reference wing should be given firstly. Necessary non-dimensional parameters to solve the flutter determinant in Eq. (5.47) of the reference Wortmann FX 76-120 wing are $x_\theta = 0.241,\ r_\alpha^2 = 0.406,\ \varphi_{0.75} = 0.157,\ \varphi_{0.95} = 0.124,\ \mu_m = 2.40$. In [23], C_{L_α} of the wing is given as 6.15; therefore, F_f is obtained as 0.98.

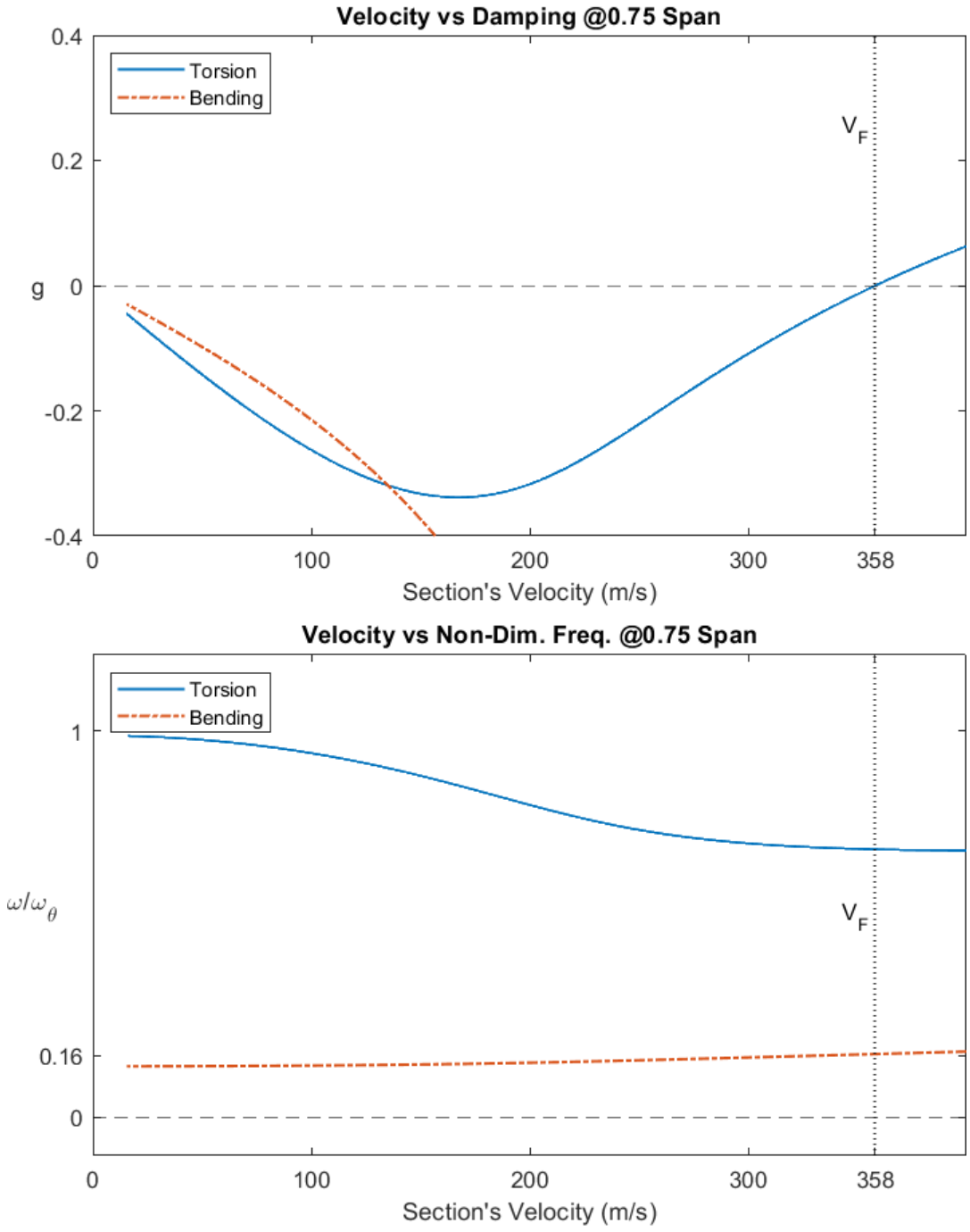

Figure 5.20. Section's velocity versus damping and modal frequency at %75 span of the reference Wortmann FX 76-120 symmetrical wing under Theodorsen's unsteady aerodynamic loads with structural damping (K-Method).

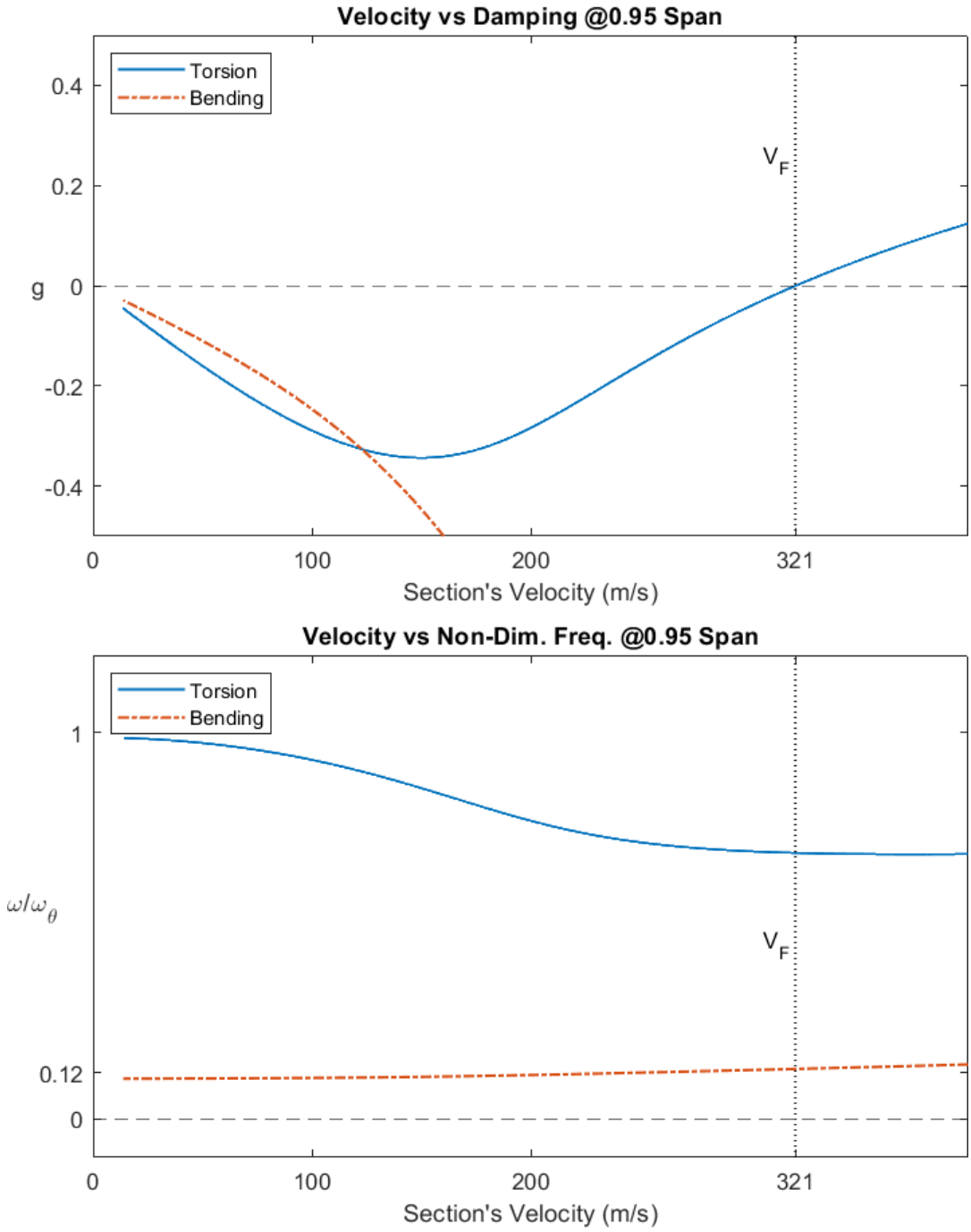

Figure 5.21. Section's velocity versus damping and modal frequency at %95 span of the reference Wortmann FX 76-120 symmetrical wing under Theodorsen's unsteady aerodynamic loads with structural damping (K-Method).

According to K-Method, flutter speed of the reference Wortmann FX 76-120 wing is found as 358 m/s if the section is taken from %75 span of the reference wing. If the section is taken from %95 span, flutter speed is predicted as 321 m/s. In [21], flutter speed of the reference Wortmann FX 76-120 wing is found as 368 m/s by using MSC FlightLoads. It is observed that if the section is taken from %75 span of the wing, K-Method predicts the flutter speed very close to the finite element analysis with a deviation of %2.7; however, if the section is taken from %95 flutter speed prediction of K-Method deviates %12.8 from Ref. [21]. Therefore, it could be concluded that K-Method could be used to obtain a robust flutter speed prediction by taking the section from %75 span, whereas flutter speed is found conservatively if the section taken from %95 span.

Another important conclusion regarding the results given in Figure 5.20 and Figure 5.21 is that predicted flutter speed is lower if the section is taken from %95 span in contrast to the reference helicopter blade's flutter predictions in which flutter speed is found higher if the section is taken from the %95 radius. Hence, it could be stated that if the flutter speed is intended to be found by implementing sectional analysis, usage of different sections would be wise to be on the safe side.

5.8 Comparison of the Predicted Flutter Speeds

Table 5.1 Comparison of flutter speed predictions of the methods used for %75 and %95 radius of the blade.

Method	%75 Radius	%95 Radius
Steady Loads	459 m/s	444 m/s
Theodorsen	481 m/s	457 m/s
Theodorsen K-Method	481 m/s	457 m/s
Loewy K-Method	463 m/s	474 m/s
Finite Wake K-Method	463 m/s	474 m/s

According to Table 5.1, predicted flutter speeds of the reference blade by the steady load assumption are the lowest ones for both sections. The main reason behind this fact is that in unsteady aerodynamic theories there are some terms which act as a damping in the Lagrangians of the typical section. However, these aerodynamic damping terms do not exist in the steady load. Therefore, steady loads method predicts the lowest flutter speed.

Another observation from Table 5.1 is that Theodorsen's unsteady aerodynamic theory predicts same flutter speed whether K-Method is implemented or not. In [10], an example for which Theodorsen's unsteady aerodynamic and K-Method predicted same flutter speed is given as well. Therefore, it could be stated that Theodorsen's unsteady aerodynamic, and K-Method predict same flutter speed by referring the obtained results and Ref. [10]. It is also seen that flutter speed predictions are identical when Loewy's unsteady aerodynamic theory and finite wake unsteady aerodynamic theories are implemented. The main reason behind this situation is that finite wake unsteady aerodynamic theory is an unsteady aerodynamic theory based on Loewy's theory such that the lift deficiency function of the finite wake unsteady aerodynamic theory is almost identical to Loewy's. Therefore, they predict same flutter speed for the reference blade.

In Table 5.1, it is observed that flutter speed predictions of steady loads, Theodorsen's unsteady aerodynamic theory and K-Method are higher if the section is taken from %75 radius. On the other hand, Loewy's unsteady aerodynamic theory and finite wake theory predicts flutter speed higher if the section is taken from %95 radius of the blade. All non-dimensional parameters given in Eq. (5.19) are same in the structural part of the flutter determinant in Eq. (5.40) except the ratio of the natural frequencies φ, whereas in the aerodynamic part in Eq. (5.40) is different for each aerodynamic theory which makes the solution of the flutter determinant different than each other. If the solutions of the flutter determinant are inspected in detail it is seen that solution of the determinant is non-linearly dependent on the ratio of the natural frequencies φ and aerodynamic terms. Therefore, changing the φ non-linearly affects the solution of the flutter determinant as it could be seen in Table 5.1. Hence, how changing φ and aerodynamic terms will affect the flutter determinant may not be predicted easily.

Although predicted flutter speed values are well beyond the flight envelope, found flutter speeds are different for each aerodynamic theory. As discussed in Section 5.5, Loewy's unsteady aerodynamic theory is valid for only in hover and near hover flight conditions. Therefore, it could be concluded that for a helicopter blade, different theories should be used to predict the flutter speed since they are valid for different flight conditions and they give different results from each other.

CHAPTER 6

DISCUSSIONS AND FUTURE WORK

The main purposes of this work are to determine whether the divergence or flutter would occur in the flight envelope and to examine how valid the torsionally rigid blade assumption is.

It is found that no divergence is expected since the shear center is located in front of the aerodynamic center. It is also found that including the effects of the torsional twist of the blade do not change the results considerably in a level flight compared to the rigid blade assumption since the distance between the aerodynamic center and the shear center is very low. Especially the required powers are almost identical. The only noticeable difference is found between the necessary collective inputs. It is found that required collective input for a trimmed level flight is only 0.05 degree is higher if the blade is assumed to be elastic in the torsional direction. The reason behind this situation is that the shear center is forward of the aerodynamic center. Therefore, any aerodynamic lift causes a negative torsional twist of the blade which decreases effective angle of attack; as a result, an increase in the collective input is needed to compensate the lift loss due to the negative torsional twist. If the required inputs are compared with each other, it could be concluded that assuming the blade is torsionally rigid is a valid assumption.

For the flutter analyses, the reference blade is found as flutter-safe in the given flight speed range. Although different theories are used to determine the flutter speed, all theories expect that the flutter speed is above 300 m/s which is much higher than the flight envelope. Therefore, it could be said that the reference blade will not experience any flutter in the current flight envelope according to the methodology proposed in this work. However, a more detailed three-dimensional or finite element analysis should be conducted to say undoubtedly that the blade will not experience any flutter in the given flight envelope.

To take this work one step further:

- In this work, only trimmed level flight is inspected. Full flight envelope including all the maneuvers and load cases of the reference helicopter could be analyzed to examine the validity of rigid blade assumption.
- Higher order harmonics are neglected and only the first harmonics are considered in this work. Including the higher harmonics and re-doing the analyses could be done to observe the effects of the higher harmonics.
- For the flapping motion, out-of-plane bending of the blades is assumed to be constant through the blades and structural damping is ignored, and the flapping motion is modeled as if the system was a pure mass-spring system. Flapping motion could be analyzed by implementing exact out-of-plane bending angles and adding the structural damping to the system.
- Inertial effects in the torsional dynamics of the blade are ignored. Analyses conducted in the static aeroelastic part could be expanded by adding the inertial effects of the torsional dynamics.
- Root's spring and damper systems could be implemented to see the effects of spring and damper.
- Inflow field of the rotor is assumed to be uniform. Different inflow models especially dynamic inflow models could be implemented into the analyses to increase the accuracy of the work.
- In static aeroelasticity part, loads are assumed to be steady, and any unsteady effects are ignored. Instead of steady aerodynamics loads, unsteady aerodynamics could be implemented.
- Aerodynamic center and elastic axis are assumed to stay constant during hover and forward flight. Change in aerodynamic center and elastic axis could be considered during the analyses.
- Flutter analyses are done w.r.t the sections taken from the reference blade's %75 and %95 span. Instead of taking a section from the blade, whole blades equation motion and aerodynamic loads could be written to obtain the flutter speed.

- Compressibility effects are ignored while calculating the unsteady aerodynamic loads. Flutter analyses could be carried by including the compressibility effects.
- Inflow effect is ignored in Theodorsen's unsteady aerodynamic theory.
- Pitching and plunging couplings coming from the rotation of the blade are ignored since the distance between the mass center and shear center is low. Flutter analyses could be re-conducted by including these couplings.
- A more sophisticated unsteady aerodynamic theory developed for helicopters in forward flight could be used to determine the flutter speed for the main rotor blades in forward flight.

REFERENCES

1. Anderson, J. D. (2017). *Fundamentals of Aerodynamics* (6th ed.). McGraw-Hill Education.

2. Akel, E. (2017). *The Effect of Blade Torsional Elasticity on Helicopter Flight Dynamics* [MSc. thesis]. METU.

3. Bielawa, R.L. (2006) *Rotary Wing Structural Dynamics and Aeroelasticity*. Reston, VA: American Institute of Aeronautics and Astronautics.

4. Bramwell, A.R.S., Done, G. and Balmford, D. (2001) *Bramwell's Helicopter Dynamics*. 2nd edn. Oxford: Butterworth-Heinemann.

5. CH-47 CHINOOK (no date) Boeing. Available at: https://www.boeing.com/defense/ch-47-chinook/ (Accessed: January 6, 2023).

6. Couch, M.A. (2003) A Three-Dimensional Flutter Theory for Rotor Blades with Trailing-Edge Flaps. thesis.

7. Çiçek, O. (2019). *Flutter Analysis of Fixed and Rotary Wings* [MSc. thesis]. METU.

8. Dowell, E.H. (2015) *A Modern Course in Aeroelasticity*.

9. Farsadi, T., & Kayran, A. (2016, August 28). Aeroelastic Instability Analysis of Composite Rotating Blades Based on Loewy's and Theodorsen's Unsteady Aerodynamics. *The 2016 World Congress on Advances in Civil, Environmental, and Materials Research (ACEM16) / The 2016 Structures Congress (Structures16)*.

10. Hodges, D.H. and Pierce, G.A. (2011) *Introduction to Structural Dynamics and Aeroelasticity*. 2nd edn. New York, NY: Cambridge University Press.

11. Johnson, W. (1994) *Helicopter Theory*. New York, NY: Dover Publications.

12. Johnson, W. (2013). *Rotorcraft Aeromechanics*. Cambridge University Press.

13. KA32 (no date) KAMOV Ka-32 | SKYbrary Aviation Safety. Available at: https://skybrary.aero/aircraft/ka32 (Accessed: January 6, 2023).

14. Leishman, J.G. (2006) *Principles of Helicopter Aerodynamics*. 2nd edn. Cambridge: Cambridge University Press.

15. Megson, T.H.G. (2022) *Aircraft Structures for Engineering Students*. 7th edn. Amsterdam: Elsevier, Butterworth-Heinemann.

16. NACA 0012 airfoils (n0012-IL). (n.d.). Retrieved October 5, 2022, from http://airfoiltools.com/airfoil/details?airfoil=n0012-il

17. Özturan, B. İ. (2019). *Multibody Simulation of Helicopter Rotor with Structural Flexibility* [MSc. thesis]. METU.

18. Padfield, G.D. (2007) *Helicopter Flight Dynamics: The Theory and Application of Flying Qualities and Simulation Modelling*. 2nd edn. Oxford: Blackwell.

19. Prouty, R.W. (2005) *Helicopter Performance, Stability and Control*. Malabar: Krieger.

20. Sieradzki, A. (2018). Aeroelastic Analysis of a Helicopter Rotor in Hover. *Journal of Physics: Conference Series*, 1101, 012033. https://doi.org/10.1088/1742-6596/1101/1/012033

21. Susuz, U. (2008). *Aeroelastic Analysis of An Unmanned Aerial Vehicle* [MSc. thesis]. METU.

22. T129 ATAK (no date). Turkish Aerospace. Available at: https://www.tusas.com/urunler/helikopter/ortak-gelistirme/t129-atak (Accessed: January 6, 2023).

23. Wortmann FX 76-120 (FX76120-IL). (n.d.). Retrieved February 26, 2023, from http://airfoiltools.com/airfoil/details?airfoil=fx76120-il

APPENDICES

A. Natural Frequencies of the Sections

In Ch. 5, sectional properties are used to predict the flutter speed of the reference blade. These sectional properties are non-dimensional radius of gyration r_a^2, mass ratio parameter μ_m, non-dimensional distance between elastic axis and shear center x_θ and the ratio of the uncoupled plunging natural frequency to the pitching natural frequency of the airfoil φ. Since the reference blade is uniform and it is assumed that shear center and center of gravity of the blade do not change with the rotation of the blade, non-dimensional parameters r_a^2, μ_m and x_θ are same for both sections taken from %75 and %95 radius of the blade. However, out-of-plane bending (plunging) and torsional (pitching) stiffnesses of the sections change with location which makes the ratios of the plunging and pitching natural frequencies different than each other although mass and inertia parameters of the sections are same.

$$\omega_{h_{0.75}} = \sqrt{\frac{k_{h_{0.75}}}{m}} \qquad \omega_{\theta_{0.75}} = \sqrt{\frac{k_{\theta_{0.75}}}{I_p}}$$
$$\omega_{h_{0.95}} = \sqrt{\frac{k_{h_{0.95}}}{m}} \qquad \omega_{\theta_{0.95}} = \sqrt{\frac{k_{\theta_{0.95}}}{I_p}} \tag{A.1}$$

where m is the blade mass per unit length, I_p is the blade mass moment inertia per unit length in pitching direction (along the blade span), k_h and k_θ are the plunging and pitching stiffnesses of the sections respectively. Spring stiffnesses of the reference blade are defined from the relations:

$$k_h = \frac{F}{\delta_h} \qquad k_\theta = \frac{M}{\delta_\theta} \tag{A.2}$$

where δ_h and δ_θ are the plunging and pitching deflections of corresponding sections of the reference blade under a load which is applied at the section's locations respectively.

To illustrate how spring stiffnesses and natural frequencies of the sections are obtained, let us consider a clamped-free, flat and uniform plate whose dimensions are 2 m in length, 20 cm in width, 1 mm in thickness.

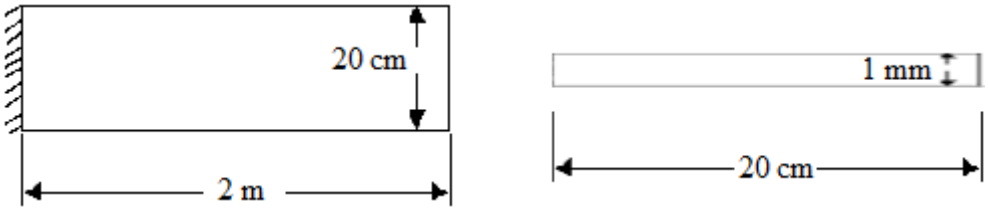

a) Top view b) Front view

Figure A.1. Flat plate dimensions.

Young's Modulus of the plate is given as 70 GPa, Poisson's ratio is 0.3, density of the plate is 2700 kg/m^3. For given dimensions and density, mass properties of the flat plate are found as $m = 0.54\ kg/m$ and $I_p = 1.8x10^{-3}\ kgm$.

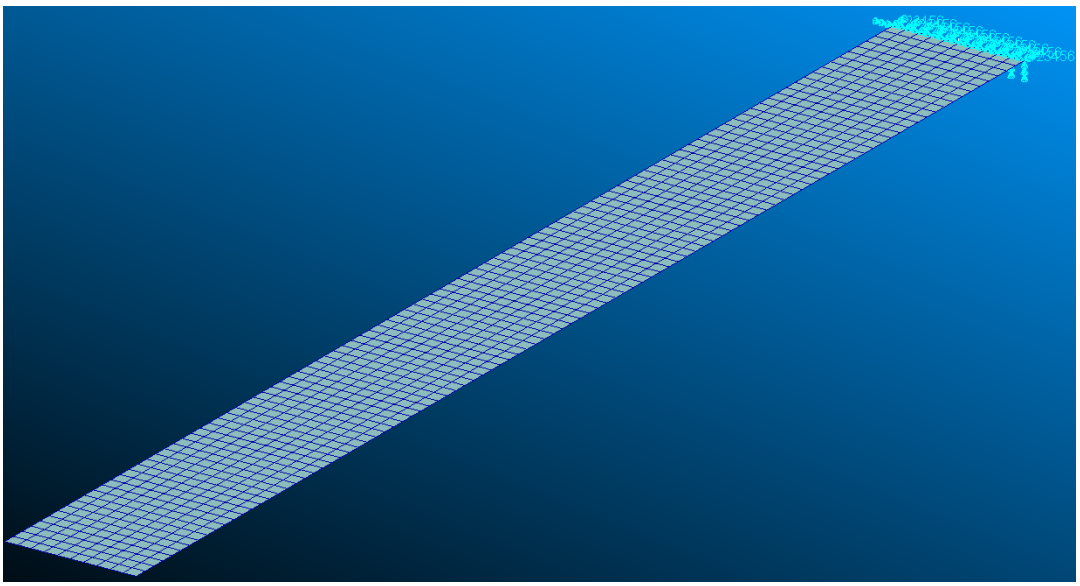

Figure A.2. Finite element mesh of the flat plate.

First out-of-plane bending and torsional natural frequencies of the plates are obtained as $\omega_h = 0.21\ Hz$ and $\omega_\theta = 4.00\ Hz$ by using MSC Nastran.

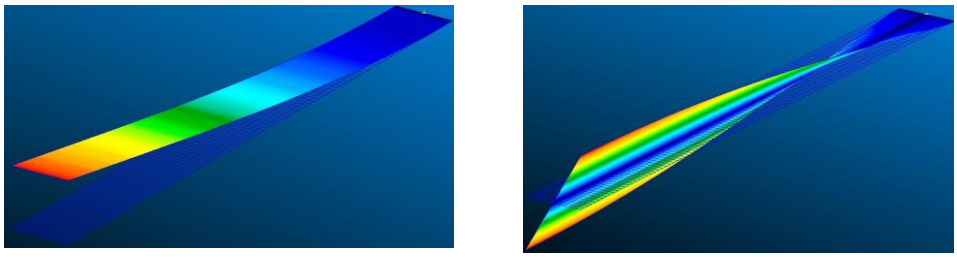

a) 1st out-of-plane bending mode b) 1st torsional mode

Figure A.3. First out-of-plane bending and torsional mode shapes.

If a $10^{-3}\ N$ force and $10^{-3}\ Nm$ moment are applied separately to the nodes where they are located %75 and %95 span of the flat plate in spanwise direction and center of gravity, displacements are obtained as $\delta_{h_{0.75}} = 0.952\ mm$, $\delta_{\theta_{0.75}} = 8.43x10^{-4}\ rad$, $\delta_{h_{0.95}} = 1.94\ mm$ and $\delta_{\theta_{0.95}} = 1.07x10^{-3}\ rad$.

By using the displacements, spring stiffnesses are found as:

$$k_{h_{0.75}} = 1.05\ N/m \qquad k_{\theta\,0.75} = 1.19\ Nm/rad$$
$$k_{h_{0.95}} = 0.52\ N/m \qquad k_{\theta\,0.95} = 0.93\ Nm/rad \tag{A.3}$$

from which natural frequencies of the sections are obtained as:

$$\omega_{h_{0.75}} = 0.22\ Hz \qquad \omega_{\theta\,0.75} = 4.09\ Hz$$
$$\omega_{h_{0.95}} = 0.16\ Hz \qquad \omega_{\theta\,0.95} = 3.63\ Hz \tag{A.4}$$

If the natural frequencies of the sections are compared with the natural frequencies of the plate, it is found that natural frequencies of the section taken from %75 span of the plate deviates about %5 and %2 from first out-of-plane bending and torsional natural frequencies of the plate. On the other hand, natural frequencies of the section from %95 span of the plate deviate about %26 for first out-of-plane bending and %10 for first torsional natural frequency of the plate. Therefore, the plate could be approximated by using its %75 span section.

In Section 5.7, a Wortmann FX 76-120 symmetrical wing whose dimensions and structural details are given from Ref. [21]. First out-of-plane bending and torsional natural frequencies of the Wortmann FX 76-120 wing are given as $\omega_h = 14.7\ Hz$ and $\omega_\theta = 98.7\ Hz$ respectively and methodology described here is applied to the wing to find flutter speed. Natural frequencies of the %75 and %95 sections are:

$$\omega_{h_{0.75}} = 15.6\ Hz \qquad \omega_{\theta_{0.75}} = 100.2\ Hz$$
$$\omega_{h_{0.95}} = 11.0\ Hz \qquad \omega_{\theta_{0.95}} = 89.0\ Hz \tag{A.5}$$

When the natural frequencies are compared with the reference, the deviations of the out-of-plane bending natural frequencies of the sections are about %6 and %25 for %75 and %95 sections respectively. Whereas the deviations for the torsional natural frequencies are about %1.5 for %75 section and %9 for %95 section.

Flutter speed of the wing is found as 368 m/s in Ref. [21] by using MSC FlightLoads, whereas by using offered K-Method flutter speed is found as 358 m/s if the %75 section is used. If the section is taken from %95 flutter speed is predicted as 321 m/s for the Wortmann FX 76 120 wing. The difference is about %2.7 and %13 respectively. When the flutter speeds predicted by K-Method are compared with the finite element analysis, it is seen that there is a correlation between the flutter speed predictions and how good approximated natural frequencies of the wings by the sections. Hence it could be concluded that if the natural frequencies of the sections are close to the natural frequencies of the system, flutter speed predictions are also close to the three-dimensional flutter predictions.